Photocatalysis under Periodic Illumination

Thesis by

Catherine J. G. Cornu

In Partial Fulfillment of the Requirements

for the Degree of

Doctor of Philosophy

California Institute of Technology

Pasadena, California

2002

(Submitted September 24, 2001)

Acknowledgements

I want to thank everybody who helped make the five years I spent as a graduate student at Caltech both fruitful and enjoyable.

First and foremost, my gratitude goes to Professor Michael Hoffmann for giving me the opportunity to pursue my Ph.D. at Caltech and to do research in his laboratory.

Dr. A. J. Colussi was a great mentor to me; discussing results and ideas with him always results in refreshing insights.

I also benefited from stimulating discussions, collaboration on experiments, demonstrations of equipment, and general companionship provided by Steve Szczepankiewicz, Yael and Yaniv Dubowski, Tim Lesko, Fok-Yan Leung, Tatiana Piatina, Jennie Stephens, Bill Balcerski, T. K. Lee, John Moss, and Nathan Dalleska, among others.

I also wish to thank my committee members, Prof. Janet Hering, Prof. Nathan Lewis, and Prof. Geoffrey Blake, for the helpful suggestions for improving this manuscript.

Last, but not least, I must acknowledge the support of my family during all the years that preceded this work, and the encouragements of my husband and my daughter.

Abstract

In the first part of this work, the use of periodic illumination is investigated as a means to improve the quantum yield of aqueous phase photocatalysis. We find that quantum yield enhancements are obtained under periodic illumination compared to those under continuous illumination with the same *maximum* photon absorption rate. This result is in agreement with previous literature reports. However, no enhancements are obtained when compared to those under continuous illumination with the same *average* photon absorption rate. Ways in which the use of periodic illumination in remediation systems might nevertheless be more cost-effective than continuous operation are discussed.

In the second part of this work, periodic illumination is applied as a tool to investigate the kinetic behavior of the intermediates involved in photocatalysis. Two transitions are observed in the quantum yield as a function of the active light period, corresponding to separate lifetimes of two intermediates. These lifetimes are found to be relatively insensitive to the physical properties of the TiO_2 photocatalyst particles, the compound being photocatalytically oxidized, or the oxygen concentration. However, a strong correlation with the pH of the solution is observed. For example, one intermediate's lifetime increases exponentially with pH, while the other one's decreases exponentially. Principles from electrochemistry, namely Nernst's law and the Butler-Volmer equation, allow us to conclude that the intermediate with a decreasing lifetime with pH is a reducing species, while the other one is an oxidizing species. The intermediates' lifetimes are equal at a pH ~ 8, concurrent with a minimum in quantum yield. Below pH 8 the

reducing species has a longer lifetime, indicating that interfacial electron transfer to oxygen is the slowest step under these conditions.

The observed lifetimes are compatible with those previously measured for superoxide radicals (reducing species), and hydroxyl radicals, surface trapped holes, or surface bound hydroxyl radicals (oxidizing species).

Table of contents

List of figures

List of tables

List of symbols

symbol		units used
$\varnothing$	dissipated heat	
A	anatase	-
a	parameter in $\phi_F = a \langle I_a \rangle^m$	
α	polarizability	
A	molecule undergoing photolysis according to the reaction mechanism on p. II-16 and VI-5	-
A	electron acceptor	-
α_{1e}	electron transfer coefficient for reduction ((7) on p. VI-10)	-
α_{2h}	electron transfer coefficient for oxidation ((8) on p. VI-10)	-
a_i	activity of component i	M
α_{ox}	electron transfer coefficient for oxidation	-
α_{red}	electron transfer coefficient for reduction	-
b	ratio of the light time to the average lifetime of D_1	-
β	parameter in $R_4 = \beta \langle I_a \rangle^n$ (Ch. 3) or $R_s = \beta I_a^n$ (Ch. 4)	
c	speed of light	$m\ s^{-1}$
C_{dl}	capacitance of the double layer	$F\ m^{-2}$
c_i	concentration of component i	M
D	diffusion coefficient	$cm^2\ s^{-1}$
δ	density	$g\ cm^{-3}$
d	depth of the reaction cell (2.5)	cm
D	electron donor	-
D^+	oxidized form of D	-
D_1	rate-controlling intermediate in photolysis reaction on p. II-16 and VI-5	-
$(\overline{D_1})$	time average concentration of D_1 under periodic illumination	
$(D_1)_s$	stationary concentration of D_1 under steady illumination	
D_2, D_3	intermediate in photolysis reaction on p. II-16 and VI-5	-
Da	Damköhler number	-
D_n	intermediate in photopolymerization reaction on p. II-16	-
E	(electrical) potential	V

e	reducing species	-
e^-	electron	-
E^{Θ}	standard electrode potential	V
$E^{\Theta'}$	formal potential	V
E^*	excess photon energy	eV
E_b	bandgap	eV
E_{CB}	conduction band edge energy	eV
E_{VB}	valence band edge energy	eV
F	Faraday's constant (96485)	C mol^{-1}
Φ	spherical coordinate	rad
ϕ	quantum yield	-
ϕ_F	quantum yield for photocatalytic formate degradation	-
γ	duty cycle	-
h	Planck's constant ($6.63\ 10^{-34}$)	J s
η	photoefficiency	-
h	oxidizing species	-
h^+	hole	-
h_t^+	trapped hole	-
i	chemical component (reagent or product)	-
I_0	incident photon rate during the light time	µEinstein L^{-1} s^{-1}
I_a	photon absorption rate	µEinstein L^{-1} s^{-1}
$\langle I_a \rangle$	average photon absorption rate	µEinstein L^{-1} s^{-1}
$I_{a,dark}$	photon absorption rate during the dark time	µEinstein L^{-1} s^{-1}
$I_{a,max}$	maximum photon absorption rate	µEinstein L^{-1} s^{-1}
I_b	back scattered photon rate	µEinstein L^{-1} s^{-1}
I_f	forward scattered photon rate	µEinstein L^{-1} s^{-1}
I_j	rate of photon absorption by the actinometer in the jacket	µEinstein L^{-1} s^{-1}
I_s	side scattered photon rate	µEinstein L^{-1} s^{-1}
I_{scat}	total scattered photon rate	µEinstein L^{-1} s^{-1}
I_t	transmitted photon rate	µEinstein L^{-1} s^{-1}
j	number of carrier traps present on a particle	-
k	wave number	
k_0	standard rate constant	
k_{01}	standard rate constant for reduction ((7) on p. VI-10)	m^2 mol^{-1} s^{-1}
k_{02}	standard rate constant for oxidation ((8) on p. VI-10)	m^2 mol^{-1} s^{-1}

k_1	rate constant for reduction ((7) on p. VI-10)	$m^2\ mol^{-1}\ s^{-1}$
k_2	rate constant for oxidation ((8) on p. VI-10)	$m^2\ mol^{-1}\ s^{-1}$
k_3	recombination rate constant	particle s^{-1}
k_{ox}	oxidation rate constant	
k_p	propagation rate constant	$cm^3\ mol^{-1}\ s^{-1}$
k_{red}	reduction rate constant	
k_t	termination rate constant	$cm^3\ mol^{-1}\ s^{-1}$
λ	wavelength of the light	nm
m	parameter in $\phi_F = a\ \langle I_a \rangle^m$	
m	$\tau_L\ k_t\ [D_1]$	-
n	number of D_1 units in a polymer chain	-
n	parameter in $R_4 = \beta\ \langle I_a \rangle^n$ (Ch. 3) or $R_s = \beta\ I_a^n$ (Ch. 4, 5)	
ν	frequency of the light	Hz
N_A	Avogadro's number ($6.0225 \cdot 10^{23}$)	molecules mol^{-1}
ν_i	stoichiometric coefficient of component i	-
Ox	oxidizing species	-
p	ratio of the dark time to the light time	-
PE	photoefficiency	-
Pot	(electrical) potential	V
θ	scattering angle	rad
θ_{window}	minimum angle for scattered light to leave the reaction cell through the front window (2.17 rad, 124.5°)	rad
R	rutile	-
r	distance	m
R	radius of the reaction cell (1.82)	cm
R	ideal gas law constant (8.314)	$J\ mol^{-1}\ K^{-1}$
$\langle r \rangle$	particle radius	nm
R_2	rate of step 2 in the reaction mechanism on p. III-12	
R_4	reaction rate (rate of step 4 in the reaction mechanism on p. III-12)	
$R_{4,max}$	largest observed R_4 per particle	mol s^{-1}
Red	reducing species	-
R_p	reaction rate under periodic illumination	nM min^{-1}
R_s	reaction rate under steady (continuous) illumination	nM min^{-1}
s	particle surface area	m^2

T	UV transmittance of suspension	-
t	time	s
T	temperature	K
τ	$\tau_L + \tau_D$	s
τ_1	characteristic time of transition at long τ_L	s
τ_2	characteristic time of transition at short τ_L	s
τ_D	dark time	s
T_{filter}	UV transmittance of neutral-density filter	-
τ_L	light time	s
v	mathematical expression, proportional to the reaction rate of the reaction mechanism on p. II-16 and VI-5	
Ω	carrier trap	-
z	number of electrons transferred	-

Chapter 1

Introduction and overview

1.1 Introduction

Photocatalysis is an advanced oxidation technology (AOT). AOTs involve the *in situ* generation of active radical species, typically the hydroxyl radical ($OH^{\bullet}$), leading to the complete destruction of the target pollutant. [1] Recently, the U.S. Environmental Protection Agency (EPA) has approved the inclusion of AOTs as a Best Available Technology (BAT). BATs have been found by the EPA to meet the standards and specifications that provide safe and sufficient pollution control of industrial processes and remediation of contaminated sites. The accepted treatment technologies applicable to aqueous phase waste streams containing organic contaminants are air stripping, adsorption onto activated carbon and bioremediation. AOT systems have the advantage of on-site destruction of contaminants with little or no air emissions, and may prove to be more economically efficient for certain remediation and pollution control applications. [2]

These technologies have been the focus of intensive research over the past two decades. Crucial insight into the chemical processes has been obtained and the use of these processes has been demonstrated on a practical level. Advantages and drawbacks relative to conventional approaches have been addressed. [3]

As a method of water purification, photocatalysis has substantial advantages. It destroys toxins rather than merely transferring them to another phase (as compared to adsorption on activated carbon and air stripping), and does so without the use of potentially hazardous oxidants (as compared to ozonolysis and chlorination for example). Removal of chlorinated hydrocarbons is of particular importance in industrial effluent treatment and has been shown to respond well to photocatalytic treatment. [3]

There are a number of problems associated with photocatalyzed treatment of wastewater, such as low photoefficiencies, which reduce the economic viability of the process and have prevented full commercialization. [4] Reactor design can alleviate some of the problems and increase the efficiency of the photocatalyzed process. Based on preliminary experiments, the use of periodic illumination has been suggested as a means to overcome the low photoefficiencies. [5,6]

The objective of this research is to contribute to the body of knowledge on photocatalytic degradation, with a particular focus on aspects of periodic illumination relevant to improving the photonic degradation efficiency.

1.2 Overview

The central theme in this work is the use of periodic illumination in photocatalysis with aqueous suspensions of TiO_2. First, in Chapter 2, a brief background pertaining to photocatalysis on TiO_2 and the use of periodic illumination is given.

The initial goal of this work is to investigate the mechanistic origins behind the reported efficiency enhancements for photocatalysis under periodic illumination. This aspect is addressed in Chapter 3. The results of a systematic study on the photocatalytic degradation of formate ion under periodic illumination are presented. An initial hypothesis to explain the observations is proposed. The comparison with continuous illumination is made, and implications for reactor design are discussed.

Based on these experiments, we noted that periodic illumination could be used as a tool for investigating the lifetimes of intermediates involved in the primary and secondary reactions of semiconductor photocatalysis. In order to determine the importance of the physical properties of the photocatalyst on the lifetimes of reaction intermediates, a comparative study, applying the technique of periodic illumination, is made of two different types of TiO_2 particles. This work is presented in Chapter 4.

In Chapter 5, the nature of the intermediates is probed. The methodology established in previous chapters is used to explore the photocatalytic degradation of methyl orange under a variety of reaction conditions. The hypothesis proposed in Chapter 3 is further refined and conditions favorable to obtaining higher photocatalytic efficiencies are deduced.

In Chapter 6, a simple kinetic model is proposed that describes the major reactions taking place and visualizes the concentrations of important intermediates during photocatalysis under continuous and periodic illumination. This model allows us to explore the effects of several experimental parameters.

The major conclusions of this work, and directions for future work are presented in Chapter 7.

1.3 References

(1) Jackman, A. P.; Powell, R. L. *Hazardous Waste Treatment Technologies*, Noyes Publications, Park Ridge, NJ, 1991.

(2) *Advanced Oxidation Technologies for Water and Air Remediation*; Al-Ekabi, H. (Ed.); Proceedings of the 4th Conference on Advanced Oxidation Technologies for Water and Air Remediation (London, Canada) 2000.

(3) *Photocatalytic Purification and Treatment of Water and Air*; Ollis, D. F., Al-Ekabi, H. (Eds.); Elsevier Science Publishers: Amsterdam, 1993, and references therein.

(4) Hoffmann, M. R.; Martin, S. T.; Choi, W.; Bahnemann, D. W. *Chem. Rev.* **1995**, *95*, 69.

(5) Sczechowski, J. G.; Koval, C. A.; Noble, R. D. in *Photocatalytic Purification and Treatment of Water and Air*; Ollis, D. F., Al-Ekabi, H. (Eds.); Elsevier Science Publishers: Amsterdam, 1993.

(6) Sczechowski, J. G.; Koval, C. A.; Noble, R. D. *J. Photochem. Photobiol. A: Chem.* **1993**, *74*, 273.

Chapter 2

Background

2.1 Titanium dioxide

Most of the semiconductor particles, which have been used for photocatalytic studies, are metal oxides, such as TiO_2, WO_3, ZnO, CdO and In_2O_3, and metal chalcogenides such as CdS, CdSe, MoS_2 and WS_2. However, TiO_2 is the most commonly used catalyst for the photocatalytic oxidation of aqueous and gaseous pollutants, because it is highly photoactive, very photostable, biologically and chemically inert, and relatively inexpensive as well. [1-6]

TiO_2 as a semiconductor

The semiconducting character of TiO_2 allows it to be used as a photocatalyst. A semiconductor or an insulator is a material whose valence (highest occupied) band and conduction (lowest unoccupied) band are separated by an energy gap or bandgap, E_b. [7] Whether the material behaves as a semiconductor or an insulator depends on the presence or absence of charge carriers. Although the wide bandgap of TiO_2 (3.2 eV) is too large to generate many charge carriers by thermal excitation, charge carriers are easily generated by absorption of photons with energy equal to or greater than 3.2 eV, which corresponds to ultra-violet light with wavelengths $\lambda < 380$ nm. [7]

TiO_2 as a mineral

The largest commercial market for titanium dioxide is as a paint pigment, because of its high refractive index. It is also used in sunblock lotions, cosmetics, pharmaceuticals, and vitamin tablets, for example. [1]

For use in photocatalysis, a distinction should be made between the three polymorphic crystalline structures TiO_2: anatase (tetragonal), rutile (tetragonal) and brookite (orthogonal). Brookite is not photoactive. Anatase is generally accepted to be (much) more photoactive than rutile, although this may not be true for all conditions or reactions. [1,3-5] This is believed to be due to the bandgap of anatase being wider than that of rutile by about 0.2 eV and a higher degree of surface hydroxylation in anatase. Rutile is the thermodynamically stable form of TiO_2, into which anatase (and brookite) convert when heated. [3,4]

Characteristics of P25 TiO_2

In order to improve the reproducibility of results between groups, many have chosen to use a particular source of TiO_2, with a recognized high photocatalytic activity, namely Degussa P25. [1-6] In the experimental work described in the subsequent chapters of this work, we also utilized Degussa P25. It comes as a powder and is produced by flame hydrolysis of $TiCl_4$ in the presence of hydrogen and oxygen, at temperatures greater than 1200 °C. The TiO_2 is treated with steam to remove HCl, which is also produced as part of the reaction. The product is 99.5% pure TiO_2 composed of a three-phase mixture of anatase, rutile – with an anatase to rutile ratio of about 70:30 – and a small fraction amorphous TiO_2. P25 is non-porous, with cubic particles with rounded edges. It has a surface area of 50 ± 15 m^2 g^{-1} and an average particle diameter by number count of 21 nm. However, the particles are known to exist in aggregates, typically approximately 0.1 μm in diameter. [1,3]

2.2 Photocatalysis on TiO_2

Mechanism

When TiO_2 is illuminated with photons with $\lambda < 380$ nm, upon absorption of a photon by the TiO_2 particle, an electron, e^-, is excited from the valence band to the conduction band, leaving a hole, h^+, behind in the valence band, as illustrated in Figure 2.1. At the TiO_2 surface, electrons and holes can participate in redox half-reactions. [1-6]

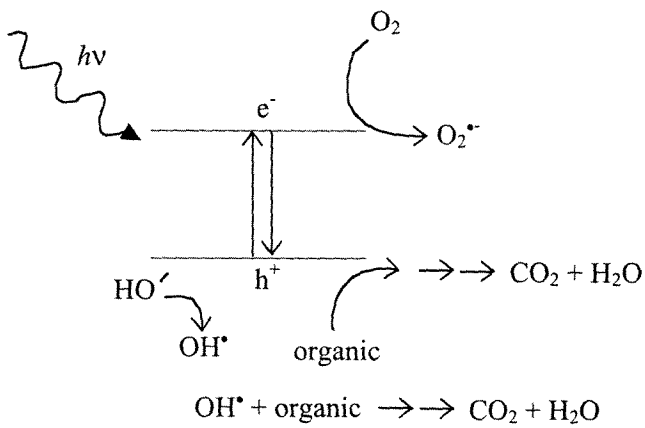

Figure 2.1. Schematic representation of the processes occurring in and on semiconductor particles during the photocatalytic mineralization of organic molecules by oxygen.

Due to the position of the valence band edge of TiO_2 (+3.1 V vs. NHE at pH 0 for anatase), the hole is a potent oxidant and can oxidize organic molecules at the surface,

eventually mineralizing them to CO_2. Similarly, the hole can oxidize water or hydroxide ions to form hydroxyl radicals, $OH^{\bullet}$, which are also efficient oxidants of organic molecules.

In order for the oxidation process to proceed effectively, the photogenerated electrons must also be removed from the TiO_2 particle. Typically, oxygen is used as the electron acceptor. Oxygen can be reduced to the superoxide, $O_2^{\bullet-}$, which may also participate in the degradation reactions of the organic molecules, or be further reduced to hydrogen peroxide or water.

When the concentrations of e^- and h^+ on the TiO_2 particle are high, they are likely to recombine to produce heat. The e^- and h^+ can also become immobilized at surface defects, called "traps." [8] While holes are usually powerful enough to initiate oxidation in either the free or trapped state, electrons can relax in traps below the reduction potential of O_2, called deep traps. The occupation of a deep electron trap inevitably leads to recombination with a hole, while the occupation of a shallow trap can also lead to transfer across the TiO_2/solution interface to O_2.

Applications

In addition to oxidation of organic pollutants by oxygen, there are reports in the literature on the photocatalytic dissociation of water, [9] destruction of gaseous pollutants (deodorization), [10-13] removal of inorganic pollutants [14] – including metal ions, [15] destruction of cancer cells, [16] and of bacteria and viruses (disinfection), [16-18] and on photocatalytic reduction of N_2 and CO_2. [19,20]

A number of photocatalytic reactors have been designed, patented and built, and have been employed in (small scale) site remediation efforts, both for gaseous (e.g., from a soil vapor extraction system) and aqueous (e.g., groundwater, wastewater or landfill leachate) contaminants. [21]

TiO_2 photocatalytic technology is also being applied in the building industry, especially in Japan, on interior construction materials as ceramic tiles and window glass. These materials are coated with transparent TiO_2 films, which perform deodorizing, self-cleaning, and antibacterial functions of the indoor air under roomlight illumination. [12,18]

Timescales

Characteristic times for the various processes occurring during photocatalysis have been determined. [22-29] Electron-hole pair generation upon absorption of a photon is extremely fast (fs). On the basis of laser flash photolysis measurements by Martin *et al.*, it was determined that trapping of electrons and holes happens on the nanosecond scale (~ 0.1-10 ns). Recombination has a characteristic time of 10 to 100 ns. Interfacial transfer of holes is slow (~ 100 ns), but the slowest step is the interfacial charge transfer of electrons to the electron acceptor (ms). [1,22,23] Gerischer and Heller have suggested that in most photocatalytic oxidations, reduction of oxygen is the rate-limiting step. [30,31]

Ohko *et al.* also deduced characteristic times, based on the photocatalytic decomposition of gaseous 2-propanol on titanium dioxide thin films under very weak UV light. The results are reprinted in Figure 2.2. [32]

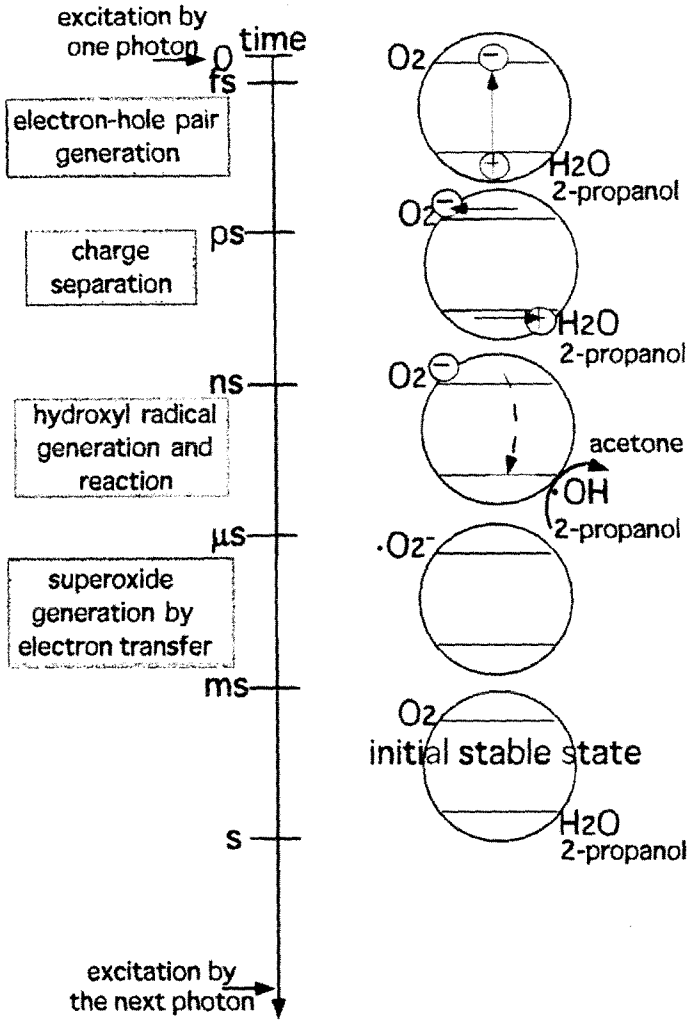

Figure 2.2. Schematic diagram of a series of photocatalytic processes along the time axis. The time interval of excitation by photons in this figure is assumed to be that for an experimental condition of 1 W cm^{-2} incident UV intensity and 1000 ppmv initial 2-propanol concentration (gas phase). [32]

2.3 Aqueous phase photocatalysis

A variety of organic molecules can be photocatalytically oxidized and eventually mineralized according to the following general reaction: [1-6]

$$\text{organic molecule} + O_2 \xrightarrow[h\nu \geq E_b]{\text{semiconductor}} CO_2 + H_2O + \text{mineral acids} \qquad (1)$$

An abbreviated list of compounds that have been demonstrated to be degradable via reaction 1 is given in Table 2.1. Often, (local) pollution problems impel researchers to investigate the degradability of a particular compound, and new compounds are continually being added to the list. [3]

Process efficiency

The efficiency with which photons of a certain wavelength λ are utilized is expressed by the quantum yield, [33]

$$\phi(\lambda) = \frac{\text{moles of molecules transformed by photons with wavelength } \lambda}{\text{moles of photons with wavelength } \lambda \text{ absorbed}}. \qquad (2)$$

When broadband UV is used, an overall quantum yield can be defined, [33]

$$\phi = \frac{\text{moles of molecules transformed}}{\text{moles of photons absorbed}}. \qquad (3)$$

For heterogeneous photocatalysis, it is experimentally difficult to determine ϕ, because of light scattering off the (semiconductor) particles. Scattering losses can be significant, and

Class	Example
alkanes	methane, isobutane, pentane, heptane, cyclohexane, paraffin
haloalkanes	mono-, di-, tri- and tetrachloromethane, tribromoethane, 1,1,1-trifluoro-2,2,2-trichloroethane
aliphatic alcohols	methanol, ethanol, isopropyl alcohol, glucose, sucrose
aliphatic carboxylic acids	formic, ethanoic, dimethylethanoic, propanoic, oxalic acids
alkenes	propene, cyclohexene
haloalkenes	perchloroethene, 1,2-dichloroethene, 1,1,2-trichloroethene
aromatics	benzene, naphtalene
haloaromatics	chlorobenzene, 1,2-dichlorobenzene, bromobenzene
nitrohaloaromatics	3,4-dichloronitrobenzene, dichloronitrobenzene
phenols	phenol, hydroquinone, catechol, 4-methylcatechol, resorcinol, o-, m-, p-cresol
halophenols	2-,3-,4-chlorophenol, pentachlorophenol, 4-fluorophenol, 3,4-difluorophenol
aromatic carboxylic acids	benzoic, 4-aminobenzoic, phtalic, salicylic, m- and p-hydroxybenzoic, chlorohydroxybenzoic acids
polymers	polyethylene, poly(vinyl chloride) (PVC)
surfactants	sodium dodecylsulphate (SDS), polyethylene glycol, sodium dodecyl benzene sulphonate, trimethyl phosphate, tetrabutylammonium phosphate
herbicides	methyl viologen, atrazine, simazine, prometron, propetryne, bentazon
pesticides	DDT, parathion, lindane
dyes	methylene blue, rhodamine B, methyl orange, fluorescin

Table 2.1. Some examples of organic compounds that can be photomineralized on TiO_2.[3]

have been determined to in some cases account for up to 70% of the incident photons.[3,33] To circumvent the problem of quantifying the number of photons absorbed, researchers often report photoefficiencies PE or η, where[33]

$$\eta = \frac{\text{moles of molecules transformed}}{\text{moles of incident photons}}. \quad (4)$$

ϕ and η are usually low for aqueous phase photocatalysis of organic molecules, typically around a few percent. This is the main obstacle that has prevented this technology from being widely commercialized. The primary non-productive pathways that limit the efficiency of the photocatalytic degradation process are believed to be direct and indirect electron-hole pair recombination.[1-6,25,34,35] Additional loss mechanisms include reactions of electrons and holes with solution species, such as the complete oxidation of water to molecular oxygen, or the oxidation of superoxide.[1-6]

To allow a direct comparison of the efficiency of degradation of a particular compound with photocatalysis and with other advanced oxidation technologies, figures of merit can be used.[36] Figures of merit are independent of the nature of the system, and are based on electric energy consumption (for electric energy driven systems) or collector area (for solar energy driven systems). The figures of merit are inversely proportional to fundamental efficiency factors – such as the lamp efficiency (for electrical systems), the fraction of the emitted light that is absorbed in the aqueous solution, and the quantum yield of generation of active radicals (so lower values mean higher efficiency).

Methods for improving ϕ

Most efforts to improve the quantum yield for aqueous phase photooxidation have been focused on the design of the photocatalyst, and have met with limited success. The use of dopants and the synthesis of Q-particles are amongst approaches that have been pursued in our laboratory in the past. [37-41]

Since the rate-controlling step in photocatalysis is believed to be the charge transfer of electrons to O_2, metal atoms or clusters are added to the surface of the TiO_2 to facilitate the removal of electrons. The effects of metal ions in the crystal lattice have also been examined, and the results suggest that the concentration, valence state, and distribution of the dopants within the TiO_2 lattice are all important in determining their effects, making structure-activity correlations very complex. [37-39]

Q particles are small (nanometer sized) colloidal particles, which exhibit a size quantization effect that widens the bandgap, thus increasing the reactivity of electrons and holes. In addition, the small crystallite size increases the available reactive surface area and decreases light scattering. Despite these physical advantages, the general photocatalytic efficiency of TiO_2 Q particles has not been demonstrated to (significantly) exceed that of their larger counterparts. [22,40,41]

In 1993, the first report was published in which periodic illumination was applied to photocatalysis and higher quantum yields were observed. We will review these and subsequent observations in the next section. [42]

2.4 Periodic illumination

Periodic illumination is obtained by a square-wave modulation of the light intensity, as illustrated in the schematic diagram shown below.

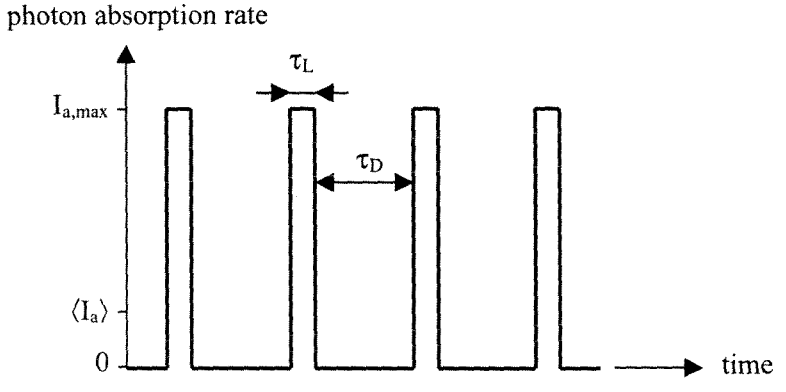

Figure 2.3. Schematic representation of periodic illumination.

The parameters that have been used to describe periodic illumination in previous literature are the light time τ_L – which is the length of time the light is actually on – and the dark time τ_D – which is the length of time the light is off in between two light times.[42-47] We found it useful to introduce the concept of duty cycle, γ, based on these two parameters, as $\gamma = \tau_L/(\tau_L + \tau_D)$. The duty cycle gives the fraction of the time the light is on.

The important photon rates are the incident photon rate, I_0, the maximum photon absorption rate, $I_{a,max}$, and the average photon absorption rate, $\langle I_a \rangle$. I_0 is the amount of

light (expressed in Einstein, i.e., moles of photons) entering the reaction solution, per unit time and volume of reaction solution. The light is then scattered, transmitted, or absorbed. The photon absorption rate by the TiO_2 particles during the time the light is on is termed $I_{a,max}$. Per definition, $\langle I_a \rangle = \gamma \times I_{a,max} + (1 - \gamma) \times I_{a,dark}$, with $I_{a,dark}$ the photon absorption rate during the dark time. Usually $I_{a,dark}$ is negligible, resulting in $\langle I_a \rangle = \gamma \times I_{a,max}$.

Periodic illumination applied to photocatalysis on TiO_2

A relationship between the photoefficiency and the periodicity of illumination of the photocatalyst was first reported by Sczechowski *et al.*, for the photocatalytic oxidation of formate (Figure 2.4).[42,43] A five-fold increase over continuous illumination was obtained using periodic illumination of a TiO_2 slurry in a flow through reactor, with τ_L = 72 ms and τ_D = 1.45 s.

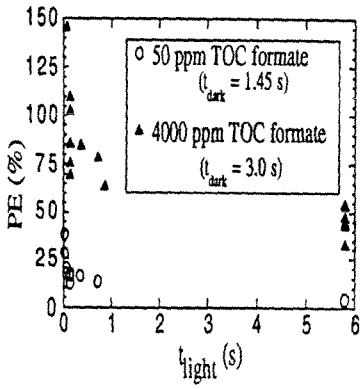

Figure 2.4. Photoefficiency vs. t_{light} (= τ_L) for the photocatalytic oxidation of formate.[43]

The explanation put forward was that the accumulation of photogenerated intermediates favors reactions resulting in the recombination of electron-hole pairs or other redox processes that do not oxidize the organic compound, and that periodic illumination reduces the build-up of intermediates, and thus the occurrence of these undesirable reactions.

In subsequent studies by Buechler *et al.*, photoefficiency improvements were observed under some conditions.[44,45] Stewart and Fox, using laser excitation pulses, found a 1.8-fold rate improvement for the photocatalytic oxidation of 1-octanol by increasing the dark interval from 0.1 s to 1 s, but detected no improvement in the photocatalytic reduction of p-nitroacetophenone under the same conditions.[46]

It should be pointed out that in the cases where improvements using periodic illumination were observed, it was in systems that were not limited by mass transfer. Obviously, when mass transfer to and from the photocatalyst surface is the rate limiting step, the reaction rate is independent of the photon absorption rate, and any reduction in incident photon rate – including the insertion of a dark time – will improve the quantum yield, as observed in Buechler *et al.*'s latest work.[47]

Aside from this body of work focusing on efficiency enhancements, there are also a few reports suggesting a change in the product distribution by applying periodic illumination.[44,48-50] This holds promise for developing methodologies for destroying compounds which generate hazardous intermediates or byproducts (such as phosgene).

Periodic illumination applied to photochemistry

Periodic illumination can be used as a tool to determine lifetimes of rate-controlling intermediates and rate constants of photochemical reactions. [51-55] Periodic illumination is usually provided by rotating a slotted wheel in front of the light source. By changing the rotation speeds, the light time can be varied. The main principle is that at high rotation speeds (short light times) the system behaves as if illuminated continuously, with a light intensity that is reduced compared to the full intensity by a factor given by the ratio between the light time and the total (= light + dark) time. At slow rotation speeds, on the other hand, the system experiences continuous illumination with the full intensity, but only a fraction of the time, given – also – by the ratio between the light time and the total time. If the reaction rate is not linear with the light intensity, the measured rates at low and high rotation speeds will be different. The light time at which the rate transitions from high to low depends on the reaction, and is related to the average lifetime of the rate-controlling intermediate involved in the reaction.

For the low temperature photolysis of aldehyde and for many photopolymerizations, assumptions [(*)] can be made that simplify the rate equations so that an analytical solution can be found. This analytical solution is represented graphically in Figure 2.5. It allows the determination of the lifetime of the rate-controlling intermediate with just a few experiments. [52]

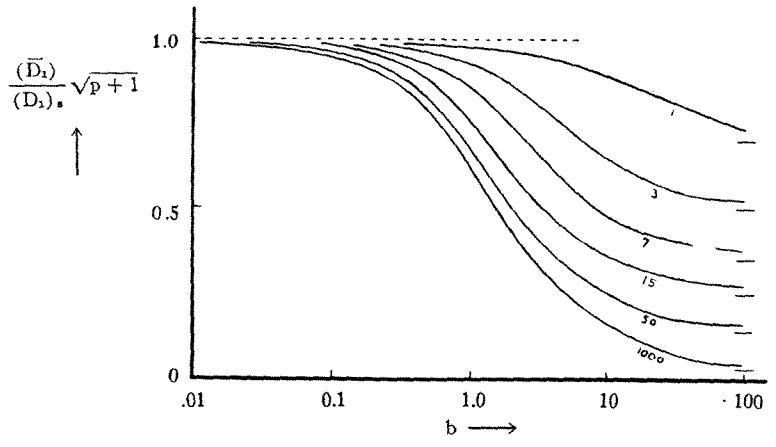

Figure 2.5. Variation in ratio $(\overline{D_1})/(D_1)_s$ with b for various values of p.

$(\overline{D_1})$ is the time average concentration of the rate-controlling intermediate D_1 under

---

(*) The general reaction scheme for aldehyde photolysis is:

initiation: $A + h\nu \rightarrow D_1 + D_2$

propagation: $D_1 + A \rightarrow B + D_3$

$D_3 \rightarrow D_1 + C$

termination: $D_1 + D_1 \rightarrow D$

where D_1, D_2, and D_3 are free radicals, and B, C, and D stable product molecules ($A = C_2H_4O$, $D_1 = CH_3$, $D_2 = CHO$, $D_3 = CH_3CO$, $B = CH_4$, $C = CO$, and $D = C_2H_6$).

An analytical solution for the reaction rate can be obtained if the concentration of the rate-controlling radical D_1 is determined by the rates of the initiation (generation of D_1) and termination (consumption of D_1) steps only. This occurs, e.g., when the second step of the propagation is much faster than the first, such that there is no net consumption (nor generation) of D_1 during the propagation. This condition is met for aldehyde photolysis at moderate temperatures, rather than at high temperature. For photopolymerizations – following a reaction scheme involving chain initiation, propagation ($D_1 + D_n \rightarrow D_{n+1}$, where n denotes the number of D_1-units in the polymer chain), and termination – an analytical solution can be obtained if the reactivities of D_1, D_n and D_{n+1} are equal, which is often a good approximation.

periodic illumination, $(D_1)_s$ the stationary concentration of D_1 under steady illumination. The ratio $(\overline{D_1})/(D_1)_s$ is equal to the ratio of the observed rates under periodic and steady illumination. b is the ratio of the light time to the average lifetime of D_1 under steady illumination of the same intensity, p is the ratio of the dark time to the light time. Ordinates are multiplied by $(p + 1)^{1/2}$ to produce a common asymptote of unity with decreasing b. Values of p from 1 to 1000 are illustrated. [52]

2.5 Effects of experimental parameters

The rate of photomineralization of an organic compound by a photocatalysis on semiconductor depends mainly on the nature of the semiconductor photocatalyst, the photon absorption rate I_a (and therefore the incident photon rate and the load of TiO_2), the oxygen concentration, the nature and concentration of the compound, the temperature, the pH and the presence of interfering adsorbing species. In subsequent chapters we will vary a number of these parameters, the principal ones being I_a and pH.

Effect of light intensity

For a simple set of reactions including only charge carrier generation, recombination, reduction and oxidation, it is easily derived that at low I_a and correspondingly low carrier concentrations, the rate of oxidation of a particular compound is proportional to I_a, while at higher I_a the rate is dominated by (second-order) charge carrier recombination and has a square-root dependence on I_a. Many researchers have verified this behavior

experimentally, [56-60] even though it has been argued that charge carrier recombination is not a second-order process, [61,62] and deviations of the square-root dependence have been observed. [63] The transition from one regime to the other depends on the photocatalyst material, but is typically above 1 sun equivalent ($7 \cdot 10^{-5}$ Einsteins m^{-2} s^{-1}). [57]

Increasing the incident photon rate invariably results in an increase in volumetric reaction rate, until the mass transfer limit is encountered. This transition depends on the (immobilized) catalyst configuration and on the flow regime in the photoreactor, and varies with each application. [57]

The observation that the quantum yield decreases with increasing levels of illumination indicates an efficiency penalty for intense lamps or concentrated solar sources.

Effect of pH

The pH of an aqueous solution significantly affects all oxide semiconductors, including the surface charge on the semiconductor particles, the size of the aggregates formed and the energies of the conduction and valence bands.

TiO_2 particles suspended in water are known to be amphoteric. [41] The principal amphoteric surface functionality is the "titanol" surface group, ≡TiOH. The surface density of ≡TiOH is typically 10^{12} - 10^{15} cm^{-2}. [3]

Hydroxyl groups on the TiO_2 surface undergo the following acid-base equilibria:

$\equiv TiOH_2^+ \leftrightarrow \equiv TiOH + H^+, \quad pK_{a1}$

$\equiv TiOH \leftrightarrow \equiv TiO^- + H^+, \quad pK_{a2}$

where ≡ denotes a surface group.

The pK_a values for P25 have been measured as 4.5 for pK_{a1} and 8 for pK_{a2}, which results in a pH of zero point charge, $pH_{ZPC} = 0.5\ (pK_{a1} + pK_{a2})$, of 6.25.[41] At pH < 6 the TiO_2 surface accumulates a net positive charge due to the increasing fraction of total surface sites present as $\equiv TiOH_2^+$. At high pH, the surface has a net negative charge due to a significant fraction of total surface sites present as $\equiv TiO^-$.

In accordance with Nernst's law, varying the pH of the solution also shifts the energies of the valence and conduction band edges, by 0.059 V per pH unit (at ambient temperature).[64-65] This results in the valence band electrons becoming more potent and the conduction band holes less potent at higher pH.

2.6 Concluding remarks

The performance enhancements using periodic illumination reported to date are based on the comparison of photoefficiencies obtained under widely different average light intensities. In the experiments by Sczechowski *et al.*, the average light intensity is a factor of 21 lower for the optimal case than for the continuous photolysis used as a reference.[42,43] In the study by Stewart and Fox, there is a factor of 10 difference.[46] Furthermore, the enhancements are in the range of those expected by proportionately reducing the light intensity. Little attention has been given to this fact in the literature.

Thus, in investigating the effects of periodic illumination, it is important to design a set-up in which the light intensity can easily be varied, to determine how the quantum yield

varies with the light intensity. This will allow a comparison between periodic illumination and continuous illumination with the same average intensity, and enable us to distinguish between effects of pulsing the light and of reducing the average light intensity. This will be the focus of the next chapter.

It should also be noted that to our knowledge periodic illumination has not been used as a tool in photocatalytic studies. If the reaction conditions are well chosen, however, it should be possible to gain valuable information on the kinetics of the photocatalytic reactions. Though we will briefly touch on this in the next chapter, we will provide details on the determination of kinetic information in Chapters 5 and 6.

2.7 References

(1) Hoffmann, M. R.; Martin, S. T.; Choi, W. Y.; Bahnemann, D. W. *Chem. Rev.* **1995**, *95*, 69.

(2) Herrmann, J. *Catalysis Today* **1999**, *53*, 115.

(3) Mills, A.; Le Hunte, S. *J. Photochem. Photobiol. A* **1997**, *108*, 1.

(4) Stafford, U.; Gray, K. A.; Kamat, P. V. *Heterogeneous Chemistry Reviews* **1996**, *3*, 77.

(5) Ollis, D. F.; Al-Ekabi, H. (Eds.) *Photocatalytic Purification and Treatment of Water and Air*, Elsevier Science Publishers: Amsterdam, 1993.

(6) Linsebigler, A.; Lu, G.; Yates, J. T. *Chem. Rev.* **1995**, *95*, 735.

(7) Boer, K. W. *Survey of Semiconductor Physics*, Van Nostrand Reinhold: New York, 1990.

(8) Szczepankiewicz, S. H.; Colussi, A. J.; Hoffmann, M. R. *J. Phys. Chem. B* **2000**, *104*, 9842.

(9) Karakitsou, K. E.; Verykios, X. E. *J. Phys. Chem.* **1993**, *97*, 1184.

(10) Suzuki, K. in *Photocatalytic Purification and Treatment of Water and Air*, Ollis, D. F.; Al-Ekabi, H. (Eds.), Elsevier Science Publishers: Amsterdam, 1993.

(11) Mikula, M.; Brezova, V.; Ceppan, M.; Pach, L.; Karpinsky, L. *J. Mater. Sci. Lett.* **1995**, *14*, 615.

(12) Negishi, N.; Iyoda, T.; Hashimoto, K.; Fujishima, A. *Chem. Lett.* **1995**, 841.

(13) Matsubara, H.; Takada, M.; Koyama, S.; Hashimoto, K.; Fujishima, A. *Chem. Lett.* **1995**, 767.

(14) Ranjit, K. T.; Viswanathan, B. *J. Photochem. Photobiol. A* **1997**, *108*, 73.

(15) Schiavello, M. *Photocatalysis and Environment*, Kluwer Academic Publishers: Dordrecht, 1988.

(16) Blake, D. M.; Maness, P. C.; Huang, Z.; Wolfrum, E. J.; Huang, J.; Jacoby, W. A. *Separation and Purification Methods* **1999**, *28*, 1.

(17) Lawton, L. A; Robertson, P. K.; Cornish, B. J. P. A.; Jaspars, M. *Environ. Sci. Technol.* **1999**, *33*, 771.

(18) (a) Sunada, K.; Kikuchi, Y.; Hashimoto, K.; Fujishima, A. *Environ. Sci. Technol.* **1998**, *32*, 726.

(b) Kikuchi, Y.; Sunada, K.; Iyoda, T.; Hashimoto, K.; Fujishima, A. *J. Photochem. Photobiol.* **1997**, *106*, 51.

(19) Gratzel, M. (Ed.) *Energy Resources through Photochemistry and Catalysis*, Academic Press: New York, 1983.

(20) Davies, J. A.; Boucher, D. L.; Edwards, J. G. *Adv. Photochem.* **1995**, *19*, 235.

(21) Al-Ekabi, H. (Ed.) *TiO_2 Photocatalytic Purification and Treatment of Water and Air*, Proceedings of the 5th Conference on TiO_2 Photocatalytic Purification and Treatment of Water and Air (London, Canada) 2000.

(22) Martin, S. T.; Herrmann, H.; Choi, W.; Hoffmann, M. R. *J. Chem. Soc. Faraday Trans.* **1994**, *90*, 3315.

(23) Martin, S. T.; Herrmann, H.; Hoffmann, M. R. *J. Chem. Soc. Faraday Trans.* **1994**, *90*, 3323.

(24) Rothenberger, G.; Moser, J.; Gratzel, M.; Serpone, N.; Sharma, D. K. *J. Am. Chem. Soc.* **1985**, *107*, 8054.

(25) Colombo, D. P.; Bowman, R. M. *J. Phys. Chem.* **1995**, *99*, 11752.

(26) Bahnemann, D. W.; Hilgendorff, M.; Memming, R. *J. Phys. Chem.* **1997**, *101*, 4265.

(27) Furube, A.; Asahi, T.; Masuhara, H.; Yamashita, H.; Anpo, M. *J. Phys. Chem. B* **1999**, *103*, 3120.

(28) Serpone, N.; Lawless, D.; Khairutdinov, R.; Pelizzetti, E. *J. Phys. Chem.* **1995**, *99*, 16655.

(29) Stopper, K.; Dohrmann, J. K. *Zeitschrift fur Physikalische Chemie* **2000**, *214*, 555.

(30) Gerischer, H.; Heller, A. *J. Phys. Chem.* **1991**, *95*, 5261.

(31) Gerischer, H. in *Photocatalytic Purification and Treatment of Water and Air*, Ollis, D. F.; Al-Ekabi, H. (Eds.), Elsevier Science Publishers: Amsterdam, 1993.

(32) Ohko, Y.; Hashimoto, K.; Fujishima, A. *J. Phys. Chem. A* **1997**, *101*, 8057.

(33) (a) Serpone, N.; Salinaro, A. *Pure Appl. Chem.* **1999**, *71*, 303.

(b) Salinaro, A.; Emeline, A. V.; Zhao, J. C.; Hidaka, H.; Ryabchuk, V. K.; Serpone, N. *Pure Appl. Chem.* **1999**, *71*, 321.

(34) Kesselman, J. M.; Shreve, G. A.; Hoffmann, M. R.; Lewis, N. S. *J. Phys. Chem.* **1994**, *98*, 13385.

(35) Ishibashi, K.; Fujishima, A.; Watanabe, T.; Hashimoto, K. *J. Phys. Chem.* **2000**, *104*, 4934.

(36) Bolton, J. R.; Bircher, K. G.; Tumas, W.; Tolman, C. A. *Pure Applied Chem.* **2001**, *73*, 627.

(37) Martin, S. T.; Morrison, C. L.; Hoffmann, M. R. *J. Phys. Chem.* **1994**, *98*, 13695.

(38) Choi, W. Y.; Termin, A.; Hoffmann, M. R. *J. Phys. Chem.* **1994**, *98*, 13669.

(39) Choi, W. Y.; Termin, A.; Hoffmann, M. R. *Angew. Chem. Int. Edit.* **1994**, *33*, 1091.

(40) Hoffman, A. J.; Mills, G.; Yee, H.; Hoffmann, M. R. *J. Phys. Chem.* **1992**, *96*, 5546.

(41) Kormann, C.; Bahnemann, D. W.; Hoffmann, M. R. *J. Phys. Chem.* **1988**, *92*, 5196.

(42) Sczechowski, J. G.; Koval, C. A.; Noble, R. D. *J. Photochem. Photobiol. A: Chem.* **1993**, *74*, 273.

(43) Sczechowski, J. G.; Koval, C. A.; Noble, R. D. in *Photocatalytic Purification and Treatment of Water and Air*, Ollis, D. F.; Al-Ekabi, H. (Eds.), Elsevier Science Publishers: Amsterdam, 1993.

(44) Buechler, K. J.; Noble, R. D.; Koval, C. A.; Jacoby, W. A. *Ind. Eng. Chem. Res.* **1999**, *38*, 892.

(45) Buechler, K. J.; Nam, C. H.; Zawistowski, T. M.; Noble, R. D.; Koval, C. A. *Ind. Eng. Chem. Res.* **1999**, *38*, 1258.

(46) Stewart, G.; Fox, M. A. *Res. Chem. Intermed.* **1995**, *21*, 933.

(47) Buechler, K. J.; Zawistowski, T. M.; Noble, R. D.; Koval, C. A. *Ind. Eng. Chem. Res.* **2001**, *40*, 1097.

(48) Miller, M. L.; Borisch, J.; Raftery, D.; Francisco, J. S. *J. Am. Chem. Soc.* **1998**, *120*, 8265.

(49) Xu, W. Z.; Raftery, D. *J. Phys. Chem. B* **2001**, *105*, 4343.

(50) Nishii, J.; Fukumi, K.; Yamanaka, H.; Kawamura, K.; Hosono, H.; Kawazoe, H. *Phys. Rev. B* **1995**, *52*, 1661.

(51) Burnett, G. M.; Melville, H. W. in *Technique of Organic Chemistry, Investigation of Rates and Mechanisms of Reactions,* Friess, S. L.; Lewis, E. S.; Weissberger, A. (Eds.), 2nd Ed., Interscience Publishers: New York, 1963, Vol. VIII - Part II, Chapter 20.

(52) Noyes, W. A., Jr.; Leighton, P. A. in *The Photochemistry of Gases*, Reinhold Publishing Corp., 1941, Chapter IV.

(53) Haden, W. L.; Rice, O. K. *J. Chem. Phys.* **1942**, *10*, 445.

(54) Burnett, G. M.; Melville, H. W. *Nature* **1945**, *156*, 661.

(55) Bartlett, B. D.; Swain, C. G. *J. Am. Chem. Soc.* **1945**, *67*, 2273 and **1946**, *68*, 2381.

(56) Okamoto, K.; Yamamoto, Y.; Tanaka, H.; Itaya, A. *Bull. Chem. Soc. Jpn.* **1985**, *58*, 2023.

(57) Ollis, D. F.; Pelizzetti, E.; Serpone, N. *Environ. Sci. Technol.* **1991**, *25*, 1522-1529.

(58) Kormann, C.; Bahnemann, D. W.; Hoffmann, M. R. *Environ. Sci. Technol.* **1991**, *25*, 494-500.

(59) Ohko, Y.; Ikeda, K.; Rao, T. N.; Hashimoto, K.; Fujishima, A. *Zeitschrift fur Physikalische Chemie* **1999**, *213*, 33.

(60) Mills, A.; Wang, J. *Zeitschrift fur Physikalische Chemie* **1999**, *213*, 49.

(61) Grela, M. A.; Coronel, M. E. J.; Colussi, A. J. *J. Phys. Chem.* **1996**, *100*, 16940.

(62) Grela, M. A.; Colussi, A. J. *J. Phys. Chem.* **1996**, *100*, 18214.

(63) Bahnemann D.; Bockelmann D.; Goslich R. *Solar Energy Materials* **1991**, *24*, 564-583.

(64) Nozik, A. J.; Memming, R. *J. Phys. Chem.* **1996**, *100*, 1306.

(65) Matsumoto, Y. *J. Solid State Chem.* **1996**, *126*, 227.

Chapter 3

Quantum yields of the photocatalytic oxidation of formate in aqueous TiO_2 suspensions under continuous and periodic illumination

(published in part in *J. Phys. Chem. B* **2001**, *105*, 1351)

3.1 Abstract

Quantum yields ϕ_F for the oxidation of formate in periodically illuminated TiO_2 suspensions are always *smaller* than, but approach, at sufficiently high intermittence, the ϕ_F's measured under continuous exposure at equivalent *average* photon absorption rates $\langle I_a \rangle$. We find that $\phi_{F,cont} = (0.031 \pm 0.003) \times I_a^{-0.39 \pm 0.03}$ in the range $0.089 \leq I_a/\mu\text{Einstein } L^{-1} s^{-1} \leq 2.0$. Under periodic illumination with maximum photon absorption rate $I_{a,max} = 2.0$ μEinstein $L^{-1} s^{-1}$, ϕ_F begins to rise from its minimum value: $\phi_{F,long\ \tau} = \phi_{F,cont}(I_{a,max}) = 0.021$, for light periods $\tau_L \leq 1$ s, regardless of the duty cycle γ. Thereafter, ϕ_F climbs to its upper limit: $\phi_{F,short\ \tau} = \phi_{F,cont}(\langle I_a \rangle = \gamma\ I_{a,max})$, after a single inflection at $\tau_L \sim 200$ ms for $\gamma = 0.35$, but only after a second inflection at $\tau_L \sim 10$ ms for $\gamma = 0.05$. Thus, the photocatalytic oxidation of formate in ~10 nm TiO_2 nanoparticle suspensions under periodic illumination behaves kinetically as a homogeneous photochemical system; i.e., ϕ_F's are not limited by mass diffusion, or by adsorption/desorption, but by carrier recombination. The latter has a characteristic time of about 0.1 s under present conditions. Sparse carriers, such as those present in $\gamma = 0.05$ experiments at short τ_L's, are deactivated within ~ 6 ms. Therefore, photocatalytic quantum yields on nanoparticle surfaces are actually insensitive to events in the sub-milliseconds domain.

3.2 Introduction

The low quantum yields for the oxidation of aqueous pollutants on illuminated TiO_2 interfaces currently prevent the application of photocatalysis for large scale water remediation.[1,2] Much effort has been devoted to understanding the fundamental and engineering aspects of semiconductor photocatalysis with the goal of improving its efficiency.[3] Remarkably, whereas quantum yields in dilute aqueous solutions typically remain below ~10%, those measured for the oxidation of atmospheric organic species exceed 50% under very weak illumination.[2,4,5] The presumed slowness of electron scavenging by O_2 at the aqueous semiconductor interfaces vs. carrier trapping and/or recombination, as well as mass transfer control into and from the surrounding medium, have been invoked to account for these observations.[6-8] Since many one-electron transfers are required to fully oxidize organic substrates into CO_2, the competition for the primary oxidizing species by any chemical intermediates will also result in inefficient reactant degradation. [9]

One of the approaches recently proposed to overcome dissipative effects in TiO_2 photocatalysis involves periodic illumination. [10-15] The tacit assumption was that charge and concentration gradients developing during light exposure would eventually relax in the ensuing dark period, thereby removing the efficiency losses associated with irreversibility.[8] The two-electron oxidation of formate into CO_2 seems to be particularly appropriate for testing this hypothesis, since the number of intermediates is kept to a minimum. In 1993, Sczechowski *et al.* reported a five-fold increase in the

photoefficiency of formate oxidation in concentrated TiO_2 aqueous slurries by using τ_L = 72 ms, $\tau_{D(ark)}$ = 1.45 s cycles, apparently confirming the above expectations. [15] However, the average incident photon flux under such conditions is 21 times smaller than in the continuous photolysis regime relative to which the comparison is based. A subsequent study by Buechler *et al.* also compares quantum efficiencies based on lamp output rather than on average photon flux. [10,11] Stewart and Fox claim a 1.8-fold rate improvement for the photocatalytic oxidation of 1-octanol by decreasing the repetition rate of the applied laser pulses from 10 to 1 Hz, a procedure that effectively amounts to a ten-fold reduction in the average photon flux. [16] Thus, it appears that the alleged performance enhancements induced by discontinuous illumination are actually based on quantum yields (or efficiencies, see below) determined under widely different average photon fluxes. The distinction between the quantum yields ϕ's, i.e., the ratio of photochemical over photon *absorption* rates, reported in some experiments vs. the quantum efficiencies η's, i.e., the number (frequency) of photochemical events over the number (frequency) of *incident* photons, reported in other studies neither invalidates the preceding objection, nor impairs the transferability of periodic illumination effects among different sets of data. [17]

In this chapter, we present the results of a quantitative study on the photocatalytic oxidation of formate in dilute (6 mg/L) suspensions of small ($\langle r \rangle \sim 10$ nm) TiO_2 particles that are fully consistent with the known kinetic behavior of a photochemical reaction occurring in a homogeneous (i.e., lacking kinetically relevant gradients) system under periodic illumination.[18] More specifically, we find that the quantum yields measured under sufficiently high-frequency periodic illumination approach those measured under continuous illumination at the same average absorbed photon flux. Hence, no advantage

accrues from the use of periodic illumination over the continuous regime. Buechler *et al.* have very recently reached a similar conclusion, which is at variance, however, with their previous analysis of these phenomena. [19]

3.3 Experimental Section

Materials

Titanium dioxide (Degussa P25), and formic acid (EM Science) were used as received. Suspensions were prepared by 20 min sonication of deionized water (MilliQ-UV-Plus, 18.2 MΩ·cm resistivity) loaded with 6 mg/L TiO_2, and later adjusted to 0.1 mM in formic acid at pH = 4.2. Solutions were sparged with neat oxygen at a flow rate of 20 mL min^{-1} for 15 min prior to, and at 4 mL min^{-1} during photolysis, while being magnetically stirred.

Photoreactor

The light source was an ozone-free, 1000 W Xenon arc lamp (Oriel). Its output traversed 10 cm of water to remove IR radiation, then a 320 nm high-pass filter, and finally a 340-380 nm band-pass filter. The light beam was subsequently focused onto the flat window of a jacketed, cylindrical fused silica reaction cell (26 mL, 2.5 cm optical path), whose temperature was maintained at 10 °C by means of a refrigerated circulating bath to prevent evaporative losses during prolonged sparging.

Light pulses were generated by means of either a mechanical shutter (Uniblitz VS14, 14 mm aperture, driven by a Uniblitz T132 controller), or an optical chopper (Oriel model

75155 with 2 model 75162 chopper blades offset with respect to each other, driven by a model 75095 chopper controller), located at the focal point of 2 focusing lenses. The shutter was used for slow pulsing and the chopper for fast pulsing, with the crossover at 5 Hz. The pulsed light beam fully illuminated the volume of the reaction cell. For the continuous photolyses, the shutter was left in place in the "open" position, and the light intensity was varied using neutral-density filters (Melles Griot).

Analysis

Sample aliquots (1 mL) were withdrawn at appropriate intervals, filtered through a 0.2 μm polysulfone syringe filter (Gelman), and analyzed for $HCOO^-$ with a Dionex Bio-LC ion chromatograph (Dionex IonPac AS11/AG11 columns) equipped with a conductivity detector. Formate oxidation up to 80% conversions follows zero-order kinetics with respect to [$HCOO^-$].

Determination of the photon absorption rate

Photon absorption rate measurements were performed by chemical actinometry using (E)-α-(2,5-dimethyl-3-furylethylidene)(isopropylidene)succinic anhydride (Aberchrome 540) as actinometer.[20] The photon rate incident on the cell in the absence of neutral-density filters was $I_0 = 7.6$ μEinstein L^{-1} s^{-1}. At the low TiO_2 loads and the short (2.5 cm) optical path used, only a fraction of the incident light is absorbed. To determine the amount of scattered and transmitted vs. absorbed radiation by TiO_2 suspensions, we performed an actinometry in which the cell was filled with the reaction solution, and the cell jacket with the actinometer. The jacket was externally shielded to exclude spurious light. In this

configuration, I_0 photons L^{-1} s^{-1} enter the cell through the front window, of which I_b are scattered backwards, I_a are actually absorbed by TiO_2, and the rest proceeds into the actinometer after being transmitted I_t, scattered forward I_f through the back window, or scattered through the cell side I_s. Therefore, the rate of photon absorption by the actinometer in the jacket I_j is given by: $I_j = I_t + I_f + I_s = I_0 - I_b - I_a$. On the other hand, if T is the transmittance of these solutions measured with the UV spectrophotometer: $T\ I_0 = I_0 - I_b - I_f - I_s - I_a$. Notice that I_f also represents a loss in this case, because only a negligible fraction of the diffuse radiation scattered forward is viewed by the collimated UV detector. Assuming Rayleigh scattering ($\lambda >>$ average particle radius) and integrating over all scattering angles we estimate that in our setup the geometric factor $I_b/(I_b + I_f + I_s) = 0.265$ applies. [21] Furthermore, considering that, on average, the optical path lengths for scattered and transmitted photons inside the cell do not differ significantly, the coupling between absorption and scattering can be neglected. Therefore, from the experimental values of $I_j = 5.0$ μEinsteins L^{-1} s^{-1}, and $T = 0.449$ that apply to 6 mg L^{-1} TiO_2 suspensions in the 2.5 cm length reaction cell, we obtain $I_{a,max} = 2.0$ μEinsteins $L^{-1}s^{-1} = 1.2 \times 10^{18}$ photons L^{-1} s^{-1}. For spherical TiO_2 particles of radius $\langle r \rangle = 10$ nm, [22] and density $\delta = 3.7$ g cm^{-3}, the number density in the suspension is 3.9×10^{14} particles L^{-1}. Therefore, $I_{a,max}$ corresponds to the absorption of about 3000 photons $particle^{-1}$ s^{-1}. In contrast with laser photolysis, which delivers similar photon loads within nanoseconds, i.e., instantaneously in this context, the absorption of 3000 photons $particle^{-1}$ s^{-1} does not imply the simultaneous presence of an equivalent number of carriers, because extensive recombination (as evidenced by the low quantum yields) takes place at comparable rates.

Determination of the quantum yield

The effective photon absorption rate $\langle I_a \rangle$ in a particular pulsed experiment is given by the product of I_a times the fraction of the time the shutter is open [i.e., the duty cycle $\gamma = \tau_L/(\tau_L + \tau_D)$]: $\langle I_a \rangle = \gamma\, I_{a,max}$. For the continuous photolyses, the effective photon absorption rate is given instead by the product of $I_{a,max}$ times the transmittance of the interposed neutral-density filter: $\langle I_a \rangle = T_{filter}\, I_{a,max}$. The quantum yield for the photocatalytic degradation of formate, ϕ_F, was calculated in all cases as the degradation rate divided by the effective photon absorption rate, $\langle I_a \rangle$:

$$\phi_F = -\frac{1}{\langle I_a \rangle} \cdot \frac{d[HCOO^-]}{dt} \qquad (1)$$

3.4 Results

ϕ_F under periodic illumination

We measured ϕ_F's under periodic illumination conditions in which the incident photon rate was kept constant at $I_0 = 7.6$ μEinsteins L^{-1} s^{-1}, while the light times τ_L were varied over several orders of magnitude at fixed duty cycles of $\gamma = 0.05$ and 0.35. These correspond to average photon absorption rates $\langle I_a \rangle = \gamma\, I_{a,max}$ of 0.10 and 0.71 μEinstein L^{-1} s^{-1}, respectively. The results are shown in Figure 3.1, in which error bars represent 95% confidence intervals. The error bars do not take into account the accuracy of the assumptions made. Specifically, the possible systematic errors associated with our

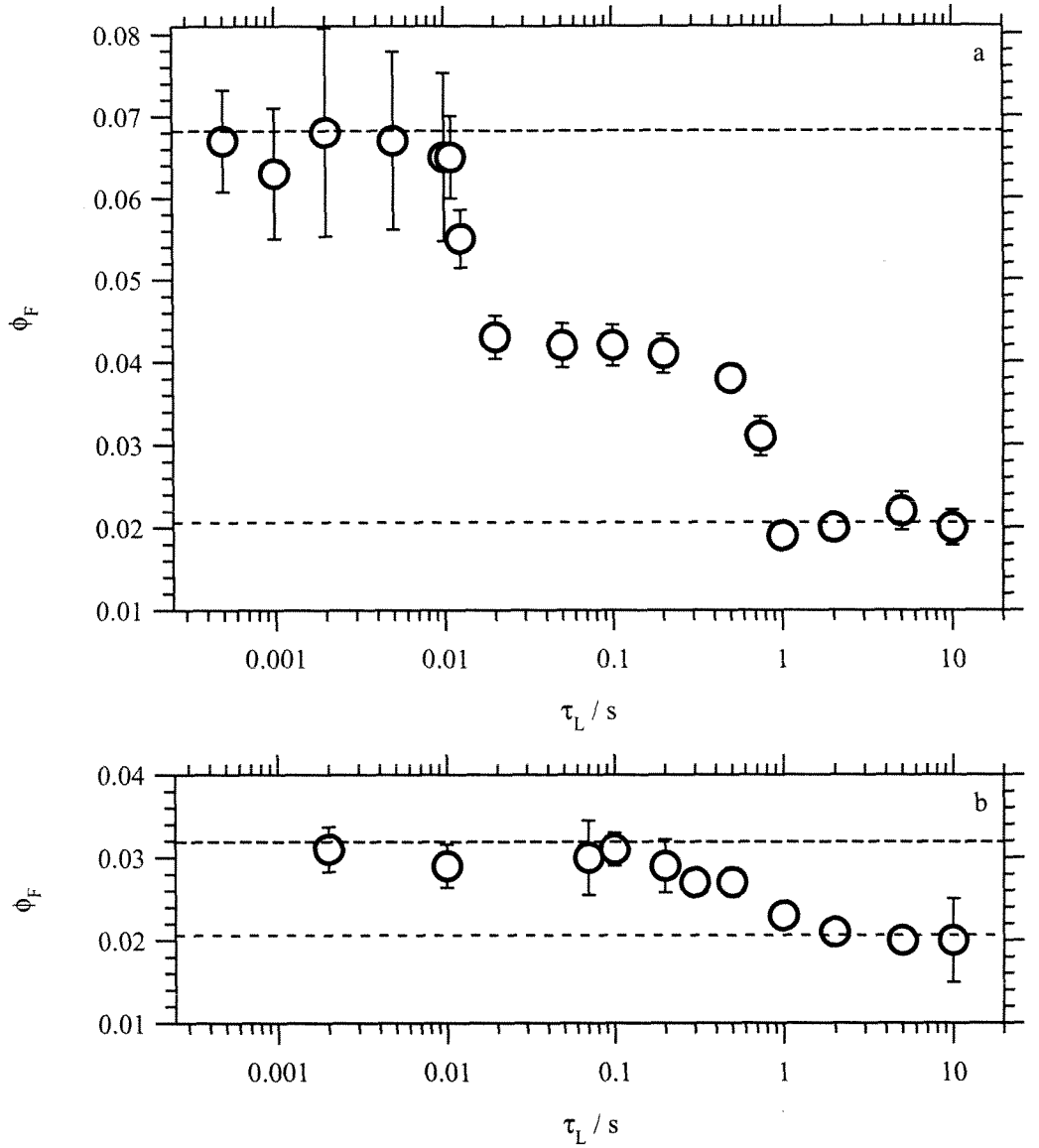

Figure 3.1. Quantum yields for formate photocatalytic oxidation under periodic illumination, at duty cycles γ: (a) 0.05, (b) 0.35. The upper dashed lines in each plot correspond to the quantum yields determined under continuous illumination at equivalent average photon absorption rates $\langle I_a \rangle = \gamma I_{a,max}$. The lower dashed lines in each plot correspond to the quantum yield measured under continuous illumination at $I_{a,max} = 2.0$ μEinsteins L^{-1} s^{-1}.

procedure for estimating light absorption rates (see above) are not included in the reported error bars, a shortcoming that would not affect, however, the relative quantum yield values on which most of the ensuing discussion is based. Quantum yields approach a common, minimum value of $\phi_{F,long\ \tau} = 0.021 \pm 0.003$ for both $\gamma = 0.05$ and 0.35 at $\tau_L \geq 2$ s. At shorter τ_L's, ϕ_F jumps to constant values of 0.042 ($\gamma = 0.05$) and 0.031 ($\gamma = 0.35$), between 500 and 50 ms. For $\gamma = 0.05$, a second jump to $\phi_F = 0.068$ occurs at $\tau_L \leq 15$ ms.

ϕ_F under continuous illumination

As a benchmark for quantum yield improvements over those merely due to a decrease in average photon absorption rate, we performed a series of continuous illumination photolyses with attenuated light beams. The results of these experiments are shown in Figure 3.2. ϕ_F increases monotonically with decreasing photon absorption rate from $\phi_{F,cont} = 0.021$ at $I_a = I_{a,max} = 2.0$ μEinsteins L^{-1} s^{-1} (without attenuation), to $\phi_{F,cont} = 0.074$ for $I_a = 0.089$ μEinstein L^{-1} s^{-1} (95.6% attenuation). The solid line in Figure 3.2 corresponds to a power-law regression $\phi_F = a \langle I_a \rangle^m$ to the data points. The best fit is obtained for $a = 0.031 \pm 0.003$, $m = -0.39 \pm 0.03$.

Comparison of ϕ_F under periodic and continuous illumination

From these results one can evaluate the quantum yields that would be attained under continuous illumination at the average absorbed photon flux prevalent in the pulsed experiments at $\gamma = 0.05$ and 0.35. These limits are indicated as dashed lines in Figure 3.1. Therefore, under present experimental conditions, the quantum yield for periodic illumination is smaller than or equal to the quantum yield for continuous illumination at

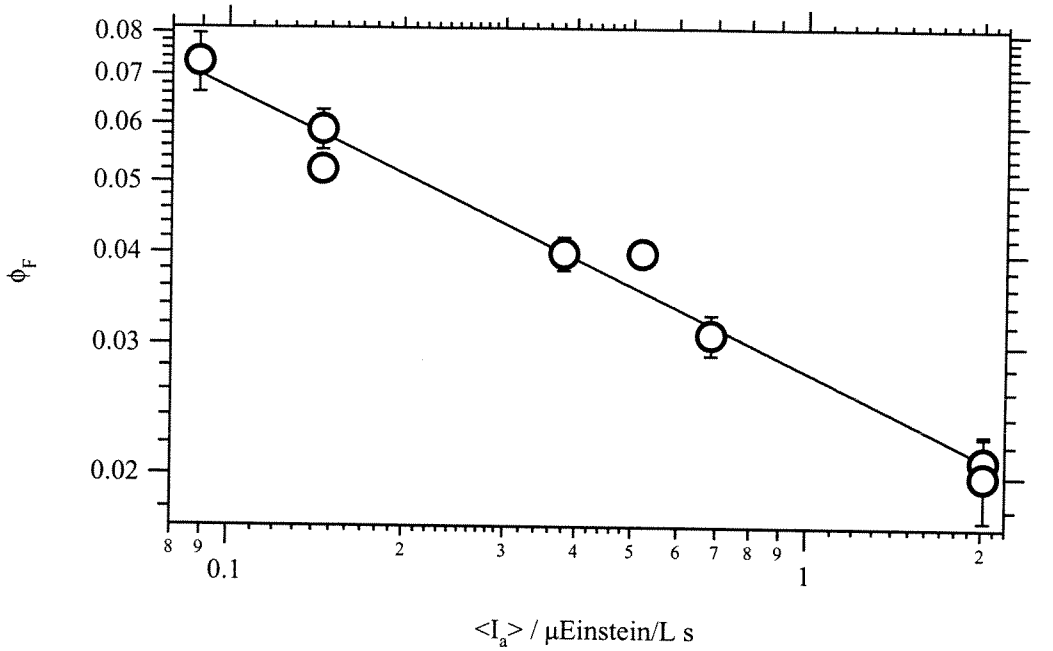

Figure 3.2. Quantum yields for formate photocatalytic oxidation under continuous illumination at $\langle I_a \rangle$. The solid line corresponds to a power-law regression to the data: $\phi_F = (0.031 \pm 0.003) \langle I_a \rangle^{-0.39 \pm 0.03}$ in the range investigated.

the same average photon absorption rate, but larger than or equal to the quantum yield for continuous illumination at the maximum photon absorption rate $I_{a,max}$ = 2.0 μEinsteins L^{-1} s^{-1}. Additional experiments for light times of 5 s and 200 ms performed with duty cycles of γ = 0.15 and 0.25 (see Figure 3.3) confirm this conclusion. The quantum yields for any of the τ_L = 5 s photolyses are the same within the experimental error: $\phi_{F,long\ \tau}$ = 0.022.

3.5 Discussion

Occurrence of inflections

The above results can be rationalized with reference to the following mechanism taking place in a homogeneous system:

$$h\nu \Rightarrow e^- + h^+ \quad (2)$$

$$e^- + O_2 \Rightarrow O_2^{\bullet -} \quad (3)$$

$$H^+ + O_2^{\bullet -} \Leftrightarrow HO_2^{\bullet} \quad (3')$$

$$h^+ + HCOO^- \Rightarrow H^{\bullet} + CO_2 \quad (4)$$

$$H^{\bullet} + O_2 \Rightarrow HO_2^{\bullet} \quad (4')$$

$$e^- + h^+ \Rightarrow \varnothing \quad (5)$$

$$h^+ + \Omega_j \Rightarrow h_t^+ \quad (6)$$

$$h_t^+ + O_2^{\bullet -} \Rightarrow \varnothing + O_2 \quad (7)$$

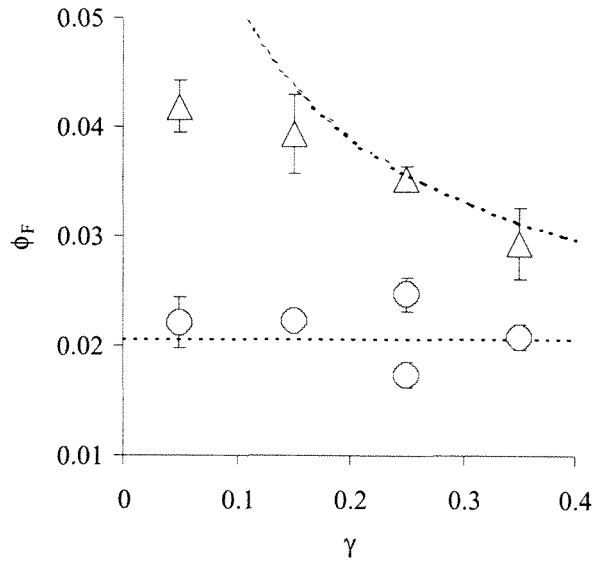

Figure 3.3. Quantum yields for formate photocatalytic oxidation under periodic illumination as a function of the duty cycle γ, with $I_{a,max}$ = 2.0 μEinsteins L^{-1} s^{-1}, and light times τ_L: (○) 5 s, (Δ) 0.2 s. The upper dashed line corresponds to the quantum yields determined under continuous illumination at equivalent average photon absorption rates $\langle I_a \rangle = \gamma \times I_{a,max}$. The lower dashed line corresponds to the quantum yield measured under continuous illumination at $I_{a,max}$.

where e^- and h^+ stand for photogenerated electrons and holes, respectively, and Ω_j for one of the *j* traps available per particle. This mechanism leads to reaction rates R_4 and quantum yields $\phi_F = R_4/I_a$ where $I_a \equiv R_2$: [18]

$$R_4 = \beta \langle I_a \rangle^n, \quad \phi_F = \beta \langle I_a \rangle^{n-1}, \quad 0.5 \leq n \leq 1 \tag{8}$$

where β is a proportionality constant independent of I_a. The condition $0.5 \leq n \leq 1$ follows from the simultaneous occurrence of first- and second-order carrier recombination steps. At sufficiently long τ_L values the system reaches steady state during the illuminated periods, and the overall reaction rate under pulsed illumination is equivalent to that of having the reaction taking place under $I_{a,max}$ for γ of the time, i.e.,

$$R_{4,\text{long}\,\tau} = \beta \gamma I_{a,max}^{\ n} \tag{9}$$

and $\phi_{F,\text{long}\,\tau} = \beta \gamma I_{a,max}^{\ n} / (\gamma I_{a,max}) = \beta I_{a,max}^{\ n-1}$, independent of γ, as observed. On the other hand, at very short τ_L's the system cannot adjust to the modulated photon flux, and effectively behaves as irradiated under the average photon rate $\langle I_a \rangle = \gamma I_{a,max}$:

$$R_{4,\text{short}\,\tau} = \beta (\gamma I_{a,max})^n \tag{10}$$

and $\phi_{F,\text{short}\,\tau} = \beta (\gamma I_{a,max})^n / (\gamma I_{a,max}) = \beta (\gamma I_{a,max})^{n-1}$, i.e., the quantum yield under high-frequency pulsing is identical to that obtained at constant illumination at $\langle I_a \rangle = \gamma I_{a,max}$, in accord with present findings. Since $n < 1$, it follows that $\phi_{F,\text{short}\,\tau} > \phi_{F,\text{long}\,\tau}$.

Determination of charge carrier lifetimes

The kinetic response of homogeneous photochemical systems to periodic light is such that, if first-order reactions (i.e., steps 6 and 7) do not affect the concentration of the reactive intermediate, an analytical solution for ϕ as a function of τ_L and γ can be obtained. This analytical solution, illustrated in Figure 2.5 and also discussed in further detail in Section 6.2, is usually presented as a series of sigmoidal curves on a plot of normalized reaction rate versus normalized light time for different ratios of dark time to light time. The light time is here normalized with respect to the life time of the intermediates. Thus, the life time of the reactive intermediate may be estimated by comparing the position of the transition in literature tabulations of the analytical solution for the appropriate ratio of dark time to light time with the light time where the transition occurs experimentally. [18] We thus infer that carrier lifetimes toward recombination are of the order of 0.1 s for $\gamma = 0.35$ ($\tau_L \sim 5 \times$ lifetime for $\tau_D/\tau_L = 1.9$), and about 6 ms for those associated with the second inflection point in the plot ϕ_F vs. τ_L for $\gamma = 0.05$ ($\tau_L \sim 2 \times$ lifetime for $\tau_D/\tau_L = 19$). Furthermore, the transition from long to short τ_L's occurs at τ_L values that are a weakly increasing function of γ, because second-order recombination decay times and τ_D both decrease with γ.

Occurrence of a second inflection for short duty cycles

The fact that $\phi_{F,short\ \tau}$ is reached at $\tau_L \leq 200$ ms for $\gamma = 0.35$, but requires much shorter light intervals for $\gamma = 0.05$ deserves an explanation. Qualitatively, this finding implies the existence of a much faster decay channel for the charge carriers present under the specific

regime supported by the shorter duty cycles.[9] The presence of a small number *j* of carrier traps Ω per particle may account for this phenomenon. Note that about 63 carriers per particle are generated during a single 20 ms pulse, i.e., just before the onset of the second plateau in Figure 3.1a, followed by τ_D = 37 or 380 ms dark intervals at γ = 0.35 or 0.05, respectively. Traps would be eventually filled upon irradiation in both cases. However, empty traps would be available at the onset of every light period at γ = 0.05, since carriers decay more extensively during the ensuing long dark periods. In contrast, traps would remain permanently occupied over experiments performed at γ = 0.35. Thus, in order to establish a steady-state carrier population for eq. 10 to hold it is ultimately necessary to compete with fast trapping for γ = 0.05. A similar conclusion was recently arrived at in connection with experiments on metastable TiO_2 colloids at much lower I_a values. [9]

Effect of $I_{a,max}$ on the lifetimes

A series of experiments using periodic illumination was performed, with the incident and absorbed photon rates decreased by a factor of about 3 (I_0 = 2.5 μEinstein L^{-1} s^{-1}, $I_{a,max}$ = 0.69 μEinstein L^{-1} s^{-1}). This provides some information on the effect of $I_{a,max}$ on the lifetimes of the charge carriers.

In the previous experiments, with $I_{a,max}$ = 2.0 μEinsteins L^{-1} s^{-1}, the first transition occurs around τ_L = 1 s. Thus, for longer light periods (i.e., for τ_L = 5 s) $\phi_F = \phi_{F,long\ \tau}$, and independent of γ (see Figure 3.3, open circles), while for shorter light periods (i.e., for τ_L = 0.2 s) $\phi_F > \phi_{F,long\ \tau}$ (see Figure 3.3, open triangles). As mentioned before, the transition-τ_L are a (weak) function of γ, as illustrated in Figure 3.1. With $I_{a,max}$ = 2.0 μEinsteins L^{-1}

s^{-1}, the first transition (around τ_L = 1 s) occurs at slightly shorter τ_L for γ = 0.05 than for γ = 0.35: $\phi_{F,1s} = \phi_{F,long\ \tau}$ for γ = 0.05, while for γ = 0.35 $\phi_{F,1s} > \phi_{F,long\ \tau}$.

When $I_{a,max}$ is decreased to 0.69 μEinstein L^{-1} s^{-1}, the same behavior is observed around τ_L = 5 s (see Figure 3.4, open circles). For γ = 0.05 and γ = 0.15, $\phi_{F,5s} = \phi_{F,long\ \tau}$, while for γ = 0.25 and γ = 0.35 clearly $\phi_{F,5s} > \phi_{F,long\ \tau}$, suggesting the transition occurs around τ_L = 5 s. Thus, decreasing the photon absorption rate to one-third results in a longer lifetime of the long-lived charge carrier by a factor of about 5, indicating that at lower photon absorption rates, longer τ_L are needed for the system to reach steady state during the illuminated periods.

Implications

Superoxide steady-state yields and decay times on weakly illuminated (1 μW cm^{-2}) water-TiO_2 interfaces have been recently quantified. [23,24] In contrast with the typically low photooxidation yields generally reported, and at variance with the contention that O_2 reduction, step 3, is rate-controlling, Ishibashi *et al.* measured $\phi_{O_2^-} \sim 0.8$. It was also found that O_2^- decays by a pseudo-first-order process with a half-life of about 70 s, probably via step 7 above. The shorter carrier decay times (~ 0.1 s) we measure are consistent with the 1.7 mW cm^{-2} irradiances [corresponding to illumination rates of 3100 (360 nm) photons $particle^{-1}$ s^{-1}] we use. In other words, carrier lifetimes determining photocatalytic quantum yields are compatible with each other, but are much longer than those (in the nanosecond-millisecond range) previously inferred from kinetic spectroscopy. [2,25,26] A plausible, albeit tentative, interpretation of this observation is that

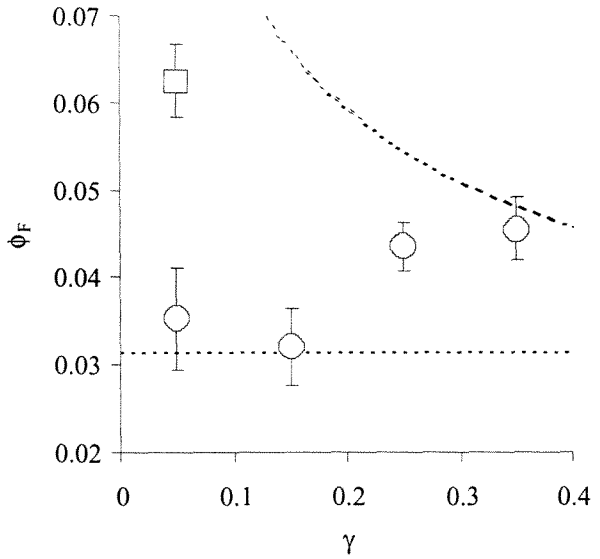

Figure 3.4. Quantum yields for formate photocatalytic oxidation under periodic illumination as a function of the duty cycle γ, with $I_{a,max}$ = 0.69 μEinstein L^{-1} s^{-1}, and light times τ_L: (○) 5 s, (□) 0.6 s. The upper dashed line corresponds to the quantum yields determined under continuous illumination at equivalent average photon absorption rates $\langle I_a \rangle = \gamma \times I_{a,max}$. The lower dashed line corresponds to the quantum yield measured under continuous illumination at $I_{a,max}$.

at least one of the primary carriers produced photochemically in step 2 is rapidly localized and, hence, less prone to recombine, with a minimum loss of chemical potential. Efficient electron trapping as O_2^-, reaction 3, followed by interfacial recombination, reaction 7, would account for the reported large $\phi_{O_2^-}$ values, and for the O_2^- long decay lifetimes. [24] This is not a trivial result, because it implies that the characteristic times of all the chemically relevant processes in semiconductor photocatalysis are longer than a few milliseconds.

Importance of mass transfer

It is instructive to assess the importance of diffusional resistance in the photochemistry of colloidal suspensions. In our system, the Damköhler number, Da, which gives the ratio of kinetic to diffusional rates, is defined as [27]

$$\mathrm{Da} = \frac{R_{4,\max}}{4\pi D\langle r\rangle[\text{reactant}]} \tag{11}$$

where $R_{4,max} = 9.9 \times 10^{-23}$ mol s^{-1} = 60 molecules s^{-1}, is the largest observed formate degradation rate per particle, $D = 1.45 \times 10^{-5}$ cm^2 s^{-1} is the diffusion coefficient of formate in water at 300 K,[28] $[HCOO^-] = 0.1$ mM, and $\langle r\rangle = 10$ nm, resulting in Da = 5×10^{-6}. Similarly, for oxygen, $R_{4,max} = 4.9 \times 10^{-23}$ mol s^{-1}, $D = 2.1 \times 10^{-5}$ cm^2 s^{-1}, and $[O_2]_{aq} = 1.3$ mM at saturation, lead to Da = 1×10^{-7}. Thus, throughout our experiments, even if sonication were not completely effective in breaking up particle aggregates, Da would be much smaller than the onset of diffusional control of chemical reactions (Da ~ 0.01). The fact that TiO_2 suspensions respond to light modulation as homogeneous media under present conditions implies that processes such as reactant adsorption and product

desorption that, besides mass diffusion, could eventually generate concentration gradients, do not contribute to the kinetics. [8]

3.6 Conclusions

We verified that, in the absence of competing intermediates, and at the slow rates typical of most photocatalytic studies, quantum yields under periodic illumination do not exceed those attained by continuous operation at equivalent average photon absorption rates. This conclusion is in accord with the theory of homogeneous photochemical reactions driven by intermittent illumination, and with estimates of the Damköhler number, which provides a measure of diffusional resistance in chemical processes, for nanoparticle suspensions. We found evidence for two distinguishable carriers, and for carrier decay lifetimes that are much longer than previously estimated.

We wish to emphasize that the preceding analysis and conclusions ultimately rest on the fundamental observation that ϕ_F values determined under periodic illumination are strictly bracketed by those calculated from the experimental $\phi_{F,cont}$ vs. I_a dependence, and on the well-established theory of photochemical reactions driven by modulated light, rather than on mechanistic assumptions.

3.7 Implications for reactor design

Optimization and characterization of reactors utilizing periodic illumination

Some photoreactors are designed such that the photocatalyst is illuminated only periodically, usually through the use of rotating components. [13,29] An example of such a reactor is the recently built batch rotating photocatalytic contactor, or RPC. [29] A schematic representation of the RPC is given in Figure 3.5. Glass discs, coated with TiO_2, partially immersed in the solution, are rotated while being illuminated. Upon rotation, a thin film of liquid from the bulk solution is entrained on the disc, and illuminated in the headspace.

Experiments on the degradation of 0.2 mM 3,4-dichlorobut-1-ene, in which the rotation speed of the discs was varied, were performed, and the results are reprinted in Figure 3.6.

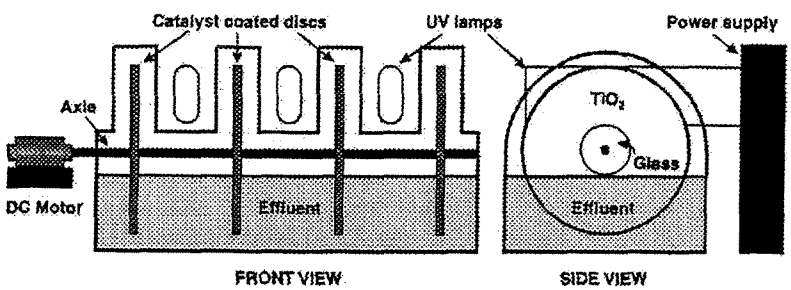

Figure 3.5. Schematic diagram of the rotating photocatalytic contactor (RPC). [29]

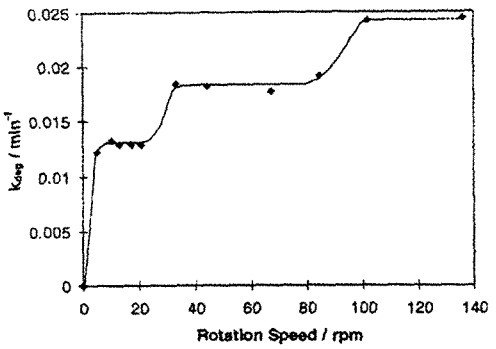

Figure 3.6. Variation in pseudo-first-order degradation rate constant with rotation speed of the degradation of 0.2 mM 3,4-dichlorobut-1-ene in the RPC. [29]

Clearly, the behavior of the rate constant as a function of rotation speed in the RPC is very similar to the behavior of the quantum yield as a function of τ_L in our slurry reactor. The incident light intensities turn out to be comparable: in the RPC it is 5.6 mW cm^{-2}, in our reactor it is 6.1 mW cm^{-2}. From the reactor geometry of the RPC, we can infer that about half the surface of the discs are illuminated at any one time. This allows conversion of rotation speeds into τ_L by τ_L (s) = 30 / rotation speed (rpm).

A first transition is then observed at $\tau_L \sim 1$ s (~ 30 rpm), and a second one at $\tau_L \sim 0.3$ s (~ 100 rpm). The occurrence of the first transition is remarkably close to our experimental results. The second transition was not observed in our work at the higher duty cycle, but the resolution of our data is not high enough to pick up separate transitions that are only a factor of 2 apart.

The likely explanation cited for these two transitions by Hamill *et al.* is a change in mass transfer properties of the system, related to the design of the reactor. [29] Comparison with our data, however, suggests the transitions may be related to lifetimes of intermediates instead.

This example illustrates how controlled experiments under periodic illumination, in a simple system similar to ours, can be useful in the interpretation of results obtained with a complex photoreactor, in which continuous illumination of the photocatalyst is not possible, and many more factors are at play. Our experiments allow us to determine which effects are due to the photocatalyst, and which are due to reactor design, and thus eliminate attempts to change the reactor design to manipulate effects that are fixed by the photocatalyst. Also, the rotation speed – and power of the motor – necessary to obtain a high quantum yield can be calculated in advance.

Another type of reactor that could perhaps benefit from our results, are fluidized-bed photoreactors. Analysis of the motion of photocatalyst granules in a vibrofluidized-bed photoreactor has shown that here too the effect of periodic illumination comes into play, resulting in a higher quantum yield compared to fixed-bed photoreactors. [30]

Use of a pulsing light source

The quantum yield is one factor that can be improved to improve the overall cost-efficiency of photocatalytic treatment processes. In our experiments, the quantum yield was compared between continuous and periodic illumination using the same light source and operating parameters. When the lamp operation is optimized for periodic illumination, other improvements besides quantum yield may be achieved. With arc

lamps for example, pulsed operation allows increased core plasma temperatures without increasing the operating temperature of the electrodes – thus, avoiding overloading of the arc tube and premature lamp failure. [31] This is desirable because the resulting spectral shift to shorter, more energetic wavelengths means a larger fraction of the light is emitted as (absorbable) UV-light, and the increase in excess photon energy E* (with $E^* = hc\lambda^{-1} - E_b$) should improve the quantum yield. [32] For arc stability, however, long pulse widths (0.2 ms vs. 0.05 ms) are desirable. [31] Our results tell us how long the pulse times can be made without impacting photocatalytic efficiency.

3.8 Concluding remarks

One of the objectives of this project was to discover the basis for the improved quantum yields observed with periodic illumination. Based on the experiments described in this chapter, we established that if the experiments are designed well, it is possible to distinguish between the effects of pulsing the light and the effects of reducing the average light intensity. This allowed us to conclude that there is no improvement in quantum yield for the photocatalytic oxidation of formate ion, if the comparison is made correctly, i.e., with respect to the quantum yield obtained under continuous illumination with the same average intensity.

While these experiments do not *per se* exclude that improvements might be obtained for the photocatalytic degradation of other compounds, we deemed it more worthwhile to look into the two transitions observed in the ϕ_F vs. τ_L plots in more detail. To shed light

on the identity of the corresponding intermediates, we will investigate how the transitions depend on the grade of TiO_2, the compound being degraded, and solution factors such as the pH. This will be described in the following chapters of this work.

3.9 References

(1) Bahnemann, D. W.; Cunningham, J.; Fox, M. A.; Pelizzetti, E.; Pichat, P.; Serpone, N. In *Aquatic and Surface Photochemistry*; Helz, G. R., Zepp, R. G., Crosby, D. G., Eds.; Lewis Publishers: Boca Raton, 1994; Chapter 21.

(2) Hoffmann, M. R.; Martin, S. T.; Choi, W.; Bahnemann, D. W. *Chem. Rev.* **1995**, *95*, 69.

(3) *Photocatalytic Purification and Treatment of Water and Air;* Ollis, D. F., Al-Ekabi, H., Eds.; Elsevier Science Publishers: Amsterdam, 1993, and references therein.

(4) Linsebigler, A.; Lu, G.; Yates, J. T., *Chem. Rev.* **1995**, *95*, 735.

(5) (a) Ohko, Y.; Hashimoto, K.; Fujishima, A. *J. Phys. Chem. A* **1997**, *101*, 8057.

(b) Ohko, Y.; Hashimoto, K.; Fujishima, A. *J. Phys. Chem. B* **1998**, *102*, 1724.

(c) Ohko, Y.; Hashimoto, K.; Fujishima, A. *J. Phys. Chem. A* **1998**, *102*, 2699.

(6) Lewis, N. S., *J. Phys. Chem. B* **1998**, *102*, 4843.

(7) Gerischer, H. In *Photocatalytic Purification and Treatment of Water and Air*; Ollis, D. F., Al-Ekabi, H., Eds.; Elsevier: Amsterdam, 1993, 1.

(8) Upadhya, S.; Ollis, D. F. *J. Phys. Chem. B* **1997**, *101*, 2625.

(9) Grela, M. A.; Colussi, A. J., *J. Phys. Chem. B* **1999**, *103*, 2614.

(10) Buechler, K. J.; Nam, C. H.; Zawistowski, T. M.; Noble, R.D.; Koval, C. A. *Ind. Eng. Chem. Res.* **1999**, *38*, 1258.

(11) Buechler, K. J.; Noble, R. D.; Koval, C. A.; Jacoby W. A. *Ind. Eng. Chem. Res.* **1999**, *38*, 892.

(12) Foster, N. S.; Koval, C. A.; Sczechowski, J. G.; Noble, R. D. *Journal of Electroanalytical Chemistry* **1996**, *406*, 213.

(13) Sczechowski, J. G.; Koval, C. A.; Noble, R. D. *Chem. Eng. Sci.* **1995**, *50*, 3163.

(14) Sczechowski, J. G.; Koval, C. A.; Noble, R. D. In *Photocatalytic Purification and Treatment of Water and Air*; by Ollis, D. F., Al-Ekabi, H., Eds.; Elsevier: Amsterdam, 1993, 121.

(15) Sczechowski, J. G.; Koval, C. A.; Noble, R. D. *J. Photochem. Photobiol. A: Chem.* **1993**, *74*, 273.

(16) Stewart, G.; Fox, M. A. *Res. Chem. Intermed.* **1995**, *21*, 933.

(17) Serpone, N., *J. Photochem. Photobiol. A: Chem.* **1997**, *104*, 1.

(18) Burnett, G. M.; Melville, H. W., in *Technique of Organic Chemistry, Investigation of Rates and Mechanisms of Reactions,* Friess, S. L.; Lewis, E. S.; Weissberger, A., Eds.; 2nd Ed., Interscience Publishers: New York, 1963, Vol. VIII - Part II, chapter 20.

(19) Buechler, K. J.; Zawistowski, T. M.; Noble, R. D.; Koval, C. A., *Ind. Eng. Chem. Res.*, **2001**, *40*, 1097.

(20) Heller, H. G.; Langan, J. R. *J. Chem. Soc. Perkin Trans. II* **1981**, *2*, 341.

(21) van de Hulst, H. C., *Light Scattering by Small Particles,* Dover, New York, 1981, p. 65.

(22) Product Information: Degussa Corporation. Product: Titanium dioxide P25 (4/96).

(23) Ishibashi, K.; Fujishima A.; Watanabe T.; Hashimoto K. *J. Phys. Chem. B* **2000**, *104*, 4934.

(24) (a) Ishibashi, K.; Nosaka, Y.; Hashimoto, K.; Fujishima, A. *J. Phys. Chem. B* **1998**, *102*, 2117. (b) Hirakawa, T.; Nakaoka, Y.; Nishino, J.; Nosaka, Y., *J. Phys. Chem. B* **1999**, *103*, 4399. (c) Nosaka, Y.; Yamashita, Y.; Fukuyama, H., *J. Phys. Chem. B* **1997**, *101*, 5822.

(25) Serpone, N.; Lawless, D.; Khairutdinov, R.; Pelizzetti, E. *J. Phys. Chem.* **1995**, *99*, 16655.

(26) (a) Martin, S. T.; Herrmann, H.; Choi, W.; Hoffmann, M. R. *J. Chem. Soc. Faraday Trans.* **1994**, *90*, 3315. (b) Martin, S. T.; Herrmann, H.; Hoffmann, M. R. *J. Chem. Soc. Faraday Trans.* **1994**, *90*, 3323.

(27) Carberry, J. J. *Chemical and Catalytic Reaction Engineering*, McGraw-Hill: New York, 1976, chapter 5.

(28) *CRC Handbook of Chemistry and Physics*; 79th Ed., CRC Press, 1998-99, p5-95.

(29) Hamill, N. A.; Weatherley, L. R.; Hardacre, C. *Appl. Catal. B-Environ.* **2001**, *30*, 49.

(30) Vorontsov, A. V.; Savinov, E. N.; Smirniotis, P. G. *Chem. Eng. Sci.* **2000**, *55*, 5089.

(31) Gu, H.; Muzeroll, M. E.; Chamberlain, J. C.; Maya, J. *Plasma Sources Sci. Technol.* **2001**, *10*, 1.

(32) Grela, M. A.; Colussi, A. J. *J. Phys. Chem. B* **1999**, *103*, 2614.

3.10 Appendices

Experimental set-up

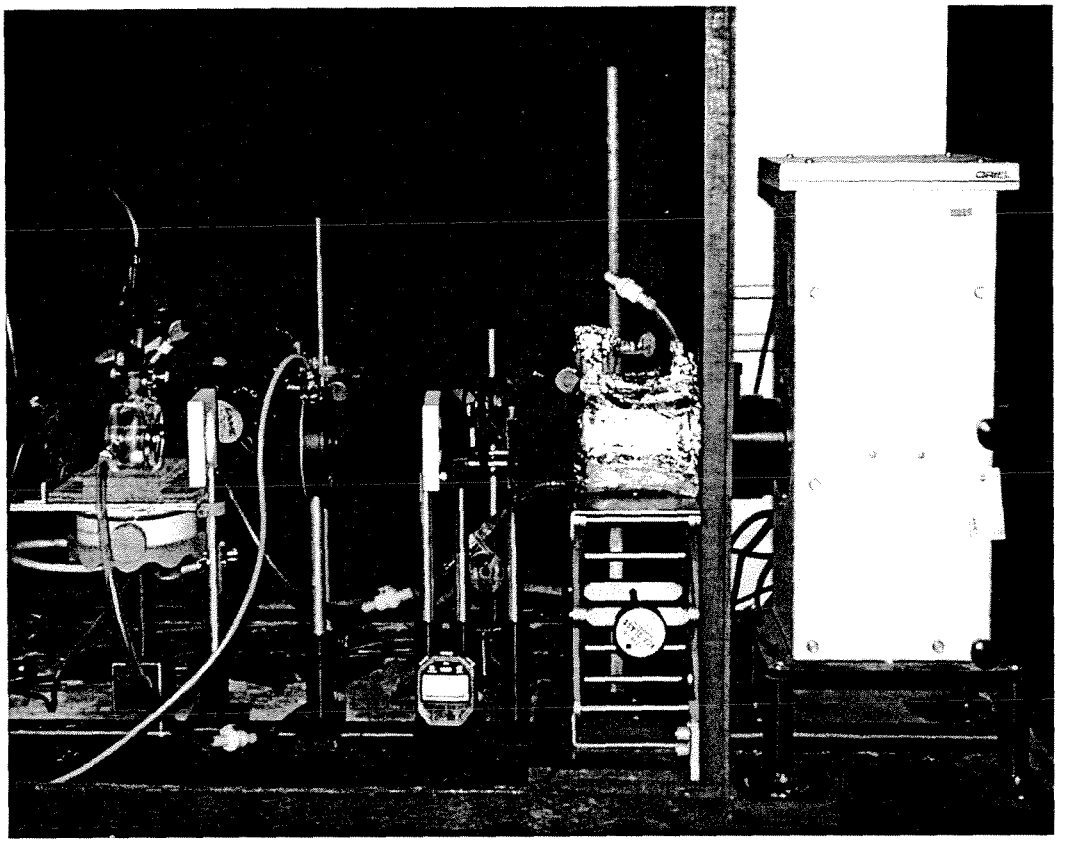

Figure 3.7. A picture of the experimental set-up.

Determination of the geometric factor

For a particle small compared to the wavelength of the incident light (Rayleigh scattering), the light intensity scattered in any given direction, I_{scat}, can be related to the incident light intensity, I_0, by

$$I_{scat} = \frac{(1 + \cos^2\theta)\, k^4\, |\alpha|^2}{2\, r^2} I_0, \qquad (12)$$

with θ the scattering angle,

k the wave number defined by $k = 2\pi/\lambda$, where λ is the wavelength of the light,

α the polarizability, and

r the distance. [21]

In the jacketed reaction cell used, with depth $d = 2.5$ cm and radius $R = 1.82$ cm, for a TiO_2 particle in the middle of the cell, $\theta_{window} = \pi/2 + \text{atan}(1.25/1.82) = 2.17$ rad (= 124.5°).

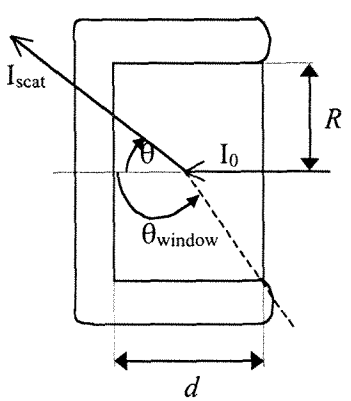

Integrated over all scattering angles, the fraction of the light scattered

$$I_{scat} \div \int_0^{2\pi} d\Phi \int_0^{\pi} (1 + \cos^2\theta) \sin\theta \, d\theta = -2\pi \int_0^{\pi} (1 + \cos^2\theta) \, d\cos\theta = 16\pi/3. \qquad (13)$$

Similarly, by integrating over all scattering angles greater that θ_{window}, the backscattered intensity I_b (i.e., the intensity of the light leaving the reaction cell through the front window) can be calculated. For the ratio of I_b to I_{scat} we then obtain

$$\frac{I_b}{I_{scat}} = \frac{2\pi (\cos\theta_{window} + 1/3 \cos^3\theta_{window} + 4/3)}{16\pi/3} . \qquad (14)$$

Thus, for $\theta_{window} = 2.17$ rad, the geometric factor $I_b/I_{scat} = 0.265$.

Data table

γ	τ_L (s)	$I_{a,max}$ μEinstein/Ls	degradation (μM/min)	95% limits (μM/min)	ϕ_F
0.05	0.0005	2.02	0.413	0.038	0.067
0.05	0.001	2.02	0.389	0.050	0.063
0.05	0.002	2.02	0.422	0.079	0.068
0.05	0.005	2.02	0.414	0.067	0.067
0.05	0.01	2.02	0.401	0.064	0.065
0.05	0.011	2.02	0.403	0.031	0.065
0.05	0.0125	2.02	0.339	0.022	0.055
0.05	0.02	2.02	0.265	0.016	0.043
0.05	0.05	2.02	0.260	0.017	0.042
0.05	0.1	2.02	0.260	0.016	0.042
0.05	0.2	2.02	0.254	0.015	0.041
0.05	0.5	2.02	0.237	0.006	0.038
0.05	0.75	2.02	0.192	0.015	0.031
0.05	1	2.02	0.119	0.008	0.019
0.05	2	2.02	0.122	0.006	0.020
0.05	5	2.02	0.134	0.014	0.022
0.05	10	2.02	0.123	0.013	0.020
0.35	0.002	2.02	1.34	0.12	0.031
0.35	0.01	2.02	1.27	0.11	0.029
0.35	0.07	2.02	1.29	0.19	0.030
0.35	0.1	2.02	1.34	0.09	0.031
0.35	0.2	2.02	1.25	0.14	0.029
0.35	0.3	2.02	1.17	0.05	0.027
0.35	0.5	2.02	1.19	0.08	0.027
0.35	1	2.02	0.993	0.047	0.023
0.35	2	2.02	0.887	0.039	0.021
0.35	5	2.02	0.884	0.048	0.020
0.35	10	2.02	0.881	0.219	0.020

Table 3.1. Degradation rates and quantum yields for the photocatalytic oxidation of 100 μM formate ion, with ϕ_F = degradation / $\gamma \times I_{a,max} \times 60$.

γ	τ_L (s)	$I_{a,max}$ μEinstein/Ls	degradation (μM/min)	95% limits (μM/min)	ϕ_F
0.15	5	2.02	0.407	0.012	0.022
0.25	5	2.02	0.527	0.034	0.017
0.25	5	2.02	0.750	0.047	0.025
0.15	0.2	2.02	0.715	0.066	0.039
0.25	0.2	2.02	1.07	0.04	0.035
1		2.02	2.57	0.22	0.021
1		2.02	2.46	0.32	0.020
1		0.685	1.29	0.08	0.031
1		0.520	1.29	0.02	0.040
1		0.381	0.926	0.049	0.040
1		0.145	0.462	0.015	0.052
1		0.145	0.528	0.033	0.059
1		0.0886	0.398	0.036	0.073
0.05	5	0.685	0.073	0.012	0.035
0.15	5	0.685	0.198	0.027	0.032
0.25	5	0.685	0.448	0.028	0.044
0.35	5	0.685	0.654	0.052	0.045
0.05	0.59	0.685	0.129	0.009	0.063
0.05	0.4	1.01	0.162	0.010	0.053

Table 3.1 (continued). Degradation rates and quantum yields for the photocatalytic oxidation of 100 μM formate ion, with ϕ_F = degradation / $\gamma \times I_{a,max} \times 60$.

Chapter 4

Determination of characteristic timescales for photocatalysis

on different titania nanoparticles

using the technique of periodic illumination

4.1 Abstract

In this work, the technique of periodic illumination, which is an established method for analyzing photokinetics in homogeneous solutions, is applied to determine the characteristic timescales of photocatalytic formate oxidation in dilute aqueous suspensions of titania nanoparticles at pH 4.2. Two characteristic times of τ_1 = 400 ms and τ_2 = 6 ms are found, which appear to be indifferent to the type of TiO_2 nanoparticles used.

4.2 Introduction

In recent years, the photocatalytic oxidation of aqueous and gaseous compounds on titania nanoparticles has been studied extensively, as a candidate technology for the destruction of environmental pollutants. The mechanistic steps are fairly well understood. [1-4] In short, upon illumination of titania with ultra-violet light (with $\lambda < 380$ nm), electrons in the valence band of titania become excited and are promoted to the conduction band, leaving a hole behind. The electrons and holes migrate to the surface of the particle, where they can participate in oxidation- reduction reactions. In most cases, oxygen is used as the electron acceptor. The holes are utilized to oxidize the (organic) pollutant of interest directly, or to produce hydroxyl radicals from the oxidation of adsorbed water or hydroxide ions. Hydroxyl radicals ($OH^{\bullet}$) are very reactive and readily attack organic molecules, eventually degrading them to CO_2 and water. Electrons and holes can also recombine, reducing the efficiency of the photocatalytic oxidation process.

The characteristic times of these steps involving electrons and holes have been determined, and range between a few femtoseconds for electron-hole pair generation, to a few milliseconds for interfacial electron transfer. [4-6] In recent studies, Nosaka *et al.* and Ishibashi *et al.* applied chemiluminescent probes to investigate some of the intermediates formed in or after these initial steps. The intermediate identified as superoxide ($O_2^{\bullet-}$) was found to have a lifetime of several tens of seconds. [7-9]

The technique of periodic illumination also provides a means to estimate lifetimes of intermediates, and is non-specific. [10-11] It has the advantage that it can be used in the actual environment of interest, with the electron and hole acceptors of interest, without adding probe molecules that might interfere with the reduction-oxidation reactions of interest. This technique has been successfully applied to study photokinetics in homogeneous solution, mainly photopolymerizations, [10-14] and its applicability for the determination of lifetimes in photocatalysis was originally demonstrated in our previous work. In our current work, we compare the characteristic times for aqueous phase photocatalysis on two different titania nanoparticles, to ascertain the relative effects of the physical properties of the titania on photoreactivity.

4.3 Particle characterization

The titania nanoparticles used were Degussa P25 and Millennium Inorganic Chemicals Tiona PC105. P25 is commonly used in photocatalytic studies, and has a high photoactivity. [1-4] It is produced by flame hydrolysis of $TiCl_4$, at temperatures in excess of 1200 °C. PC105, on the other hand, is synthesized by sol-gel techniques at much lower

temperatures. First, the titania nanoparticles were characterized. The results are summarized in Table 4.1.

	P25	PC105
phase composition	anatase + rutile	anatase
BET ($m^2 g^{-1}$)	52 ± 3	75 ± 3
particle size (nm)	300	100, 500

Table 4.1. Particle characterization of P25 and PC105 TiO_2.

The phase composition was determined by X-ray diffractometry (XRD), using an inel CPS120 detector with a Co K_α radiation source. As illustrated in Figure 4.1, P25 shows diffraction peaks characteristic of both anatase and rutile, while for PC105 only anatase could be detected. Five-point BET surface area measurements were performed on a Micromeritics Gemini 2360. For P25 we obtained a surface area of 52 ± 3 $m^2 g^{-1}$, for PC105 75 ± 3 $m^2 g^{-1}$. Assuming a spherical particle with density of 3.7 g cm^{-3}, this corresponds to particle diameters of 31 nm and 22 nm respectively. Particle sizes were also determined in sonicated suspensions, similar to those used in the photocatalysis experiments (see below), by laser light scattering off the particles, with a Malvern Instruments Zetasizer. For P25, we found an average particle size by number of 300 nm, but also detected a few large (> 1 μm) particles. This implies that the applied sonication is not completely effective in breaking up aggregates, since the observed particle dimensions are larger than the reported crystallite size (≈ 20 nm). Comparison with the particle size based on the BET suggests that the crystallites are only loosely aggregated,

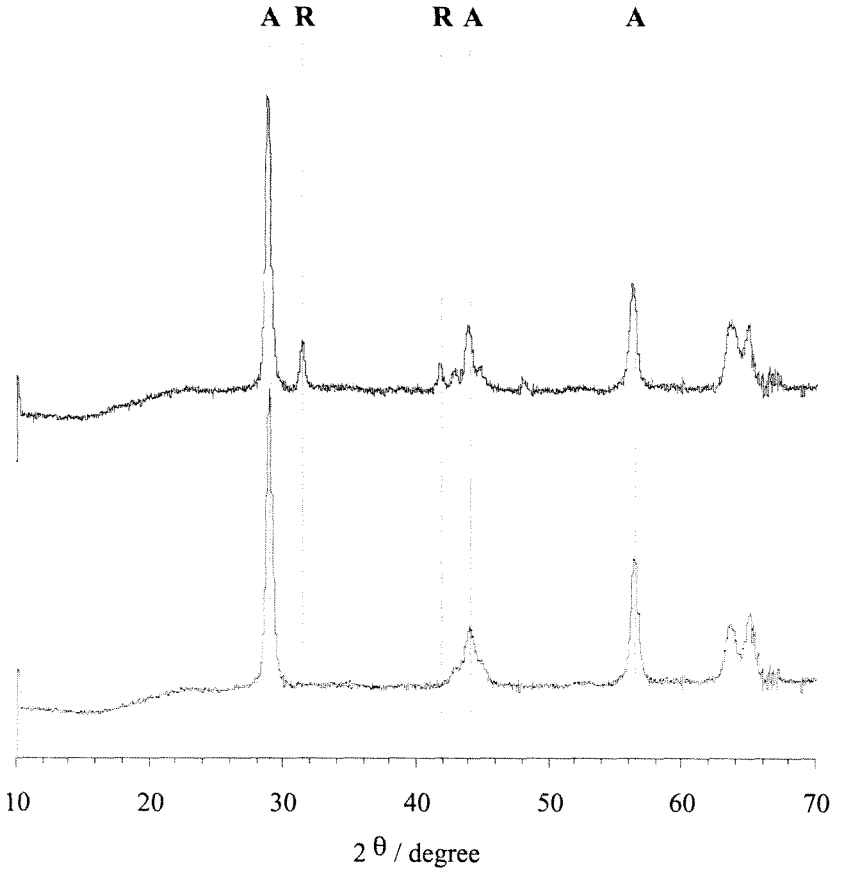

Figure 4.1. XRD patterns of P25 (top) and PC105 (bottom), normalized with respect to the highest intensity. A number of characteristic peaks for anatase (**A**) and rutile (**R**) are marked.

and that most of the particle surface is still available for reaction. For PC105 the particle size exhibited a bimodal distribution, with a majority sized around 100 nm and a minority around 500 nm. In summary, from this ensemble of experiments, we conclude that P25 and PC105 are quite different, in phase composition, surface area and particle size.

4.4 Periodic illumination

Before we commence with describing the photocatalysis experiments, we will give a brief background on the technique of periodic illumination. [10-11] In the application of this technique the light is chopped into pulses of light period τ_L, separated by dark periods τ_D. The fraction of the time that the light is on, $\gamma = \tau_L/(\tau_L + \tau_D)$, is called the duty cycle. If τ_L and τ_D are long compared to the lifetime of the active intermediates formed, periodic illumination is equivalent to illuminating the system continuously for a fraction γ of the total time, and the reaction rate (per unit of total time elapsed), $R_{p,long\ \tau} = \gamma \times R_s(I_{a,max})$, with R_s the rate under steady (continuous) illumination, and $I_{a,max}$ the corresponding absorbed light intensity. On the other hand, using periodic illumination with short τ_L and τ_D is equivalent to cutting down the light intensity to the fraction γ, and the reaction rate becomes $R_{p,short\ \tau} = R_s(\gamma \times I_{a,max})$. Providing that R_s does not vary linearly with the absorbed light intensity, $\gamma \times R_s(I_{a,max})$ and $R_s(\gamma \times I_{a,max})$ are different. The transition between these two values is an indication of the average lifetime of the intermediates.

In this manner, by applying periodic illumination with a constant γ and a range of τ_L (and τ_D) spanning several orders of magnitude, the lifetimes of the intermediates important in aqueous phase photocatalysis were determined for the two grades of titania nanoparticles.

4.5 Experimental details

The particles were used as received for the photocatalysis experiments. We worked with a (dilute) slurry as opposed to a fixed photocatalyst to avoid problems of reproducibility often observed with films and coatings, and to ensure that the degradation reaction is not mass transfer limited. [15] The reaction conditions (and the photoreactor) were designed to minimize the gradient in light intensity across the reaction volume. This reduces effects of TiO_2 particles undergoing variations in illumination when being mixed, obscuring the effects we want to observe with the technique of periodic illumination. Slurries were prepared by adding a low load of either 6 mg P25 or 18 mg PC105 to 1 L deionized water.

Photon absorption rates

In our previous study, we used 6 mg L^{-1} of P25 TiO_2, which was found to provide an appropriate compromise between a fast degradation rate and a low fraction of the incident photons absorbed. Photon absorption rates were determined by chemical actinometry with Aberchrome 540. [17] The photon rate incident on the cell during illumination, I_0, was 7.6 μEinstein L^{-1} s^{-1}. The values of the experimental parameters necessary to estimate the fraction of the incident light absorbed by the photocatalyst particles are listed in Table

4.2. For details on this procedure we refer to Chapter 3. For P25, we found that the photon absorption rate in the absence of any neutral-density filters is $I_{a,max}$ = 2.0 μEinstein L^{-1} s^{-1}, corresponding to 27% of the incident photon rate.

	P25	PC105
load (mg L^{-1})	6	18
T	0.449	0.429
I_0 (μEinstein L^{-1} s^{-1})	7.6	7.6
I_j (μEinstein L^{-1} s^{-1})	5.0	4.7
$I_{a,max}$ (μEinstein L^{-1} s^{-1})	2.0	2.4

Table 4.2. Experimental design parameters for the photocatalysis experiments on P25 and PC105 TiO_2.

Matching of $I_{a,max}$

At the end of Chapter 3, we determined that (at least one of) the characteristic times depend(s) on $I_{a,max}$, so it is important to obtain the same the photon absorption rate with PC105. Because particle size affects the absorption vs. scattering and transmission behavior of the suspensions (and PC105 and P25 have different particle sizes), the particle load of PC105 needed to be adjusted. As a starting point for determining the load of PC105 required to match $I_{a,max}$ = 2.0 μEinstein L^{-1} s^{-1}, we determined the load of PC105 required to match T, the transmittance of the suspension, which is easily measured in a spectrophotometer. This occurs with a load of 18 mg L^{-1} PC105. With this load $I_{a,max}$ = 2.4 μEinstein L^{-1} s^{-1}, corresponding to 32% absorption of the incident photon rate. The

$I_{a,max}$ with PC105 and with P25 differ by 20%, which is about the magnitude of the accuracy of the chemical actinometry technique, so no more efforts were undertaken to improve the match.

Methodology

The slurries were sonicated for 20 min, and then adjusted to 0.1 mM formic acid (EM Science), resulting in a pH of 4.2. The volume used in each photocatalysis experiment was 26 mL. The suspensions were sparged with oxygen at a flow rate of 20 mL min^{-1} for 15 min before, and at 4 mL min^{-1} during photocatalysis, while being stirred with a magnetic stirring bar.

Photoreactor

The light source was an ozone-free, 1000 W Xenon arc lamp (Oriel model 6271). Its output traversed an IR filter (10 cm of water), then a 320 nm high-pass filter, and finally a 340-380 nm band-pass filter. The light beam was subsequently focused onto the flat window of a jacketed, cylindrical, fused silica reaction cell, with a volume of 26 mL, and an optical path of 2.5 cm. Its temperature was maintained at 10 °C by means of a refrigerated circulating bath. The light beam fully illuminated the volume of the reaction cell. Light pulses were generated by means of either a mechanical shutter (Uniblitz VS14, 14 mm aperture, driven by a Uniblitz T132 controller), or an optical chopper (Oriel model 75155 with 2 model 75162 chopper blades offset with respect to each other, driven by a model 75095 chopper controller), located at the focal point of 2 focusing lenses. The shutter was used for generating long τ_L and the chopper for short τ_L, with the crossover at

10 ms. The entrance aperture of the chopper was adjusted to give the same $I_0 = 7.6$ μEinstein L^{-1} s^{-1} as measured with the shutter in place.

Dark conditions

The photon rate incident on the cell in the dark, i.e., with the shutter "closed," was determined to be more than three orders of magnitude smaller than with the shutter "open," so the effective photon absorption rate, $\langle I_a \rangle$, in an experiment using periodic illumination was calculated by $\langle I_a \rangle = \gamma \times I_{a,max}$.

Analysis

Formate was chosen as the target compound. Its degradation was measured by withdrawing sample aliquots (1 mL) at appropriate intervals, filtering them through a 0.2 μm polysulfone syringe filter (Gelman), and analyzing them for $HCOO^-$ with a Dionex Bio-LC ion chromatograph (Dionex IonPac AS11/AG11 columns) equipped with a conductivity detector, using a 3 mM NaOH eluent (1 mL min^{-1}). Formate oxidation up to 80% conversion was found to follow zero-order kinetics with respect to $[HCOO^-]$, so the degradation rate was calculated by a least-square linear regression to the data. A typical conversion was ~ 40%, as illustrated in Figure 4.2.

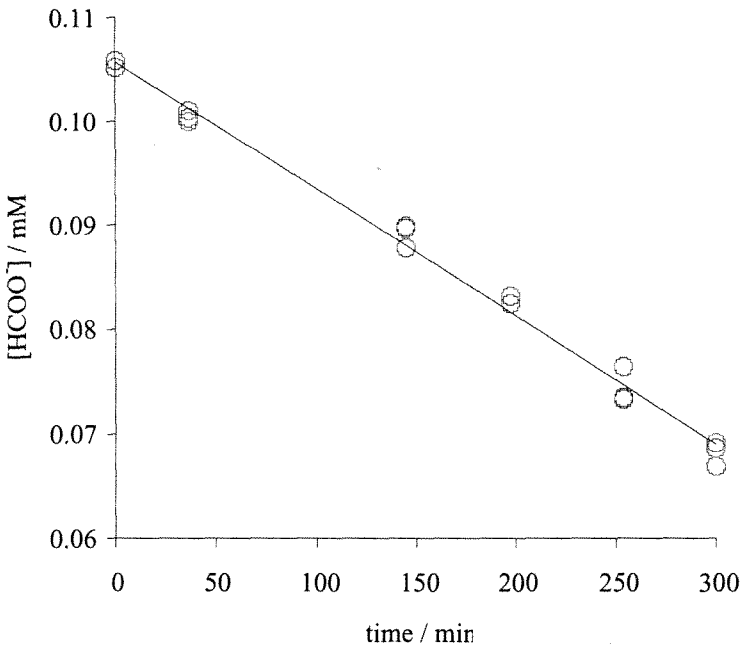

Figure 4.2. Formate concentration as a function of time during photocatalytic oxidation (with $I_{a,max}$ = 2.0 μEinstein L^{-1} s^{-1}, τ_L = 2 s, γ = 0.05, load = 6 mg L^{-1} P25). The solid line is a least-square linear regression to the data, whose slope gives the degradation rate.

4.6 Results and discussion

Photocatalytic formate oxidation under steady illumination

Before starting the experiments with periodic illumination, we determined the degradation rates for the limiting cases, i.e., under steady illumination with $I_{a,max}$ and under steady illumination with $\langle I_a \rangle = \gamma \times I_{a,max}$, with $\gamma = 0.05$. To obtain steady illumination with $I_{a,max}$, we operated with the shutter "open." To obtain steady illumination with $\langle I_a \rangle$, we would need to interpose a neutral-density filter with $T_{filter} = 0.05$, where T_{filter} is the transmittance of the filter. The filter that came closest had $T_{filter} = 0.043$ (Melles Griot), so the degradation rate expected with $T_{filter} = 0.05$ was determined by interpolation. It has been found by several researchers that the photocatalytic reaction rate depends on the photon absorption rate, I_a, according to $R_s = \beta \times I_a^n$, with β a proportionality constant independent of I_a,[1-4,17,18] so this relationship was used for the interpolation. The results of these experiments and calculations are tabulated in Table 4.3.

	P25	PC105
$R_s(I_{a,max})$ (nM s^{-1})	42	49
$R_s(0.05 \times I_{a,max})$ (nM s^{-1})	6.9	7.2
n	0.61	0.64
β	28.9	27.8

Table 4.3. Experimental parameters obtained under steady illumination, for the photocatalytic oxidation of formate on P25 and PC105 TiO_2.

The degradation rate increases with increasing photon absorption rates, from 6.6 nM s^{-1} at I_a = 0.089 μEinstein L^{-1} s^{-1} (T_{filter} = 0.043), to 42 nM s^{-1} for $I_a = I_{a,max}$ = 2.0 μEinstein L^{-1} s^{-1} with P25 and from 6.6 nM s^{-1} at I_a = 0.11 μEinstein L^{-1} s^{-1} (T_{filter} = 0.043), to 49 nM s^{-1} for $I_a = I_{a,max}$ = 2.4 μEinstein L^{-1} s^{-1} with PC105. A least-square power-law regression results in n = 0.61 for P25, and n = 0.64 for PC105.

The n are between 1 (expected for loss of electrons and holes mainly by first order reactions, e.g., by interfacial electron or hole transfer) and 0.5 (expected for mainly second order loss, e.g., by electron-hole pair recombination), and similar on the two particles, implying that interfacial transfer and recombination are in competition with each other to roughly the same extent on both types of particles. Note that if n were 1, then the technique of periodic illumination would not be applicable.

The quantum yields at $I_{a,max}$ are 0.02 on both P25 and PC105, indicating that they are equally efficient in the utilization of photons. If expressed per m^2 of surface area or per mg of photocatalyst on the other hand, P25 turns out to be more efficient than PC105 for the oxidation of formate.

Photocatalytic formate oxidation under periodic illumination

In the application of the technique of periodic illumination, we employed a fixed duty cycle γ = 0.05 (i.e., $\tau_D = 19 \times \tau_L$), and measured the formate degradation rate for a range of τ_L spanning several orders of magnitude. The incident light intensity was kept constant at I_0 = 7.6 μEinstein L^{-1} s^{-1}, so the effective absorbed light intensity $\langle I_a \rangle = \gamma \times I_{a,max}$ in

these experiments was $0.05 \times 2.0 = 0.10$ μEinstein L^{-1} s^{-1} for P25 and $0.05 \times 2.4 = 0.12$ μEinstein L^{-1} s^{-1} for PC105. The results are shown in Figure 4.3.

Comparison of the degradation rates obtained under periodic illumination with those under steady illumination shows that they indeed converge to the limiting cases: $R_{p,short\ \tau} = R_s(0.05 \times I_{a,max})$ and $R_{p,long\ \tau} = 0.05 \times R_s(I_{a,max})$. This assures us that the time-window of our experiments was sufficiently wide. Short τ corresponds to $\tau_L \leq 10$ ms, while long τ corresponds to $\tau_L \geq 2$s. In this time-window, two transitions are observed, which are less than two orders of magnitude apart, and are very similar for PC105 and for P25. One is centered around $\tau_L = 800$ ms (P25) or 1 s (PC105), and one around $\tau_L = 12$ ms.

Determination of charge carrier lifetimes

To relate these τ_L to lifetimes of intermediates, we need a reaction mechanism and the corresponding rate constants. Since at this point we do not have enough information to obtain these values, we will draw on previous literature on the application of the technique of periodic illumination in homogeneous photopolymerization. [10-14] It should be pointed out that in these cases only one transition is observed, and typically $R_s = \beta \times I_a^{0.5}$. With photocatalysis on the other hand, two reactions – reduction and oxidation – involving different intermediates occur on the photocatalyst particles, and two transitions are observed. Also $n = 0.5$ is often not strictly obeyed. Nevertheless, we infer that for $\gamma = 0.05$, the ratio of the τ_L at the transition to the average lifetime of the intermediate is ~ 2. [11] This results in lifetimes on the order of 400-500 ms and 6 ms for the two intermediates observed in this work.

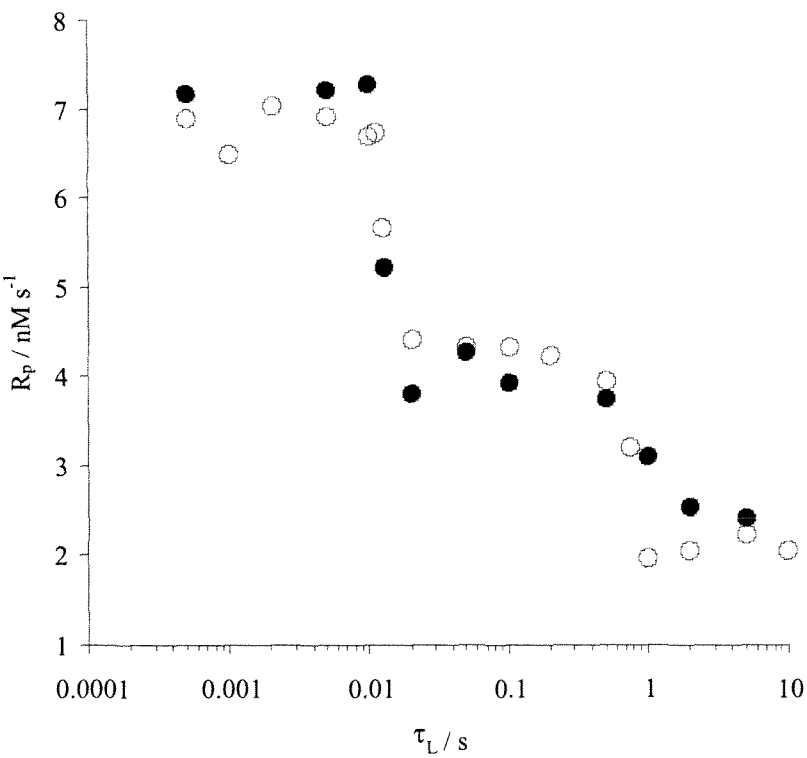

Figure 4.3. Formate photocatalytic oxidation rates under periodic illumination with γ = 0.05 on P25 (○) and PC105 (●).

4.7 Concluding remarks

Though the production method and corresponding particle characteristics have been found to be important factors for the quantum yield, and the lifetimes of electrons and holes, [5,6] in this study it turned out that when the photon absorption rates are matched, the quantum yields for photocatalytic formate oxidation are identical for the two grades of TiO_2 particles employed. The physical characteristics of the different titania nanoparticles used (i.e., phase composition, surface area and particle size) were also found to, at first sight, have little effect on the characteristic times of aqueous phase photocatalysis. Two distinct characteristic times are observed, in agreement with the occurrence of reduction and oxidation reactions on the photocatalyst particles. Corresponding lifetimes of intermediates on the order of 400 ms and 6 ms are calculated.

In the following chapter, we will further investigate the nature of the observed intermediates by assessing the effects of the compound being degraded, and of solution factors such as pH and oxygen concentration.

4.8 References

(1) *Photocatalytic Purification and Treatment of Water and Air;* Ollis, D. F., Al-Ekabi, H., Eds.; Elsevier Science Publishers: Amsterdam, 1993, and references therein.

(2) Linsebigler, A.; Lu, G.; Yates, J. T., *Chem. Rev.* **1995**, *95*, 735.

(3) Mills, A.; Le Hunte, S. *J. Photochem. Photobiol. A: Chem.* **1997**, *108*, 1.

(4) Hoffmann, M. R.; Martin, S. T.; Choi, W.; Bahnemann, D. W. *Chem. Rev.* **1995**, *95*, 69.

(5) Martin, S. T.; Herrmann, H.; Choi, W.; Hoffmann, M. R. *J. Chem. Soc. Faraday Trans.* **1994**, *90*, 3315.

(6) Martin, S. T.; Herrmann, H.; Hoffmann, M. R. *J. Chem. Soc. Faraday Trans.* **1994**, *90*, 3323.

(7) Nosaka, Y.; Yamashita, Y.; Fukuyama, H. *J. Phys. Chem. B* **1997**, *101*, 5822.

(8) Ishibashi, K.; Nosaka, Y.; Hashimoto, K.; Fujishima, A. *J. Phys. Chem. B* **1998**, *102*, 2117.

(9) Ishibashi, K.; Fujishima A.; Watanabe T.; Hashimoto K. *J. Phys. Chem. B* **2000**, *104*, 4934.

(10) Burnett, G. M.; Melville, H. W., in *Technique of Organic Chemistry, Investigation of Rates and Mechanisms of Reactions,* Friess, S. L.; Lewis, E. S.; Weissberger, A., Eds.; 2nd Ed., Interscience Publishers: New York, 1963, Vol. VIII - Part II, chapter 20.

(11) Noyes, W. A., Jr.; Leighton, P. A., in *The Photochemistry of Gases*, Reinhold Publishing Corp., 1941, chapter IV.

(12) Haden, W. L.; Rice, O. K. *J. Chem. Phys.* **1942**, *10*, 445.

(13) Burnett, G. M.; Melville, H. W. *Nature* **1945**, *156*, 661.

(14) Bartlett, B. D.; Swain, C. G. *J. Am. Chem. Soc.* **1945**, *67*, 2273 and **1946**, *68*, 2381.

(15) Turchi, C. S.; Ollis, D. F. *J. Phys. Chem.* **1998**, *92*, 6852.

(16) Heller, H. G.; Langan, J. R. *J. Chem. Soc. Perkin Trans. II* **1981**, *2*, 341.

(17) Ohko, Y.; Ikeda, K.; Rao, T. N.; Hashimoto, K.; Fujishima, A. *Zeitschrift fur Physikalische Chemie* **1999**, *213*, 33.

(18) Mills, A.; Wang, J. *Zeitschrift fur Physikalische Chemie* **1999**, *213*, 49.

4.9 Appendices

Data table

γ	τ_L (s)	$I_{a,max}$ μEinstein/Ls	degradation (μM/min)	95% limits (μM/min)	ϕ_F
0.05	0.0005	2.42	0.431	0.074	0.059
0.05	0.005	2.42	0.433	0.052	0.060
0.05	0.01	2.42	0.436	0.120	0.060
0.05	0.013	2.42	0.313	0.014	0.043
0.05	0.02	2.42	0.228	0.029	0.031
0.05	0.05	2.42	0.256	0.019	0.035
0.05	0.1	2.42	0.235	0.027	0.032
0.05	0.5	2.42	0.224	0.044	0.031
0.05	1	2.42	0.186	0.009	0.026
0.05	2	2.42	0.152	0.025	0.021
0.05	5	2.42	0.145	0.024	0.020
1		2.42	2.933	0.132	0.020
1		0.106	0.395	0.041	0.062

Table 4.4. Degradation rates and quantum yields for the photocatalytic oxidation of 100 μM formate ion on PC105, with ϕ_F = degradation / $\gamma \times I_{a,max} \times 60$. For the results on P25, see Table 3.1.

Chapter 5

Effects of solution factors on the lifetimes

of oxidizing and reducing intermediates

during photocatalysis in aqueous TiO_2 suspensions

5.1 Introduction

Several techniques have been used to determine the lifetimes of charge carriers and/or intermediates in TiO_2 photocatalysis in the past decade. [1-9] In our laboratory for example, Martin *et al.* used time-resolved microwave conductivity on TiO_2 pastes, detecting transient signals from electrons over several milliseconds. [1] Szczepankiewicz *et al.* analyzed dry TiO_2 surfaces using diffuse reflectance infrared Fourier transform spectroscopy, and found evidence that electrons can persist for days in traps under vacuum or dry oxygen, but only a few minutes in the presence of humid oxygen. [2]

As a result, a wide range of lifetimes are now available, depending on the specific conditions of the experiments. Extending these results to conditions prevalent in remediation systems can be problematic. Knowledge of these parameters in aqueous phase under actual experimental conditions would be useful, and might provide insights into the low quantum efficiency often observed in aqueous phase photocatalysis.

In previous chapters, we reported on the use of the technique of periodic illumination to determine lifetimes of intermediates involved in photocatalysis. This approach has the advantage it can be applied in the environment relevant to photocatalytic remediation, both in aqueous and in gas phase. In this chapter, we explore the nature of the intermediates involved by applying the technique of periodic illumination to the photocatalytic bleaching of methyl orange in aqueous TiO_2 suspensions, under various reaction conditions.

5.2 The technique of periodic illumination

The technique of periodic illumination was devised by Chapman and Briers in 1928 to determine the lifetimes of highly reactive intermediates, and in some cases individual absolute rate constants for the reactions in which they participate. [10] It has been used successfully for a number of homogeneous photochemical reactions. [10-14] Application of this technique involves light modulation into pulses of any selected frequency, usually through the use of a slotted wheel rotating between the light source and the cell. As a general rule, periodic illumination will affect reaction rates and quantum yields if the reaction rate under steady illumination, R_s, is not (linearly) proportional to the photon absorption rate I_a.

Many kinetic studies in the field of photocatalysis have focused on the dependence of the degradation rate versus light intensity. [15-19] At sufficiently low photon fluxes, photochemical reaction rates are proportional to the light intensity: $R_s \propto I_a$. At higher photon fluxes on the other hand, the reaction rate becomes proportional to the square root of light intensity: $R_s \propto I_a^{0.5}$. The light intensity at which this transition occurs depends on the catalyst material, but is typically above 1 sun equivalent ($7 \cdot 10^{-5}$ Einsteins m^{-2} s^{-1}). [20] For an immobilized catalyst, at even higher photon fluxes, dependent on the configuration and flow, the mass transfer limit can be encountered, in which case the reaction rate becomes independent of I_a. [17,20] In summary, for photocatalysis, three regimes can be distinguished – low, intermediate and high photon absorption rate – in which the rate R_s varies as I_a^n, with $n = 1$, $n \sim 0.5$, and $n = 0$, respectively. Thus, if

experiments are performed in the intermediate light intensity regime, periodic illumination will have kinetic consequences.

Let the light period be τ_L and the dark period τ_D, then the fraction of the time that the light is on, $\gamma = \tau_L/(\tau_L + \tau_D)$, is called the duty cycle. If the time between light periods is long compared to the lifetime of the active intermediates formed, the measured reaction rate with intermittent light with slow sector speed, $R_{p,long\ \tau}$, is merely the time average of the rate under steady illumination, $R_s = \beta \cdot I_{a,max}^{n}$, and the zero rate for the dark periods: $R_{p,long\ \tau} = \beta \cdot \gamma \cdot I_{a,max}^{n}$, with β a proportionality constant independent of I_a. For fast sector speeds, where the time between flashes is short compared to the lifetimes of intermediates, the effective photon absorption rate $\langle I_a \rangle = \gamma \cdot I_{a,max}$, and the measured rate becomes $R_{p,short\ \tau} = \beta \cdot (\gamma \cdot I_{a,max})^{n}$. The ratio of the rate with intermittent illumination to that under steady illumination changes from $R_{p,long\ \tau}/R_s = \gamma$, at slow sector speeds, to $R_{p,short\ \tau}/R_s = \gamma^{n}$ at fast sector speeds. When n is not unity, γ and γ^{n} are different. The transition between these two values occurs when the period of time between light flashes is of the order of magnitude of the lifetime of the rate-controlling intermediate. [10-14]

In this manner, the lifetimes of the intermediates important in aqueous phase photocatalysis on TiO_2 can be determined.

5.3 Experimental

Materials

Titanium dioxide (Degussa P25) was used as received. Suspensions were prepared by sonication of 1 L of deionized water loaded with 6.24 mg P25 for 20 min, of which 25 mL were dispensed in the reaction cell, together with 1 mL of a 52 μM methyl orange (J.T. Baker) stock solution, resulting in a TiO_2 load of 6.0 mg L^{-1} and a methyl orange concentration of 2 μM. The resulting pH of these suspensions was 6.0. For the preparation of suspensions with a different pH (2.5, 8.0, and 11.4), a few drops of HCl (J.T. Baker, 36.5-38%) or NaOH (EM Science, 50%) were added to an aliquot of the methyl orange stock solution. Suspensions were sparged with oxygen at a flow rate of 20 mL min^{-1} for 15 min prior to, and at 4 mL min^{-1} during photocatalysis (unless otherwise noted), while being stirred with a magnetic stirring bar.

Photoreactor

The light source was an ozone-free, 1000 W Xenon arc lamp (Oriel). Its output traversed an IR filter (10 cm of water), then a 320 nm high-pass filter, and finally a 340-380 nm band-pass filter. The light beam was subsequently directed onto the flat window of a jacketed, cylindrical fused silica reaction cell (26 mL, 2.5 cm optical path), whose temperature was maintained at 12 °C by means of a refrigerated circulating bath. The light beam fully illuminated the volume of the reaction cell. Light pulses were generated by means of either a mechanical shutter (Uniblitz VS14, 14 mm aperture, driven by a

Uniblitz T132 controller), or an optical chopper (Oriel model 75155 with 2 model 75162 chopper blades offset with respect to each other, driven by a model 75095 chopper controller), located at the focal point of 2 focusing lenses. The shutter was used for slow pulsing and the chopper for fast pulsing, with the crossover at 5 Hz. The entrance aperture of the chopper was adjusted to obtain the same incident photon rate as with the shutter.

Analysis

Methyl orange bleaching was measured by withdrawing sample aliquots (0.5 mL) at appropriate intervals, filtering them through a 0.2 μm polysulfone syringe filter (Gelman), allowing them to equilibrate to room temperature, and analyzing them with a Hewlett Packard 8452A diode array spectrophotometer. Concentrations were determined based on the net absorption at the peak wavelength, i.e., at 464 nm above the pK_a of 3.46, [21] and at 508 nm below, with a calibration curve for each experiment. The absorption was corrected by subtracting the average background signal over the range of 600 to 650 nm. Methyl orange (MO) bleaching was found to follow first-order kinetics, so the degradation rate was calculated by a least-square regression of ln[MO] vs. time. A typical extend of methyl orange degradation at the end of an experiment was ~ 25%.

Light intensities

Light intensity measurements were performed by chemical actinometry using (E)-α-(2,5-dimethyl-3-furylethylidene)(isopropylidene) succinic anhydride (Aberchrome 540) as actinometer. [22] The incident photon rate, I_0, was 7.6 μEinstein L^{-1} s^{-1}. The procedure used

to estimate the fraction of the incident light absorbed by the photocatalyst particles has been described in detail in Chapter 3. We find that 27% of the light is absorbed by the TiO_2 particles, so $I_{a,max} = 2.0$ μEinstein L^{-1} s^{-1}. The photon rate incident on the cell in the dark, i.e., with the shutter "closed," was determined to be more than three orders of magnitude smaller than the incident photon rate with the shutter "open," so the effective photon absorption rate $\langle I_a \rangle$ in a particular experiment using intermittent light is indeed given by $\langle I_a \rangle = \gamma \cdot I_{a,max}$. While investigating the methyl orange bleaching rate under steady illumination, the shutter was left "open," and the photon absorption rate was varied by interposing neutral density filters (Melles Griot).

5.4 Results

Methyl orange absorption

Methyl orange, $(CH_3)_2NC_6H_4N{=}NC_6H_4SO_3^-$, is an azo dye. At a pH above the pK_a of 3.46, it has an absorption maximum at 464 nm (orange), while the protonated form has an absorption peak centered around 508 nm (red). [21]

Methyl orange can undergo both photooxidation and photoreduction. [23-25] In our experiments, no peak growth was observed in the 200-800 nm range while the absorption peak of methyl orange was bleached, so the degradation products do not absorb UV or visible light. It is known that the reduction product of methyl orange, a hydrazine derivative, absorbs light at 247 nm. [25] Since no growth is observed at this wavelength, we can conclude methyl orange is bleached mainly by oxidation in our experiments.

Methyl orange bleaching

In a series of preliminary experiments, we looked at methyl orange bleaching under steady illumination ($I_{a,max}$ = 2.0 μEinstein L^{-1} s^{-1}), with and without TiO_2 photocatalyst, at the pHs we will use throughout this work. The measured bleaching rates in the presence of TiO_2, R_s, are tabulated in Table 5.1.

pH	R_s	*n*
	nM/min	
2.5	53	0.53
6.0	46	0.62
8.0	20	
11.4	85	0.69

Table 5.1. Parameters from methyl orange photocatalytic bleaching as a function of pH.

Figure 5.1 shows that no methyl orange bleaching occurred in the absence of TiO_2 at pH 6.0 and 11.4. At pH 2.5 on the other hand, methyl orange is susceptible to photodegradation, with a degradation rate of 6.9 nM/min, which is 13% of the degradation rate of 53 nM/min observed in the presence of TiO_2 under $I_{a,max}$ = 2.0 μEinstein L^{-1} s^{-1}. Since this is a minor contribution – whose dependence on I_a has not been examined, but is expected to remain minor – and since the goal of this work is not to precisely quantify rates, we will neglect direct photolysis, and treat the bleaching rates in the presence of TiO_2 as photocatalytic bleaching rates.

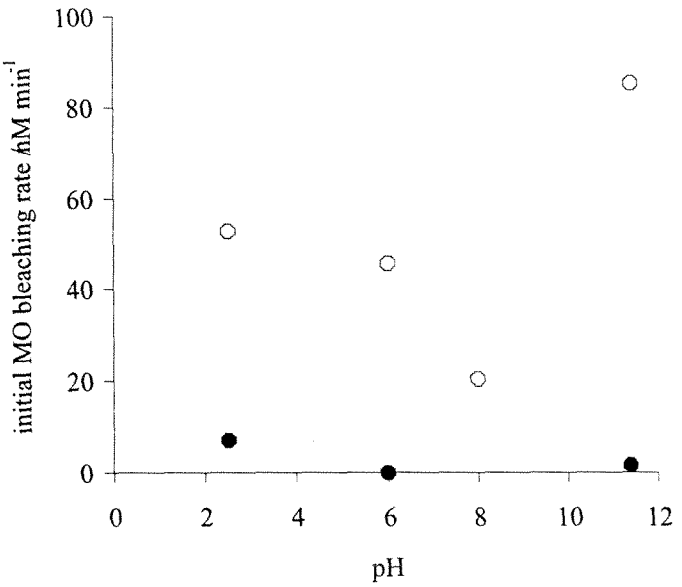

Figure 5.1. Effect of the presence of TiO_2 and of the pH on the methyl orange (MO) bleaching rate under steady illumination. Solid symbols: ●, no TiO_2 present; open symbols: ○, 6 mg L^{-1} P25.

$[MO]_{t=0}$ = 2 μM, temperature = 12 °C, I_a = 2.0 μEinstein L^{-1} s^{-1}, oxygen saturated.

The observed degradation rates result in quantum yields of $4.4 \cdot 10^{-4}$, $3.8 \cdot 10^{-4}$, $1.7 \cdot 10^{-4}$ and $7.0 \cdot 10^{-4}$, at pH 2.5, 6.0, 8.0, and 11.4 respectively. This agrees well with previous literature reports ($\eta = 5 \cdot 10^{-5}$ - 10^{-3}), considering the differences in experimental conditions. [23-25]

Methyl orange photocatalytic bleaching under steady illumination

We examined the effect of the photon absorption rate on the observed bleaching rate at the different pH values under steady illumination, for I_a ranging between 0.089 and 2.0 μEinstein L^{-1} s^{-1}. At high and low pH the bleaching rates are faster than those measured at near-neutral pH over the range of light intensities investigated. As can be seen in Figure 5.2, pH not only influences the methyl orange bleaching rate, but also the dependence of the bleaching rate on the light intensity. The exponents in the power-law regressions, *n*, are also tabulated in Table 5.1.

Since the exponents *n* in all cases lie between 1 and 0.5, we can conclude that in this setup photocatalytic methyl orange degradation is not photon-limited nor limited by mass transfer in the range of light intensities investigated. Hence, the technique of periodic illumination might provide information on the kinetics of the rate-controlling intermediates in photocatalytic methyl orange bleaching.

Methyl orange photocatalytic bleaching under periodic illumination

A series of experiments using periodic illumination with τ_L spanning 4 orders of magnitude was performed on the suspensions at pH 6.0. $I_{a,max}$ = 2.0 μEinstein L^{-1} s^{-1} was

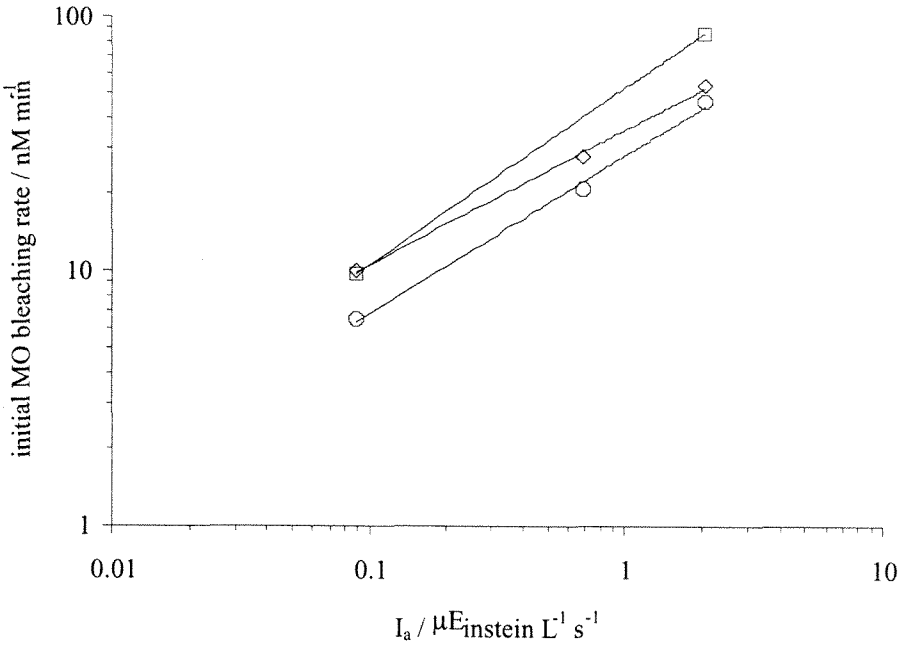

Figure 5.2. Methyl orange (MO) photocatalytic bleaching rate under steady illumination, at pH 6.0 (○), pH 11.4 (□), and pH 2.5 (◇).

The solid lines correspond to power-law regressions to the data.

$[MO]_{t=0}$ = 2 μM, load = 6 mg L^{-1} P25, temperature = 12 °C, oxygen saturated.

used, with duty cycles $\gamma = 0.05$ and 0.35, so the $\langle I_a \rangle = \gamma \cdot I_{a,max}$ obtained (0.10 and 0.71 μEinstein L^{-1} s^{-1}, respectively) are within the range of light intensities investigated in Figure 5.2.

The bleaching rate R_p is normalized relative to $R_s \cdot \gamma^n$, which corresponds to the bleaching rate under steady illumination with $\langle I_a \rangle$. The results are shown in Figure 5.3. As expected in the application of the technique of periodic illumination, the degradation rates under periodic illumination, R_p, are constrained by the degradation rates observed under steady illumination: $R_s \cdot \gamma^n \geq R_p \geq R_s \cdot \gamma$ or $1 \geq R_p/(R_s \cdot \gamma^n) \geq \gamma^{1-n}$.

For $\gamma = 0.05$, two sharp transitions are observed; one around $\tau_L = 300$ ms (τ_1) and one around $\tau_L = 25$ ms (τ_2). This corresponds to $\tau_D = 5.7$ s and 475 ms, respectively. For $\gamma = 0.35$ there appears to be only one, broader transition, centered around $\tau_L = 100$ ms or $\tau_D = 186$ ms. It should be noted that there might be two transitions for the larger duty cycle as well, but the resolution of our data does not permit us to resolve them.

This behavior is qualitatively the same as the one reported in Chapter 3 for the photocatalytic oxidation of formate ion (at pH 4.2) under the same reaction conditions. This finding indicates that the observed behavior is a general feature of photocatalytic oxidation on TiO_2 suspensions, considering that formate and methyl orange have different reactivities and degradation pathways. In fact, methyl orange is degraded about two orders of magnitude slower than formate. However, formate degradation at pH 4.2 has a τ_1 that occurs at longer τ_L (~ 800 ms) and a τ_2 at shorter τ_L (~ 12 ms) compared to methyl orange degradation at pH 6.0.

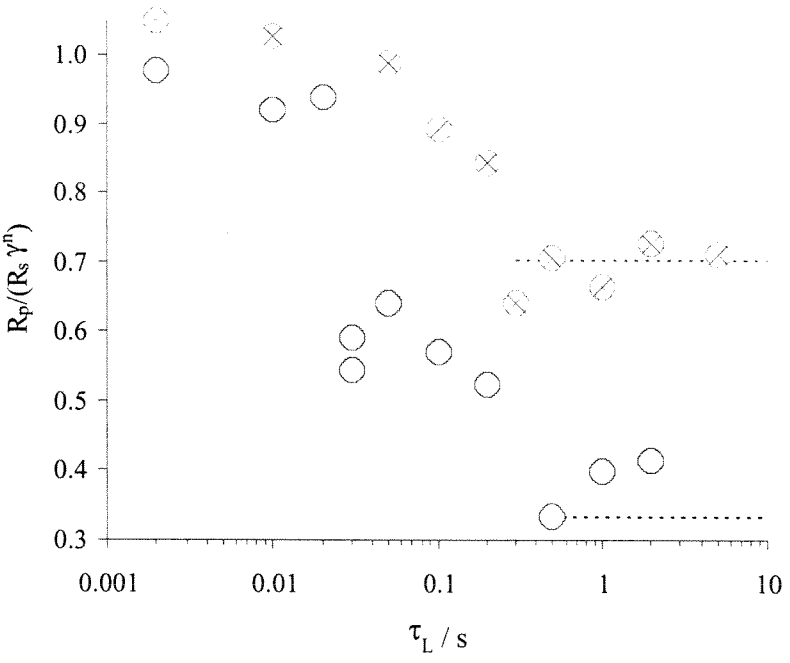

Figure 5.3. Methyl orange (MO) photocatalytic degradation under periodic illumination with $\gamma = 0.05$ and $\langle I_a \rangle = 0.10$ μEinstein L^{-1} s^{-1} (O); and with $\gamma = 0.35$ and $\langle I_a \rangle = 0.71$ μEinstein L^{-1} s^{-1} (⊗). The dashed lines correspond to γ^{1-n} for $\gamma = 0.05$ (lower) and $\gamma = 0.35$ (upper).

$[MO]_{t=0} = 2$ μM, load = 6 mg L^{-1} P25, temperature = 12 °C, oxygen saturated, pH 6.0, $I_{a,max} = 2.0$ μEinstein L^{-1} s^{-1}.

Influence of pH

In order to determine whether or not the shifts of transition times are a function of pH, we performed two series of periodic illumination experiments with $\gamma = 0.05$, on suspensions at pH 2.5 and 11.4. The results are shown in Figure 5.4. Similar to the $\gamma = 0.05$ experiments at pH 6.0, two transitions are observed at both pH values, but the width of the τ_L-window needed to capture them is significantly different. At pH 11.4, the two transitions are captured in a 10 ms to 10 s τ_L-window, while at pH 2.5, τ_2 is shifted to shorter τ_L by two orders of magnitude, resulting in an elongated constant-R_p region between the transitions.

When the transition times are plotted against pH, as seen in Figure 5.5, the strong correlation between transition-τ_L and pH becomes evident. In this figure, the width of the transition is represented by the height of the rectangular symbols used, and the position of the transition was calculated as the middle of the rectangle, i.e., by the geometric mean of the τ_L before and after the transition. The apparent crossover of τ_1 and τ_2 was confirmed by a (limited) set of experiments at pH 8.0. The exponential regressions shown have slopes of -0.50 and 0.72, and result in a crossover at pH 8.2. The data previously obtained for photocatalytic formate degradation at pH 4.2 has also been added to Figure 5.5, to illustrate that it follows the correlation established with photocatalytic methyl orange bleaching very well.

These results suggest that pH is a major factor influencing the positions of the transitions, and hence the lifetimes of the intermediates involved in photocatalysis.

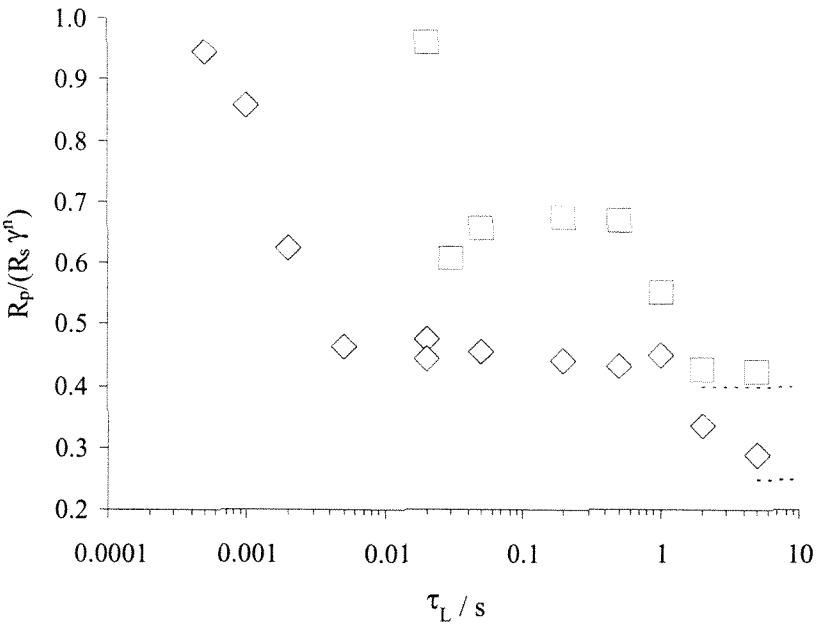

Figure 5.4. Methyl orange (MO) photocatalytic degradation under periodic illumination with $\gamma = 0.05$, at pH 11.4 (□), and at pH 2.5 (◇). The dashed lines correspond to γ^{1-n}. For values of *n* see Table 5.1.

$[MO]_{t=0} = 2\ \mu M$, load = 6 mg L^{-1} P25, temperature = 12 °C, oxygen saturated, $I_{a,max} = 2.0$ μEinstein $L^{-1}\ s^{-1}$.

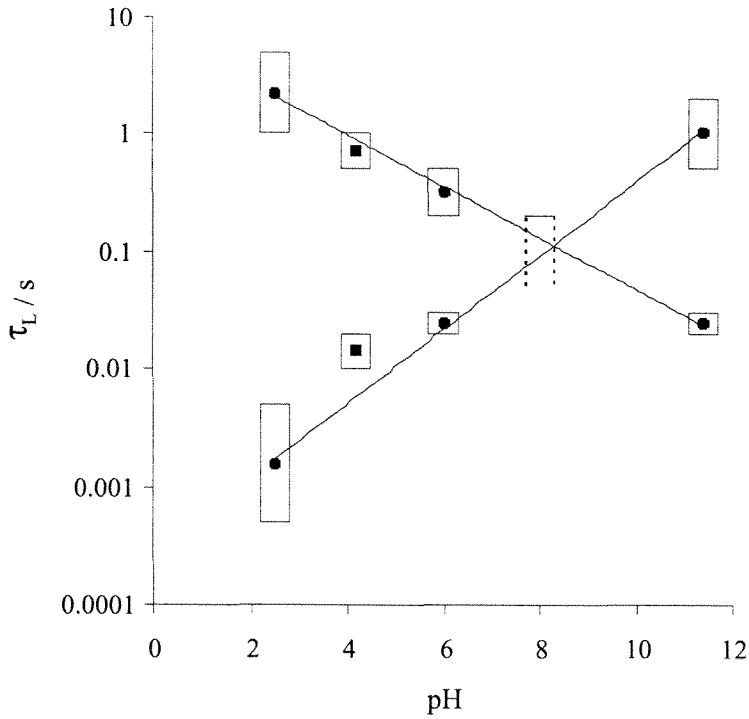

Figure 5.5. Position of the transitions as a function of pH for methyl orange (●) and formate (■). The height of the symbols represents the width of the transition. The solid lines are exponential regressions through the data points for methyl orange at pH 2.5, 6.0 and 11.4. All data for methyl orange (MO) was obtained with $[MO]_{t=0}$ = 2 μM, load = 6 mg L^{-1} P25, temperature = 12 °C, $I_{a,max}$ = 2.0 μEinstein L^{-1} s^{-1}, and oxygen saturated. The data for formate was obtained with $[HCOO^-]_{t=0}$ = 100 μM, load = 6 mg L^{-1} P25, temperature = 10 °C, $I_{a,max}$ = 2.0 μEinstein L^{-1} s^{-1}, and oxygen saturated.

Influence of oxygen concentration

Since interfacial charge transfer to oxygen is believed to be the rate-determining step in the photocatalytic oxidation of organic molecules by oxygen, [26] and superoxide has been identified as an important intermediate, [7] we also looked at the effect of the oxygen concentration. A series of periodic illumination experiments with $I_{a,max}$ = 2.0 μEinstein L^{-1} s^{-1} and γ = 0.05 was carried out on suspensions at pH 6.0 with a lower oxygen concentration, obtained by sparging the suspensions for 5 minutes with argon, at a flow rate of 10 mL min^{-1}, before illumination (no sparging was applied during the experiment). It should be pointed out that methyl orange under these conditions is still bleached mainly by oxidation. The results are shown in Figure 5.6. Comparison with Figure 5.3 shows that the oxygen concentration has little effect on the transition times. The methyl orange bleaching rates on the contrary are affected; they are decreased by a factor of about 2.7.

Summary of results

In summary, from these results we can conclude that the technique of periodic illumination reveals two intermediates, whose lifetimes (1) are very sensitive to pH, (2) are rather insensitive to the oxygen concentration, and (3) seem unrelated to the nature of the compound being degraded. Previously, we had established that the lifetime of the long-lived intermediate at pH 4.2 is longer at lower light intensities (see Figure 3.4), and is only a weak function of the duty cycle (see Figure 3.1). Furthermore, if the two lifetimes are closer to each other, the quantum yield is significantly lowered.

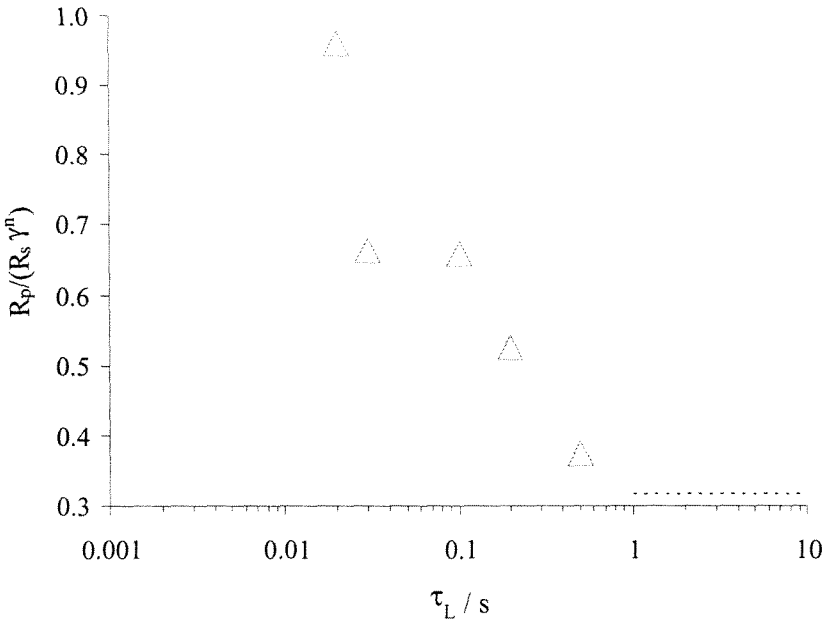

Figure 5.6. Methyl orange (MO) photocatalytic degradation under periodic illumination at $\gamma = 0.05$ with a lower oxygen concentration. Normalized assuming $n = 0.62$. The dashed line corresponds to γ^{1-n}.

$[MO]_{t=0} = 2\ \mu M$, load = 6 mg L^{-1} P25, temperature = 12 °C, pH 6.0, $I_{a,max} = 2.0\ \mu Einstein\ L^{-1}\ s^{-1}$.

5.5 Discussion

Many intermediates are possibly active in the photocatalytic degradation process. In principle, the technique of periodic illumination provides access to the lifetimes of rate-controlling intermediates without knowing their identity. However, the strong pH dependence of the lifetimes allows us to draw conclusions on the nature of these intermediates.

pH may affect photocatalytic rates by shifting the absolute potentials of the conduction and valence bands of the semiconductor photocatalyst. [27-29] It is found that in contact with an aqueous solution, the potential of the semiconductor photocatalyst and the positions of the band edges are shifted to more negative values with increasing pH, by 59 mV per pH unit at ambient temperature, over a wide pH-range. [27-29] This Nernstian behavior [(*)] has also been observed for TiO_2, for electrodes and colloidal particles. [30-32]

Thus, with increasing pH, the conduction band edge potential becomes more negative, increasing the reduction power of the conduction band electrons and the driving force for oxygen reduction, and thus by normal Marcus theory considerations increasing the electron transfer rate to oxygen across the TiO_2/solution interface. This in turn then leads to a shorter lifetime of conduction band electrons on the TiO_2 particle. Similarly, a decrease in pH results in an increased oxidation power of the valence band holes and an accelerated interfacial hole transfer, leading to a shorter lifetime of valence band holes.

However, reduction and oxidation are not always simple one-step transfers of mobile electrons or holes, but rather a cascade of electron or hole transfers from the conduction

or valence band to, for example, one or more shallow traps or intermediates to the final product. The energy levels of all traps and species on the particle are shifted with pH, along with the band edges. Thus, the lifetimes observed with the technique of periodic illumination are not *per se* the lifetimes of conduction band electrons and valence band holes, but ultimately those of reducing and oxidizing species on the TiO_2/solution interface.

(*) For half-reactions at equilibrium, the potential, E, can be related to the standard electrode potential, E^o, through Nernst's law:

$$E = E^o - (RT/zF) \Sigma \nu_i \ln(a_i)$$

where ν_i are the stoichiometric coefficients (positive for reduced species and negative for oxidized species), and a_i the activities. z is the number of electrons transferred, *F* Faraday's constant (96485 C mol^{-1}), R the ideal gas law constant (8.314 J mol^{-1} K^{-1}), and T the temperature.

In terms of concentrations, c_i, the Nernst equation can be rewritten as:

$$E = E^{o'} - (RT/zF) \Sigma \nu_i \ln(c_i)$$

in which $E^{o'}$ is the formal potential, dependent on the medium.[29]

For the protonation of the TiO_2 surface, H^+ is the only solution species participating, and

$$E = E^o + (RT/F) \ln(a_{H+}) = E^Y + (RT/F) \ln 10 \log(a_{H+}) = E^o - 0.059 \text{ pH (in V) at 298 K.}$$

Thus, the potential difference between TiO_2 and the solution changes at room temperature by 59 mV for every pH unit.

In the derivation of this equation, it is assumed that the proton activity on the surface does not change with pH. Criteria for such Nernstian behavior have been discussed by Hunter.[33] Parameters that influence the magnitude of the deviation from Nernstian behavior are, for example, the density of ionizable groups, the change of the surface charge with pH, and the difference in the equilibrium constants for the surface protonation reactions.[27]

Under illumination, TiO_2 particles may become charged with the less reactive carrier under the specific reaction conditions. The excess charge will affect the (electrical) particle potential, increasing the chemical potential of the excess carrier. The variation in electron transfer rates as a function of overpotential, $E-E^{Y'}$, is given by the Butler-Volmer equation, initially derived for electrode kinetics: [29]

$$k_{red} = k_0 \exp[-\alpha_{red}\, zF\, (E-E^{\theta'})/RT]$$

$$k_{ox} = k_0 \exp[\alpha_{ox}\, zF\, (E-E^{\theta'})/RT]$$

This equation states that the rate constants for reduction and oxidation reactions (k_{red} and k_{ox}) on the electrode depend exponentially on the electrode potential, E (with k_0 the standard rate constant, and α_{red} and α_{ox} the electron transfer coefficients).

Assuming the Butler-Volmer equation also holds for free-floating particles (though the potential in this case is not varied by applying a potential bias, but by varying the pH of the surrounding solution or by charge build-up due to different reduction and oxidation rates), and considering the lifetimes are inversely proportional to the rate constants, this results in an exponential dependence of the lifetimes of the intermediates on the particle potential and thus on the pH.

Thus, we can conclude that the intermediate observed in Figure 5.5 with an exponentially decreasing lifetime with increasing pH is a reducing species, while the intermediate with an exponentially increasing lifetime with increasing pH is an oxidizing species. The reducing species has the longer lifetime at pH values below 8.2, the oxidizing intermediate above pH 8.2. This implies that interfacial electron transfer is rate-determining at the pHs prevalent in most experimental and remediation systems,

concurring with Gerischer's suggestion.[26] It should be pointed out though that the reduction of oxygen being the rate-controlling step is characteristic of the conditions most researchers work under, rather than of photocatalysis itself.

The two transitions observed in Figures 5.3 (for $\gamma = 0.05$), 5.4 and 5.6 arise because of the different lifetimes of the reducing and oxidizing intermediates. At τ_L and τ_D longer than both the lifetimes, the system reaches steady state in the light and in the dark, and $R_{p,long\ \tau} = \beta \cdot \gamma \cdot I_{a,max}^{n}$. At τ_L and τ_D shorter than both the lifetimes, the system experiences steady illumination with an effective photon absorption rate $\langle I_a \rangle = \gamma \cdot I_{a,max}$ and $R_{p,short\ \tau} = \beta \cdot (\gamma \cdot I_{a,max})^{n}$. For intermediate τ_L and τ_D, one of the lifetimes is longer than τ_L and/or τ_D while the other one is shorter, resulting in an intermediate bleaching rate. The greater the difference in the lifetimes of the oxidizing and reducing intermediate, the longer the τ_L-window in which this intermediate R_p is observed. When the lifetimes are similar, as at pH 8 (data not shown), only one transition appears.

Other researchers have also observed two transitions, but only a factor of 3 apart, for the degradation of 3,4-dichlorobut-1-ene at pH 4.6 under periodic illumination with $\gamma \sim 0.5$.[34] In our experiments, the sampling frequency is not high enough to be able to observe transitions that close to each other as separate transitions. The observation of what appears to be only one transition for our $\gamma = 0.35$ experiments (see Figure 5.3), compared to two clearly separated transitions for the $\gamma = 0.05$ experiments under otherwise the same conditions, might suggest that (at pH 6.0) the lifetime of the reducing intermediate is linked to τ_L while the (shorter) lifetime of the oxidizing intermediate is determined by τ_D. The second transition with $\gamma = 0.05$ occurs at $\tau_D = 380$ ms ($\tau_L = 20$ ms). With $\gamma = 0.35$, τ_D

= 380 ms corresponds to τ_L = 200 ms, which is where a transition is observed, conceivably overlapping with the (first) τ_L = 200 ms transition. This aspect will be further investigated by mathematical modeling of our experimental results.

The varying lifetimes as a function of pH can also be invoked to explain the observed degradation rates. Contrary to the degradation of trichloroacetate and chloroethylammonium for example, [16] methyl orange has a high degradation rate at both high and low pH, suggesting that for methyl orange adsorption on the TiO_2 surface does not play a major role in determining the rate of the photocatalytic reaction. The shift of the particle potential with pH on the other hand, and the resulting lifetimes of reducing and oxidizing intermediates, can be related to the higher degradation rate and quantum yield observed at extreme pH. $I_{a,max}$ under our conditions corresponds to an absorption rate of about 3000 photons per particle per second; under these conditions this rate creates an electron-hole pair on average every 0.33 ms. During illumination, very likely more than one electron-hole pair is present on the particle. Interfacial electron and hole transfer are in competition with electron-hole pair recombination (as evidenced by $n \sim 0.6$). However, at (very) basic pH for example, electrons will be transferred across the TiO_2/solution interface faster, decreasing the electron concentration on the particle, thereby reducing the probability of recombination with (slow-reacting) holes left on the particle, increasing their probability to transfer across the interface. At a pH around 8, on the other hand, neither reduction nor oxidation is fast, and the reducing and oxidizing species both have a long lifetime on the TiO_2 particle, and thus are prone to recombination, resulting in a low quantum yield. Therefore, Figure 5.2 and 5.5 are consistent with each other.

Based on the work of previous researchers we can speculate about the identity of the intermediates. The observed lifetimes are too long to be those of valence band electrons and conduction band holes. Nosaka *et al.* reported the lifetime of superoxide to be 17 s at pH 11 in aqueous TiO_2 suspensions.[35] Similar experiments by Ishibashi *et al.* on TiO_2 films revealed a lifetime of superoxide of about 70 s in water.[7,36] It was observed that $O_2^{\bullet-}$ accumulates gradually with illumination time, and its number is saturated after about 20 min illumination at 1 $\mu W\ cm^{-2}$. The decay profile was found to obey first-order rate kinetics.[36] Assuming superoxide is the reducing intermediate revealed in our experiments, a first-order decay would explain the independence of the superoxide lifetime on the superoxide concentration – and thus on the concentration of oxygen, which is converted proportionally to superoxide. The results by Ishibashi *et al.* also indicate that superoxide is present at the TiO_2/solution interface, and not in the bulk solution.[37]

More reactive species were also observed, disappearing in a few seconds, and were believed to be $OH^{\bullet}$ or/and surface trapped holes.[7,36] Szczepankiewicz *et al.* determined that a hole can be trapped at the TiO_2 surface as a surface-bound hydroxyl radical.[2] The assignment of the oxidizing intermediate to species such as hydroxyl radicals, surface trapped holes, or surface-bound hydroxyl radicals, would explain why the observed lifetime is insensitive to the compound being degraded, since only a small fraction of those are used for the degradation, and their lifetimes are determined by other reactions, such as recombination with superoxide.

5.6 Conclusions

The application of the technique of periodic illumination reveals two lifetimes, belonging to two intermediates involved in photocatalysis. By varying the pH of the TiO_2 suspensions, we obtained information on the nature of these intermediates. They were found to be a reducing and an oxidizing species on the TiO_2/solution interface. The lifetime of the reducing species decreases with pH, while the lifetime of the oxidizing species increases, as a result of the shift in potential of the TiO_2 particle. Thus, at low pH the interfacial electron transfer to oxygen is slower, and at high pH the interfacial hole transfer to the organic compound. Since the crossover is at pH 8.2, in most applications the reduction of oxygen will be the slowest step. The exponential dependence of the lifetimes of on the pH was explained on the basis of the Butler-Volmer equation. The lifetimes of the intermediates are consistent with those of superoxide radicals (reducing intermediate) and hydroxyl radicals, surface-bound hydroxyl radicals and/or surface trapped holes (oxidizing intermediate).

5.7 References

(1) Martin, S. T.; Herrmann, H.; Choi, W.; Hoffmann, M. R. *J. Chem. Soc. Faraday Trans.* **1994**, *90*, 3315. Martin, S. T.; Herrmann, H.; Hoffmann, M. R. *J. Chem. Soc. Faraday Trans.* **1994**, *90*, 3323.

(2) Szczepankiewicz, S. H.; Colussi, A. J.; Hoffmann, M. R. *J. Phys. Chem. B* **2000**, 104, 9842.

(3) Bahnemann, D. W.; Hilgendorff, M.; Memming, R. *J. Phys. Chem.* **1997**, *101*, 4265.

(4) Furube, A.; Asahi, T.; Masuhara, H.; Yamashita, H.; Anpo, M. *J. Phys. Chem. B* **1999**, *103*, 3120.

(5) Serpone, N.; Lawless, D.; Khairutdinov, R.; Pelizzetti, E. *J. Phys. Chem.* **1995**, *99*, 16655.

(6) Stopper, K.; Dohrmann, J. K. *Zeitschrift fur Physikalische Chemie* **2000**, *214*, 555.

(7) Ishibashi, K.; Nosaka, Y.; Hashimoto, K.; Fujishima, A. *J. Phys. Chem.* **1998**, *102*, 2117.

(8) Rothenberger, G.; Moser, J.; Gratzel, M.; Serpone, N.; Sharma, D. K. *J. Am. Chem. Soc.* **1985**, *107*, 8054.

(9) Colombo, D. P.; Bowman, R. M. *J. Phys. Chem.* **1995**, *99*, 11752.

(10) Burnett G. M., Melville H. W. in *Technique of Organic Chemistry, Investigation of Rates and Mechanisms of Reactions,* Friess, S. L.; Lewis, E. S.; Weissberger, A., Eds., 2nd Ed., Interscience Publishers: New York, 1963, Vol. VIII - Part II, Chapter 20.

(11) Noyes, W. A., Jr.; Leighton, P. A. in *The Photochemistry of Gases*, Reinhold Publishing Corp., 1941, Chapter IV.

(12) Haden, W. L.; Rice, O. K. *J. Chem. Phys.* **1942**, *10*, 445.

(13) Burnett, G. M.; Melville, H. W. *Nature* **1945**, *156*, 661.

(14) Bartlett, B. D.; Swain, C. G. *J. Am. Chem. Soc.* 1945, *67*, 2273 and 1946, *68*, 2381.

(15) Okamoto, K.; Yamamoto, Y.; Tanaka, H.; Itaya, A. *Bull. Chem. Soc. Jpn.* **1985**, *58*, 2023.

(16) Kormann, C.; Bahnemann, D. W.; Hoffmann, M. R. *Environ. Sci. Technol.* **1991**, *25*, 494.

(17) Ohko, Y.; Ikeda, K.; Rao, T. N.; Hashimoto, K.; Fujishima, A. *Zeitschrift fur Physikalische Chemie* **1999**, *213*, 33.

(18) Mills, A; Wang, J. *Zeitschrift fur Physikalische Chemie* **1999**, *213*, 49.

(19) Bahnemann, D.; Bockelmann, D.; Goslich, R. *Solar Energy Materials* **1991**, *24*, 564.

(20) Ollis, D. F.; Pelizzetti, E.; Serpone, N. *Environ. Sci. Technol.* **1991**, *25*, 1523.

(21) Skoog, D. A.; West, D. M.; Holler, F. J. in *Fundamentals of Analytical Chemistry, 7th edition*, Saunders College Publishing, 1946, p.191.

(22) Heller, H. G.; Langan, J. R. *J. Chem. Soc. Perkin Trans. II* **1981**, *2*, 341.

(23) Chen, L. C.; Chou, T. C. *J. Mol. Catal.* **1993**, *85*, 201.

(24) Brown, G. T.; Darwent, J. R. *J. Phys. Chem.* **1984**, *88*, 4955.

(25) Brown, G. T.; Darwent, J. R. *J. Chem. Soc., Faraday Trans. I* **1984**, *80*, 1631.

(26) Gerischer, H. in *Photocatalytic Purification and Treatment of Water and Air*; Ollis, D. F., Al-Ekabi, H., Eds.; Elsevier: Amsterdam, 1993, 1.

(27) Gratzel, M. in *Heterogeneous Photochemical Electron Transfer*, CRC Press, 1989, Chapter 3.

(28) Bard, A. J.; Faulkner, L. R. in *Electrochemical Methods; Fundamentals and Application*, Wiley-Interscience: New York, 1980.

(29) Brett, C. M. A.; Oliveira-Brett, A. M. in *Electrochemistry: Principles, Methods, and Applications*, Oxford University Press, 1993.

(30) Duonghong, D.; Ramsden, J.; Gratzel, M. *J. Am. Chem. Soc.* **1982**, *104*, 2977.

(31) Nozik, A. J.; Memming, R. *J. Phys. Chem.* **1996**, *100*, 1306.

(32) Matsumoto, Y. *J. Solid State Chem.* **1996**, *126*, 227.

(33) Hunter, R. J. in *Zeta Potential in Colloidal Science*, Academic Press: London, 1981.

(34) Hamill, N. A.; Weatherley, L. R.; Hardacre, C. *Appl. Catal. B: Environ.* **2001**, *30*, 49.

(35) Nosaka, Y.; Yamashita, Y.; Fukuyama, H. *J. Phys. Chem.* **1997**, *101*, 5822.

(36) Ishibashi, K.; Fujishima, A.; Watanabe, T.; Hashimoto, K. *J. Phys. Chem.* **2000**, *104*, 4934.

(37) Ishibashi, K.; Fujishima, A.; Watanabe, T.; Hashimoto, K. *Electrochemistry* **2001**, *69*, 160.

5.8 Appendices

Data table

γ	τ_L (s)	$I_{a,max}$ μEinstein/Ls	degradation (nM/min)	O_2 sat.	pH
0.05	0.0005	2.02	9.99	x	2.5
0.05	0.001	2.02	9.06	x	2.5
0.05	0.002	2.02	6.61	x	2.5
0.05	0.005	2.02	4.89	x	2.5
0.05	0.02	2.02	5.02	x	2.5
0.05	0.02	2.02	4.67	x	2.5
0.05	0.05	2.02	4.80	x	2.5
0.05	0.2	2.02	4.66	x	2.5
0.05	0.5	2.02	4.56	x	2.5
0.05	1	2.02	4.74	x	2.5
0.05	2	2.02	3.54	x	2.5
0.05	5	2.02	3.06	x	2.5
0.05	0.002	2.02	6.67	x	6.0
0.05	0.01	2.02	6.28	x	6.0
0.05	0.02	2.02	6.41	x	6.0
0.05	0.03	2.02	3.71	x	6.0
0.05	0.03	2.02	4.03	x	6.0
0.05	0.05	2.02	4.36	x	6.0
0.05	0.1	2.02	3.89	x	6.0
0.05	0.2	2.02	3.58	x	6.0
0.05	0.5	2.02	2.28	x	6.0
0.05	1	2.02	2.71	x	6.0
0.05	2	2.02	2.82	x	6.0
0.05	0.05	2.02	2.06	x	8.0
0.05	0.2	2.02	0.820	x	8.0

Table 5.2. Degradation rates for the photocatalytic bleaching of 2 μM methyl orange.

γ	τ_L (s)	$I_{a,max}$ μEinstein/Ls	degradation (nM/min)	O_2 sat.	pH
0.05	0.02	2.02	10.2	x	11.4
0.05	0.03	2.02	6.47	x	11.4
0.05	0.05	2.02	6.97	x	11.4
0.05	0.2	2.02	7.17	x	11.4
0.05	0.5	2.02	7.10	x	11.4
0.05	1	2.02	5.87	x	11.4
0.05	2	2.02	4.52	x	11.4
0.05	5	2.02	4.51	x	11.4
0.35	0.01	2.02	23.3	x	6.0
0.35	0.05	2.02	22.4	x	6.0
0.35	0.1	2.02	20.2	x	6.0
0.35	0.2	2.02	19.1	x	6.0
0.35	0.3	2.02	14.6	x	6.0
0.35	0.5	2.02	16.0	x	6.0
0.35	1	2.02	15.1	x	6.0
0.35	2	2.02	16.5	x	6.0
0.35	5	2.02	16.1	x	6.0
1		2.02	52.9	x	2.5
1		0.685	27.8	x	2.5
1		0.089	10.0	x	2.5
1		2.02	45.6	x	6.0
1		0.685	20.6	x	6.0
1		0.089	6.46	x	6.0
1		2.02	20.3	x	8.0
1		2.02	85.0	x	11.4
1		0.089	9.72	x	11.4
0.05	0.02	2.02	2.44		6.0
0.05	0.03	2.02	1.69		6.0
0.05	0.1	2.02	1.68		6.0
0.05	0.2	2.02	1.34		6.0
0.05	0.5	2.02	0.952		6.0
1		2.02	16.2		6.0

Table 5.2 (continued). Degradation rates for the photocatalytic bleaching of 2 μM methyl orange.

Chapter 6

Mathematical modeling

of photocatalysis in aqueous TiO_2 suspensions

under continuous and periodic illumination

6.1 Introduction

Modeling of photocatalysis

Although it is known that the reaction mechanism for photocatalytic degradation of organic compounds can involve complex networks of reactions involving many intermediates, numerical solutions to complex models are of little practical value because of the difficulty in measuring or estimating the large number of parameters involved in the process. [1]

Our goal for the modeling presented in this chapter is not to provide an exhaustive description of an entire photocatalytic system under periodic illumination, but rather to find a minimal set of reactions and/or processes needed to explain the main features of the experimental results presented in previous chapters.

Nosaka and Fox used a simple mechanism involving only charge carrier generation, recombination, electron transfer and hole transfer to calculate the quantum yield for the reduction of methyl viologen, using laser pulse-irradiated colloidal semiconductors, as a function of pulse width. [2] Upadhya and Ollis [3] added adsorption kinetics to explain quantum yield improvements reported by Sczechowski *et al.* [4,5] for the photocatalytic oxidation of formate on P25. (Note that the results of Chapter 3 show conclusively for the same system that the quantum yield improvements with respect to continuous illumination at the maximum photon absorption rates do not require mass transfer limitations.)

Limitations

A significant limitation of the chemical kinetics modeling approach, where mass balances are written in terms of continuous variables, whose evolution is determined by a set of differential equations, is the implicit assumption that the evolution of an ensemble of molecules can be described by the rate equations applied to the average over the ensemble. In effect, the ensemble of TiO_2 particles is treated as one large particle. When the number of charge carrier pairs per particle is not much larger than one, this is inaccurate. A stochastic approach – such as Monte Carlo simulations – should be employed in this case. [6]

Butler-Volmer equation

The key feature for describing variations with pH in our model is the Butler-Volmer equation. Butler-Volmer describes the dependence of electron transfer reaction rates on the electrochemical driving force, i.e., the electrical potential. [7] The potential of a free-floating particle is determined by the accumulated charge on the particle and the polarization of the surrounding solution in the double layer. [7] In accordance with the principle of Le Chatelier-van 't Hoff, the Butler-Volmer formulation for electron transfer kinetics thus provides a negative feedback mechanism keeping charge build-up in check.

The electrical potential of the particle is also affected by the pH; when the pH of the solution surrounding the particle is varied, its potential shifts by 0.059 mV per pH unit. [7]

Under steady state conditions, the Butler-Volmer equation merely offsets the electron transfer rate constants by some factor, making the reduction and oxidation rates equal.

Under transient conditions, however, it is not *a priori* true that charge is conserved for each particle, so that the instantaneous reduction and oxidation rates may be different. By incorporating the Butler-Volmer equation in the model, we are taking into account that under periodic illumination, there would be an associated periodic variation in the particle charge if the steady-state potential varies with light intensity.

Outline

In the next section, we will validate our implementation of the numerical simulation with periodic illumination with a brief look at homogeneous photochemistry, where literature results for periodic illumination include analytical expressions. [8] We will then apply periodic illumination to a simple model of photocatalysis in section 6.3. This model includes only light absorption, reduction and oxidation, and recombination. A key feature in our model is the Butler-Volmer formulation for the reduction and oxidation rates, so first we will estimate the parameters that go into this formulation. In a second phase the pH-dependence of the degradation rates and the transitions will be tackled.

This modeling will then allow us to, for example:

- visualize the concentrations of the intermediates during photocatalysis,
- explore the effects of parameters such as the photon absorption rate, the duty cycle, the pH, the bandgap of the semiconductor, etc., and
- determine the relationship between the transition times and the lifetimes of the intermediates involved.

This will be discussed in section 6.4.

6.2 Validation of the numerical methodology

The numerical simulations of the photocatalytic reaction kinetics under periodic illumination were performed using Igor Pro, a commercial data analysis package. Igor Pro includes a built-in facility for calculating numerical solutions to initial-value problems involving stiff sets of ordinary differential equations with user-defined derivative functions. By defining a function that, given the concentrations of the various species and a set of rate constants, calculates the reaction rates of those species, any chemical kinetic reaction mechanism can be modeled. Because the user-defined derivative functions can depend explicitly on the independent variable, the implementation of chemical kinetics under time-varying conditions, e.g., pulsed illumination, is straightforward. To verify that our implementation in Igor of such models is correct, our results for (homogeneous) pulsed photolysis were compared with the analytical solution, which exists for the following chain reaction mechanism: [8]

initiation:	$A + h\nu \rightarrow D_1 + D_2$ $(I_a*\phi)$	(1)
propagation:	$D_1 + A \rightarrow B + D_3$ (k_p)	(2)
propagation:	$D_3 \rightarrow D_1 + C$ (fast)	(3)
termination:	$D_1 + D_1 \rightarrow D$ (k_t)	(4)

with D_1, D_2, and D_3 free radicals, and B, C, and D stable product molecules. Aldehyde photolysis at moderate temperatures ($A = C_2H_4O$, $R_1 = CH_3$, $R_2 = CHO$, $R_3 = CH_3CO$, $B = CH_4$, $C = CO$, and $D = C_2H_6$) and many photopolymerizations follow this general reaction scheme.

For this reaction mechanism the reaction rate (and therefore the quantum yield), under pulsed illumination is found to be proportional to

$$v = \frac{1}{p+1}\left(1+\frac{1}{m}\ln\left(\frac{pm}{1+\dfrac{2(pm+\tanh(m))}{pm\tanh(m)+\sqrt{(pm\tanh(m))^2+4(pm+\tanh(m))\tanh(m)}}}+1\right)\right) \tag{5}$$

with $p = \tau_D/\tau_L$ and $m = \tau_L k_t [D_1]$.

This analytical expression is plotted as a function of m for p =19 (corresponding to a duty cycle of 0.05) in Figure 6.1. In the same figure, the results of numerical simulation after 20 illumination periods are shown. For long light times, the agreement is excellent. For shorter light times, the reaction rates calculated in the numerical simulation are too low. For these short light times, the result under pulsed illumination can be described as a sawtooth superimposed on the result for continuous illumination with the average intensity. As can be seen in Figure 6.2, the reaction rates for short light times are underestimated because the total elapsed time in the simulation is shorter than the time required to reach steady state under continuous illumination with the average intensity. This situation is easily remedied by setting the initial concentration of D_1 in the simulation to the steady state concentration for continuous illumination with the average intensity. For sufficiently long simulation times, the result converges to the steady state value regardless of the initial conditions, but through judicious choice of the initial conditions the simulation time required can be reduced to a minimum. Figure 6.3 shows that with the initial concentration of the intermediates set to their steady state

concentration, good agreement is achieved between the analytical result and the numerical simulation over the entire range of light times, and the number of illumination periods in the simulation can be reduced from 20 to 3 with only a slight decrease in accuracy.

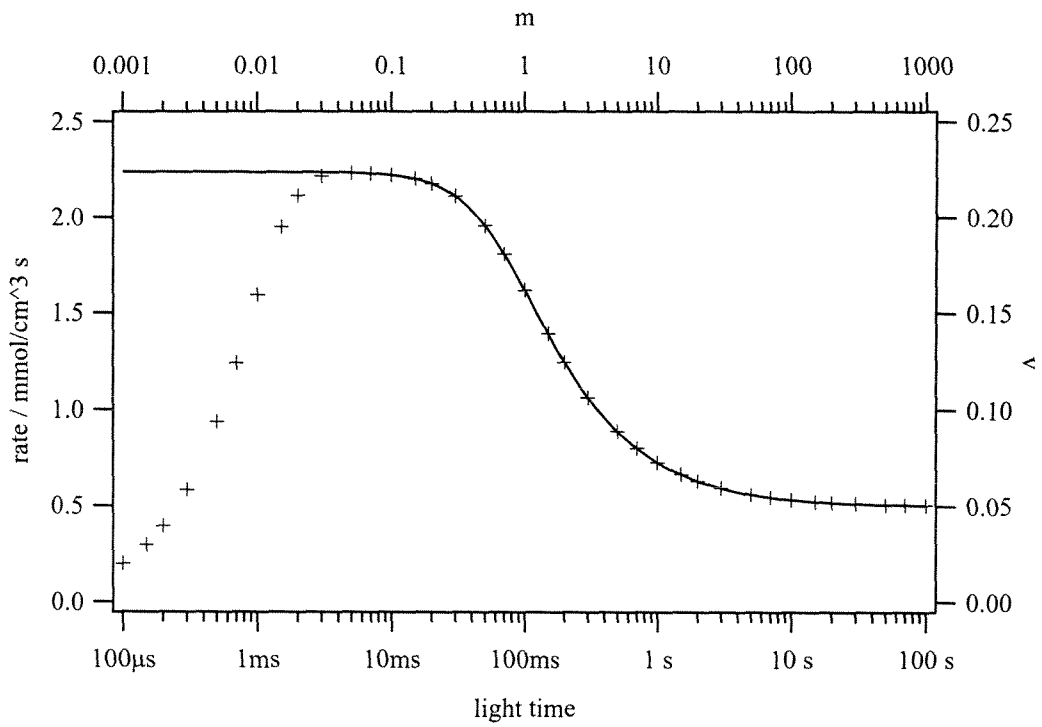

Figure 6.1. Results of the numerical simulation for the reaction mechanism presented in the text (markers), with [A] = 1 mol cm^{-3}, $I_a*\phi$ = 5 10^{-13} Einstein cm^{-3} s^{-1}, k_p = 10^{10} cm^3 mol^{-1} s^{-1}, k_t = 10^{13} cm^3 mol^{-1} s^{-1}. [8] The solid line represents the analytical solution given by equation (5).

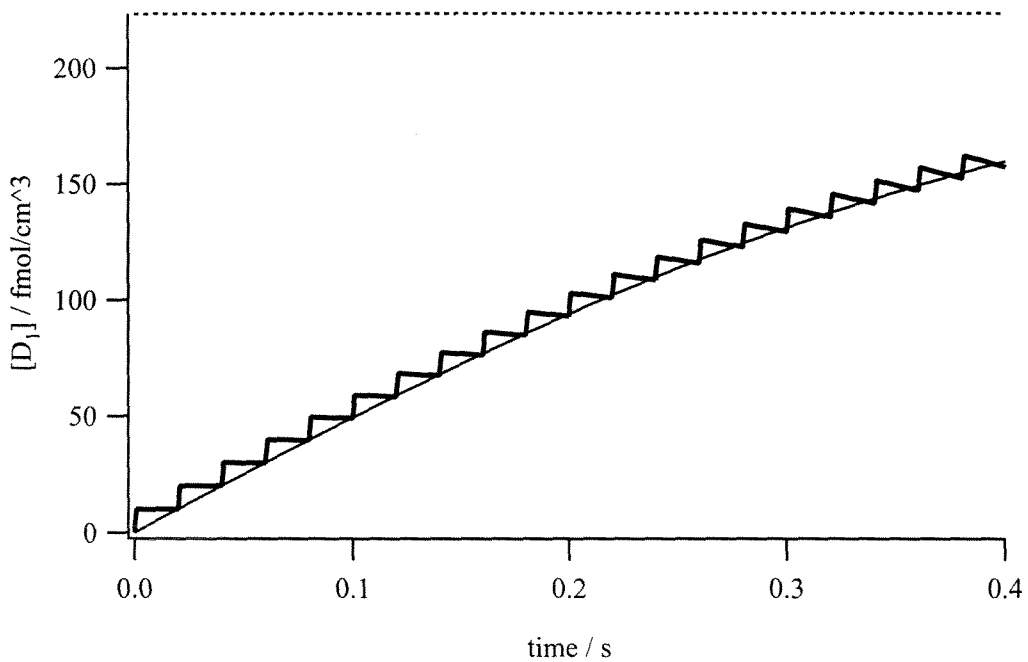

Figure 6.2. Transient concentration of intermediate D_1 as a function of time for τ_L = 10 ms and γ = 0.05. The thin and the dashed line are the transient and steady state concentrations under continuous illumination with the average photon absorption rate, respectively.

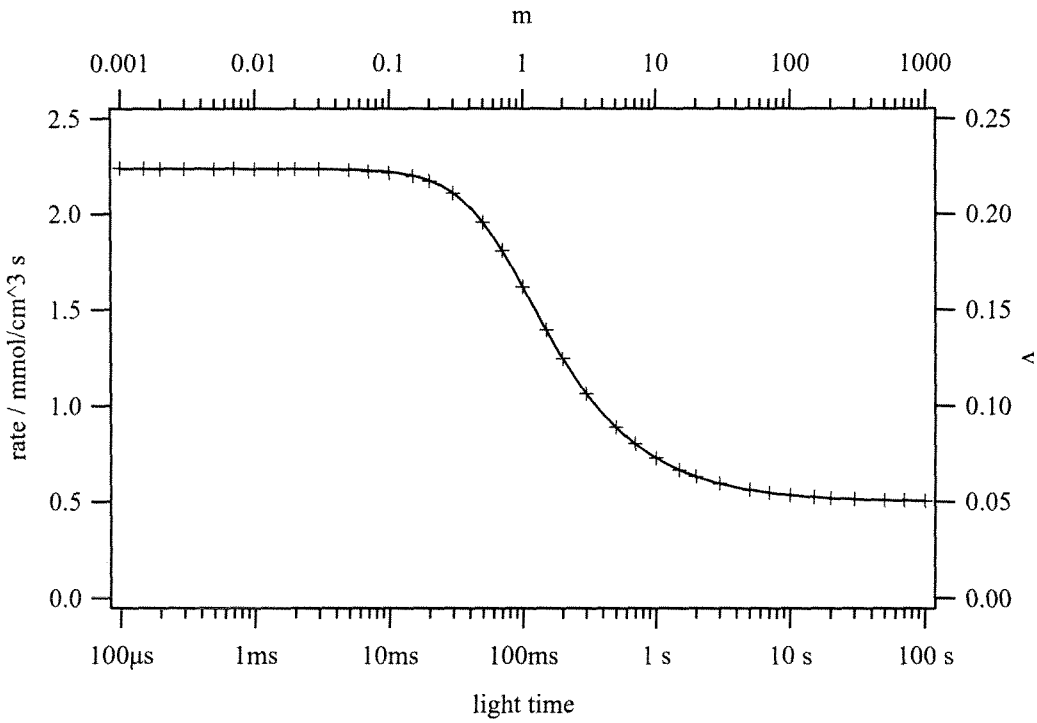

Figure 6.3. Results of the numerical simulation for the reaction mechanism presented in the text (markers), using the steady-state concentration of intermediate D_1 under continuous illumination with the average photon absorption rate as the initial conditions. The solid line represents the analytical solution given by equation (5).

It should also be noted that to avoid issues associated with the depletion of the reagent A affecting the reaction rate, the concentration of A is not actually varied, but the rate at which A is consumed is integrated using a dummy species.

6.3 Mathematical model for photocatalysis

Reactions

Many factors may affect the degradation rate of an organic compound on a TiO_2 particle, such as the incident photon rate, the presence of an appropriate electron acceptor, competing species and/or interfering ions, the depletion and replenishment of the organic compound, etc.

In a first-cut analysis we will only consider a limited number of reactions – light absorption, reduction of an electron acceptor A, oxidation of an electron donor D, and electron-hole recombination. This simple model can be expanded later on if need be.

The reactions, species and rate constants considered in this model are as follows:

	$\rightarrow e + h$	I_a	(light absorption)	(6)
$e + A$	$\rightarrow$	k_1	(electron transfer, reduction)	(7)
$h + D$	$\rightarrow D^+$	k_2	(hole transfer, oxidation)	(8)
$e + h$	$\rightarrow$	k_3	(recombination)	(9)

The species "electron" (e) and "hole" (h) represent a reducing species and an oxidizing species, respectively, not necessarily free electrons and holes. A and D stand for electron acceptor and donor respectively; D^+ stands for the oxidized form of D. The reduced form of A, the heat dissipated and the photons absorbed are not of interest, and are not identified in the program.

Rate equations

The rate equations for the species involved in these four reactions are expressed by the following stiff set of differential equations:

$$d[e]/dt = I_a - k_{01}\cdot\exp(-\alpha_{1e}\cdot(zF/RT)\cdot Pot)\cdot[e]\cdot[A] - k_3\cdot[e]\cdot[h] \quad (10)$$

$$d[h]/dt = I_a - k_{02}\cdot\exp(\alpha_{2h}\cdot(zF/RT)\cdot Pot)\cdot[h]\cdot[D] - k_3\cdot[e]\cdot[h] \quad (11)$$

$$d[A]/dt = 0 \quad (12)$$

$$d[D]/dt = 0 \quad (13)$$

$$d[D^+]/dt = k_{02}\cdot\exp(\alpha_{2h}\cdot(zF/RT)\cdot Pot)\cdot[h]\cdot[D] \quad (14)$$

The rate constants for reduction and oxidation are adjusted for the particle potential with an exponential factor, according to the Butler-Volmer equation,

with z the number of electrons transferred,

F Faraday's constant (96485 C mol^{-1}),

R the ideal gas law constant (8.314 C V mol^{-1} K^{-1}), and

T the temperature.

At 25 °C (298 K) zF/RT equates to 40 V^{-1} for a one-electron transfer reaction.

The concentrations of A and D on the particle surface are considered to be constant. Gerischer suggests that the oxygen concentration at the particle surface is constant, provided the solution remains equilibrated with oxygen. [9] This was the case in our experiments, since we continuously sparged the solution with oxygen. The same

reasoning – of a partitioning between the solution and adsorption sites on the particle – was applied for the electron donor.

Periodic illumination

Periodic illumination was imposed mathematically by modulating the light intensity with a square wave, with a duty cycle γ, using the following conditional assignment:

$$\text{If } (\text{mod}(t,\tau_L/\gamma) > \tau_L) \text{ then } I_a = I_{a,max}, \text{ else } I_a = I_{a,dark}. \quad (15)$$

The "mod" function subtracts an integer number of illumination periods (1 period = τ_L/γ) from the time, so that the remainder is smaller than one period (but larger than or equal to zero), so it returns the time into the current illumination period. If this time is smaller than τ_L, the light is on and $I_a = I_{a,max}$, otherwise the light is off and $I_a = I_{a,dark}$.

$I_{a,dark}$ corresponds to the contributions of spurious illumination and electron-hole pair creation by thermal excitation, which is negligible in TiO_2. Spurious illumination was determined experimentally to be ~ 1 nEinstein L^{-1} s^{-1} in our setup.

It should be noted that for the modeling of the homogeneous photopolymerization presented previously, we used $I_{a,dark} = 0$ to agree with the conditions for which the analytical expression was derived.

Initial concentrations

The concentrations of A and D used in the experiments described in previous chapters are bulk concentrations. Since reduction and oxidation take place on the surface of the TiO_2 particle, the available surface area should be taken into account. Oxygen seems to adsorb

on sites different from those on which organic molecules are oxidized, avoiding competition. [10] Manuera *et al.* reported coverage of water on the TiO_2 surface to be $5 \cdot 10^{14}$ cm^{-2} molecules, along with $3 \cdot 10^{14}$ cm^{-2} acidic OH groups and $2 \cdot 10^{14}$ cm^{-2} basic OH groups. [11] Upadhya *et al.* assumed $5 \cdot 10^{14}$ available surface sites per cm^2, both for oxygen and formate. [3] Under this assumption, with all available sites occupied, we obtained

$$[A]_{t=0} = [D]_{t=0} = 8.3 \cdot 10^{-6} \text{ mol m}^{-2}, \quad (16)$$

and because of equation (12) and (13), these concentrations are invariant with time.

The concentrations of electrons and holes establish themselves according to equations (10)-(11), regardless of the initial values. As initial values for an experiment with periodic illumination, we used the steady state concentrations obtained under steady illumination with photon absorption rate $\gamma \cdot I_{a,max}$, because it converges faster. As initial values for an experiment with steady illumination, we used

$$[e]_{t=0} = [h]_{t=0} = 0 \text{ particle}^{-1}. \quad (17)$$

For ease of visualization, the concentrations of electrons and holes are expressed per particle.

As the reactions progress, D^+ is formed and released to the bulk of the solution. Since the concentration of the holes is expressed per particle, the concentration of D^+ ensuing from equation (14) will also be per particle. Working with a particle load of 6 mg L^{-1}, a reactor volume of 26 mL, a particle density of 3.7 g cm^{-3} and a particle radius of 10 nm, there are 10^{13} particles in suspension in the reactor. To convert from per particle to a bulk concentration in molar, we multiply with 10^{13} and divide by Avogadro's number (N_A = $6.0225 \cdot 10^{23}$ mol^{-1}) and the reactor volume. So the formation and subsequent release of 1

molecule D^+ per particle corresponds an addition of 0.642 nM to the bulk of the solution. As initial concentration of D^+, we took

$$[D^+]_{t=0} = 0 \text{ particle}^{-1}. \quad (18)$$

Rate constants

The standard rate constants for reduction (k_{01}) and oxidation (k_{02}), and the recombination rate constant (k_3) are fitting parameters. The units of k_{01} and k_{02} are $m^2\ mol^{-1}\ s^{-1}$, the units for k_3 are particle s^{-1}. The rate constant for light absorption, I_a, is expressed in photons $particle^{-1}\ s^{-1}$, according to equation (10). In most of the experiments described in previous chapters, $I_{a,max}$ = 2.0 μEinstein $L^{-1}\ s^{-1}$ was applied, and $I_{a,dark}$ was ~ 1 nEinstein $L^{-1}\ s^{-1}$. Unless otherwise noted (Figure 6.8), these values were used, which, using the same assumptions as above, were converted to

$$I_{a,max} = 3111 \text{ photons particle}^{-1}\ s^{-1}, \text{ and} \quad (19)$$

$$I_{a,dark} = 1.6 \text{ photons particle}^{-1}\ s^{-1}. \quad (20)$$

Particle potential

The Butler-Volmer equation expresses how the rate constants for reduction and oxidation depend on the particle potential. Since the particle potential increases by 0.059 V per pH unit, we can convert from a pH scale to a potential scale by

$$Pot_{pH} = (6.25 - pH) \times 0.059 \text{ V}, \quad (21)$$

where 6.25 is the pH of zero point charge (pH_{ZPC}) of P25.

The particle can also become charged with the less reactive charge carrier, leading to a change in particle potential,

$$Pot_{e/h} = \frac{F \times ([h] - [e])}{N_A \times s \times C_{dl}} V, \quad (22)$$

with s the particle surface area, and

C_{dl} the capacitance of the double layer around the TiO_2 particle.

F/N_A represents the charge of an electron, equal to $1.6\ 10^{-19}$ C. The particle surface area, s, can be calculated based on the BET surface area (50 $m^2\ g^{-1}$ for P25) of the TiO_2 particles, resulting in

$$s = 8.1\ 10^{-16}\ m^2. \quad (23)$$

For semiconductors, the value for the double layer capacitance is typically between 0.1 and 1 F m^{-2}.[7] C_{dl} is expected to vary with parameters such as the ionic strength and the pH of the solution, but these effects were not taken into account. A constant, intermediate value of

$$C_{dl} = 0.2\ F\ m^{-2} \quad (24)$$

was used, resulting in

$$Pot_{e/h} = ([h] - [e]) \times 10^{-3}\ V. \quad (25)$$

Thus, an excess of one charge carrier relative to the other on a particle gives rise to a potential difference of 1 mV.

The combination of these two contributions to the particle potential, "Pot," results in

$$Pot = (6.25 - pH) \times 0.059 + ([h] - [e]) \times 10^{-3}\ V. \quad (26)$$

It should be noted that if the particle potential were significantly affected by the charge build-up on the particle, due to an imbalance between the oxidation and reduction rates, then the apparent proportionality factor between pH and particle potential would be smaller than 0.059 V per pH unit.

Electron transfer (Tafel) coefficients

For the one-electron transfer reaction (z = 1)

$$e^- + Ox \leftrightarrow Red \qquad (27)$$

the reduction rate constant $k_{red} = k_0 \exp(-\alpha_{red} \cdot (F/RT) \cdot Pot)$ and

the oxidation rate constant $k_{ox} = k_0 \exp(\alpha_{ox} \cdot (F/RT) \cdot Pot)$, with

$$\alpha_{red} + \alpha_{ox} = 1 \text{ and } \alpha_{red} \geq 0, \alpha_{ox} \geq 0 \qquad (28)$$

α_{red} and α_{ox} are the electron transfer coefficients or Tafel coefficients. They are a measure of the slopes of the energy profiles in the transition state zone and, therefore, of barrier symmetry. Values of α_{red} and α_{ox} can vary between 0 and 1, but for metals are around 0.5. A value of 0.5 means that the activated complex is exactly halfway between reagents and products on the reaction coordinate, its structure reflecting reagents and products equally.

For more complicated electron transfer reactions, the Tafel coefficients need not add up to unity. Also, there is no relationship expected between the α_{red} and the α_{ox} of different redox reactions taking place on the same electrode or particle.

Based on Figure 5.5 we will estimate the Tafel coefficients for the electron transfer reactions

$$A + e^- \rightarrow \qquad k_1 \tag{29}$$

$$D \rightarrow D^+ + e^- \qquad k_2 \tag{30}$$

taking place on the TiO_2 particles.

The transition times, corresponding to lifetimes of a reducing and an oxidizing intermediate, are inversely proportional to the rate constants for reduction and oxidation respectively,

$$k_1, k_2 = \tau_L^{-1} \quad (\text{in } s^{-1}). \tag{31}$$

The pH can be converted to a potential using equation (21). In this manner, Figure 6.4 was constructed. This figure illustrates clearly that electrons are removed more readily (i.e., faster) if there is an excess negative charge on the particle, and vice versa. From the exponential least-square regression, we obtain $k_1 \propto e^{-8.55 \times Pot}$ for the reduction reaction, and $k_2 \propto e^{12.2 \times Pot}$ for the oxidation reaction. Comparison with equation (14) and an analogous equation for the reduction, shows that $-\alpha_{1e} \cdot (zF/RT) = -8.55$ and $\alpha_{2h} \cdot (zF/RT) = 12.2$, so assuming one-electron transfers ($z = 1$), we obtain

$$\alpha_{1e} = 0.21 \text{ and } \alpha_{2h} = 0.30 \tag{32}$$

in the approximation that the contribution of charge build-up to the particle potential is negligible.

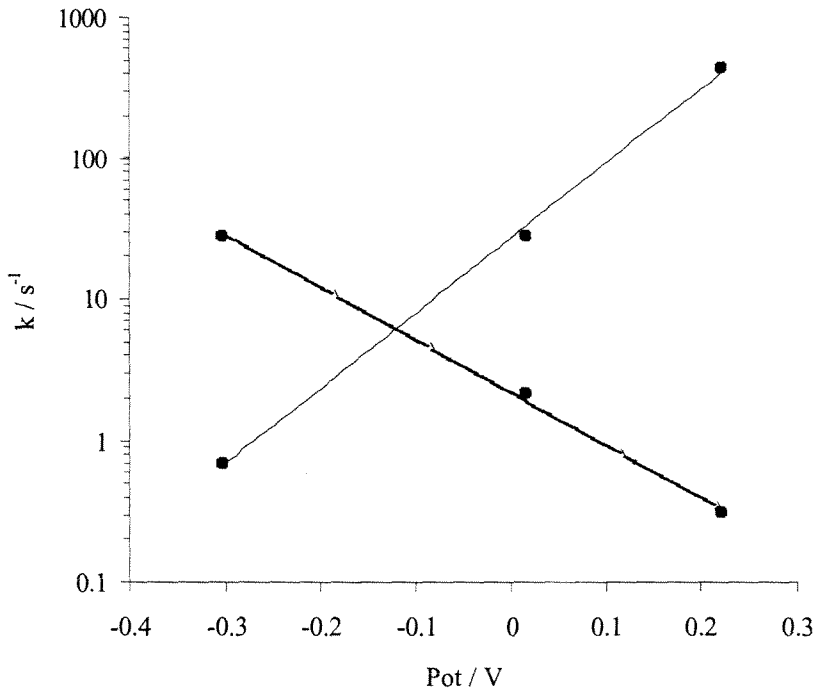

Figure 6.4. Variation of the rate constants for reduction (dotted line) and oxidation (solid line) as a function of the particle potential.

Methodology

The production of D^+ under periodic illumination was calculated for a range of τ_L from 1 ms to 100 s. The production rate was calculated as

$$d[D^+]/dt = ([D^+]_{t=4\tau} - [D^+]_{t=3\tau}) / \tau \qquad (33)$$

with $\tau = \tau_L + \tau_D$.

6.4 Results and discussion

Since there is no efficiency factor incorporated in the model to account for competing electron donors, the degradation rates will be higher than our experimental results. A simulation at pH 6 is presented in Figure 6.5. The rate constants used are: $k_{01} = 22300$ m^2 mol^{-1} s^{-1}, $k_{02} = 250000$ m^2 mol^{-1} s^{-1}, $k_3 = 0.7$ particle^{-1} s^{-1}. These rate constants were found to reproduce the main features in our experimental data.

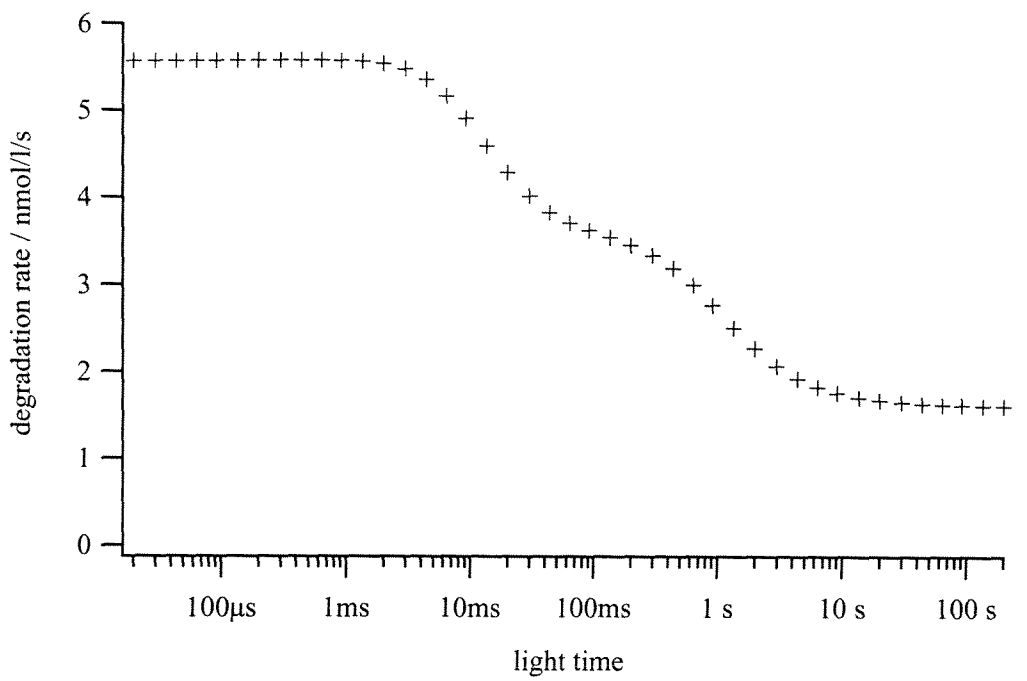

Figure 6.5. Simulation of a photocatalytic degradation at pH 6, with $\gamma = 0.05$ and $I_{a,max} =$ 3111 photons particle^{-1} s^{-1}.

As can be seen in Figure 6.5, the degradation rate rises from its lower limit to its upper limit, as the light time decreases, via two transitions. The limits are given by the degradation rates under continuous illumination with the same average, and the same maximum photon absorption rate. Hence, the simple mechanism represented by equations (6)-(9) is sufficient to explain the most prominent feature of our results. The transitions are less sharp though than those determined experimentally. It is unclear at this point what controls the sharpness of these transitions.

Effect of the light time

In Figure 6.6, we take a closer look at the concentrations of the reducing and oxidizing intermediates on the TiO_2 particle during periodic illumination. Three cases are presented, corresponding to short, intermediate, and long light times. This simulation is for pH 6, where the reducing intermediate is the majority species on the particle. The same behavior is observed however at high pH, except that the roles of the reducing and oxidizing intermediates are reversed. For short light times, the intermediates' concentrations fluctuate around their steady state concentration. For intermediate light times, during illumination there is a build-up of both intermediates. When the light is turned off, the concentrations of both intermediates rapidly decay because of recombination and interfacial transfer of the oxidizing intermediate, until the oxidizing intermediate is exhausted. The reducing intermediate then reacts (away) exponentially due to interfacial transfer, but its concentration does not reach its steady state value before the next light time begins. For long light times on the other hand, both the oxidizing and the reducing species decay away to their steady state in the dark.

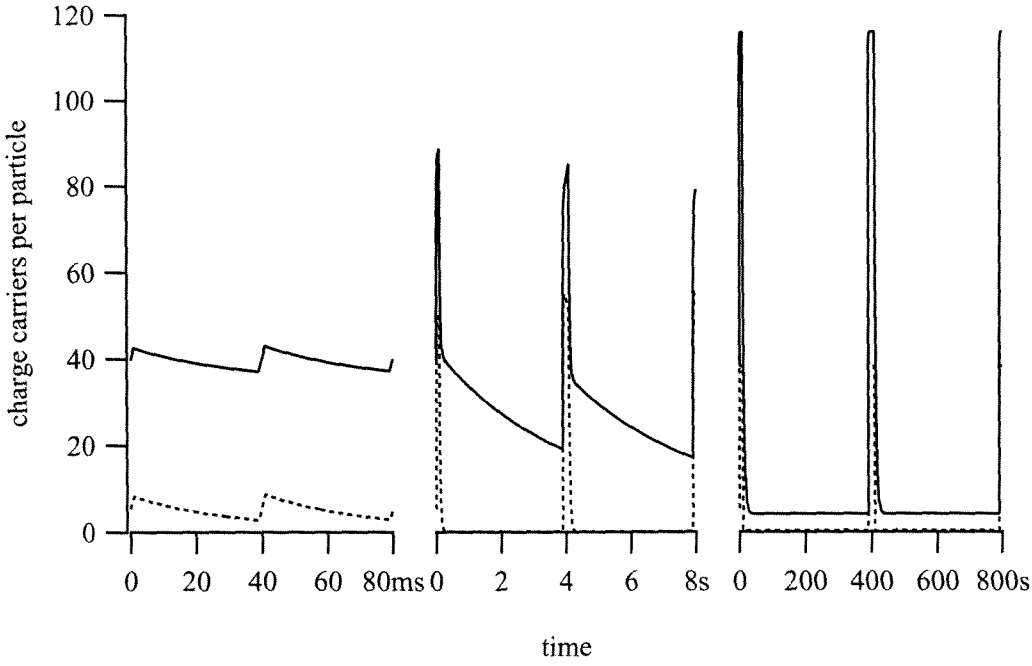

Figure 6.6. Simulated concentrations of the reducing and oxidizing intermediates on the TiO_2 particle during periodic illumination at pH 6, with $\gamma = 0.05$, $I_{a,max} = 3111$ photons particle^{-1} s^{-1} and $\tau_L = 2$ ms (first graph), $\tau_L = 200$ ms (second graph), and $\tau_L = 20$ s (third graph). The solid line is for the reducing intermediate, the dashed line for the oxidizing intermediate.

Effect of the duty cycle

In Figure 6.7, we explore the effect of the duty cycle γ. The results for four duty cycles are displayed. The top marker corresponds to the highest γ, since the degradation rates

increase with γ (but the quantum yields at high intermittence decrease with γ). Both transitions shift to longer light times with increasing duty cycle. This is because with increasing duty cycles the dark time decreases. Thus, the point at which the intermediates cannot decay away to their steady state concentration in the dark – i.e., where transitions occur – shifts to longer τ_L. This was also observed experimentally (cfr. Figures 3.1 and 3.4), though to a much lesser extent, for the first transition. The shift of the second transition, at shorter τ_L, as a function of duty cycle was never observed clearly, which could be due to either the resolution or the accuracy of our data. The fact that both transitions shift by roughly the same factor indicates that the transitions are both related to the dark time, but a different set of rate constants might change this behavior. In fact, under the conditions prevalent in our experimental setup the relationship between the transition time and τ_L or τ_D might be different than in our model.

Effect of light intensity

The effect of light intensity is more prominent for the transition at short τ_L, as illustrated in Figure 6.8. This transition is dominated by the recombination of the reducing and oxidizing intermediates. Since at lower intensities the steady state concentration to which these intermediates build up during illumination is lower, the time needed for one of the intermediates to decay away completely will be shorter, shifting the transition to shorter times. The transition at longer times is determined by interfacial transfer of the reducing or the oxidizing intermediate, depending on which is the excess carrier, and the decay time due to interfacial transfer – unlike the decay time due to recombination – does not depend on the concentration of the (other) intermediate (and is in fact constant).

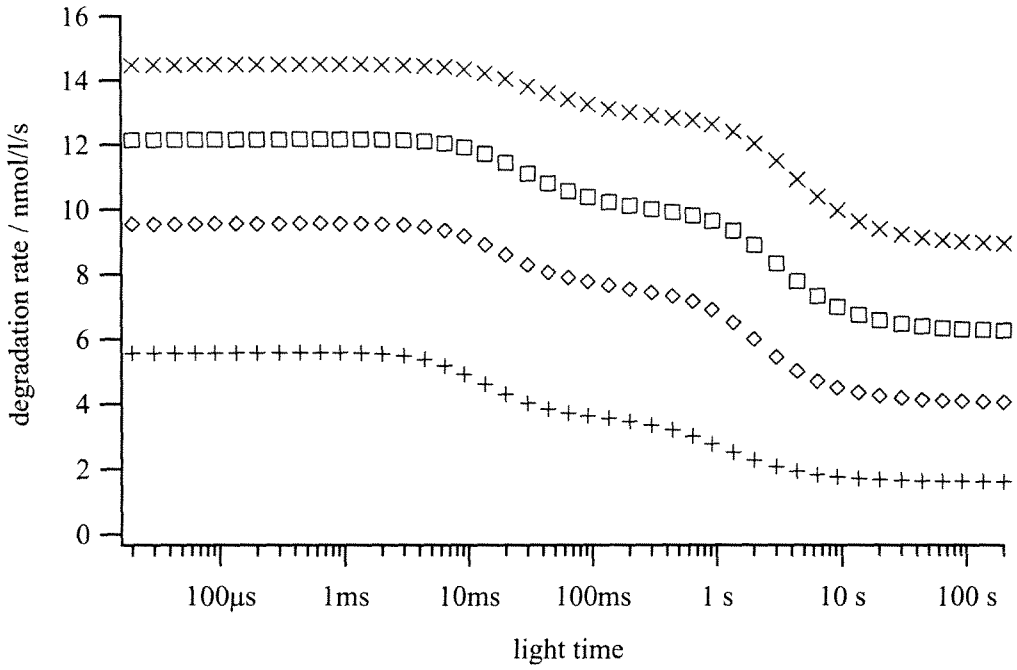

Figure 6.7. Effect of the duty cycle in the simulations, for $\gamma = 0.05$ (+), $\gamma = 0.15$ (◇), $\gamma = 0.25$ (□), and $\gamma = 0.35$ (×), at pH 6 and with $I_{a,max} = 3111$ photons particle^{-1} s^{-1}.

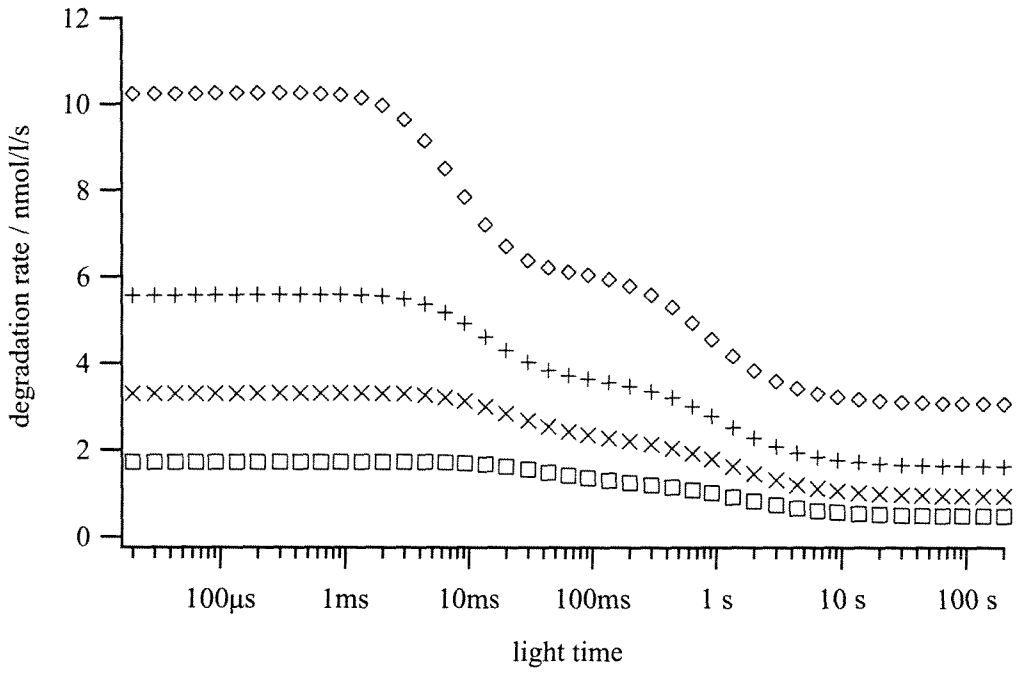

Figure 6.8. Effect of light intensity in the simulations, for I_a = 311 (□), I_a = 1089 (×), I_a = 3111 (+), and I_a = 10889 photons particle^{-1} s^{-1} (◇), at pH 6, with γ = 0.05.

Effect of pH

The effect of pH on the transitions is shown in Figure 6.9. The transitions shift with pH as observed experimentally, with a crossover at pH ~ 8. At this pH, only one transition is observed, while at the other pH values there are two. At pH 8 also the crossover from the reducing intermediate being the excess species (pH < 8) to the oxidizing intermediate

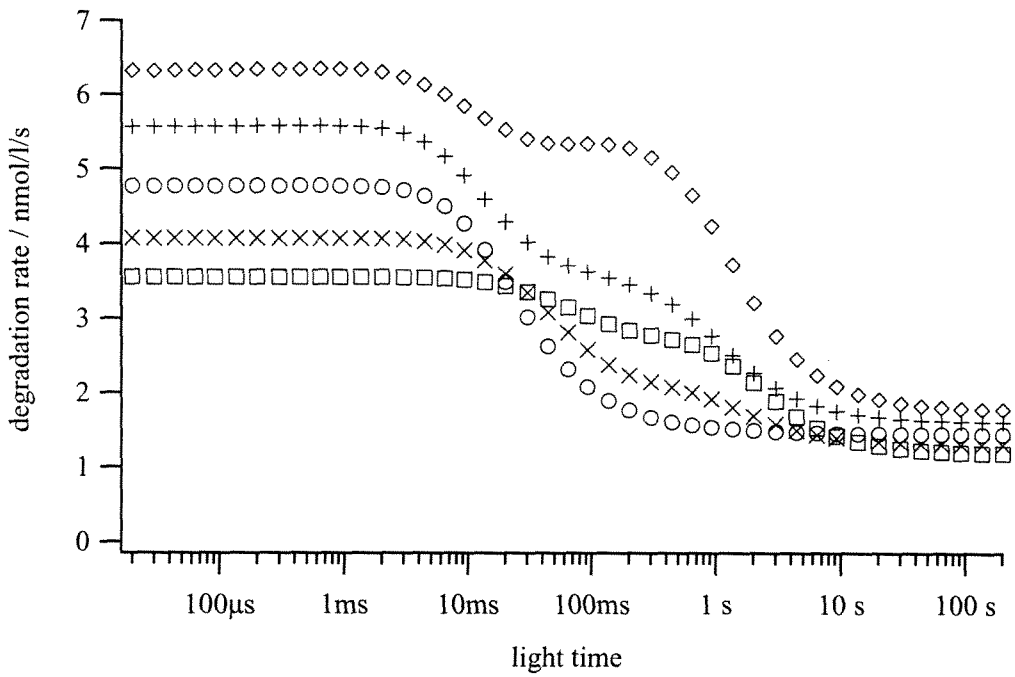

Figure 6.9. Effect of the pH in the simulations, for pH 12 (□), pH 10 (×), pH 8 (○), and pH 6 (+), pH 4 (◇), with $\gamma = 0.05$ and $I_{a,max} = 3111$ photons particle^{-1} s^{-1}.

being the excess species (pH > 8) occurs. The experimentally observed concurrent minimum in degradation rate is not reproduced: according to the modeling, the degradation rate decreases with increasing pH. Likely, the observed minimum is caused by one or more effects that enhance the degradation at high pH, that have not been incorporated in the model – such as for example an alternative degradation pathway in basic media (e.g., hydrolysis) for one of the intermediate degradation products of methyl orange (D), such that less of this intermediate is in competition with methyl orange for holes or hydroxyl radicals.

Effect of Butler-Volmer

The effect of the Butler-Volmer equation is illustrated in Figure 6.10, which shows the concentration of the reducing and oxidizing intermediates under continuous illumination at pH 6.25 (pH_{ZPC}), with and without the Butler-Volmer modulation of the rate constants. With the Butler-Volmer equation, the charge build-up quickly levels off, and the concentrations reach a steady state. Figure 6.11 shows the evolution of the particle potential and the rate constants due to Butler-Volmer during continuous illumination.

At steady state, the reaction rates for reduction (k_1 [A] [e]) and oxidation (k_2 [D] [h]) are equal. The reaction rates are affected directly by the concentrations of the reducing and oxidizing intermediate ([e] and [h]), and again indirectly via the charge imbalance and the Butler-Volmer equation ($k_1 = k_{01} \cdot \exp(-\alpha_{1e} \cdot (zF/RT) \cdot Pot)$, $k_2 = k_{02} \cdot \exp(\alpha_{2h} \cdot (zF/RT) \cdot Pot)$). When the second effect is absent, the change in the concentration of the reducing and oxidizing intermediates required to make the reaction rates equal is much greater and

takes much longer to be established than when the Butler-Volmer equation is taken into account (Figure 6.10).

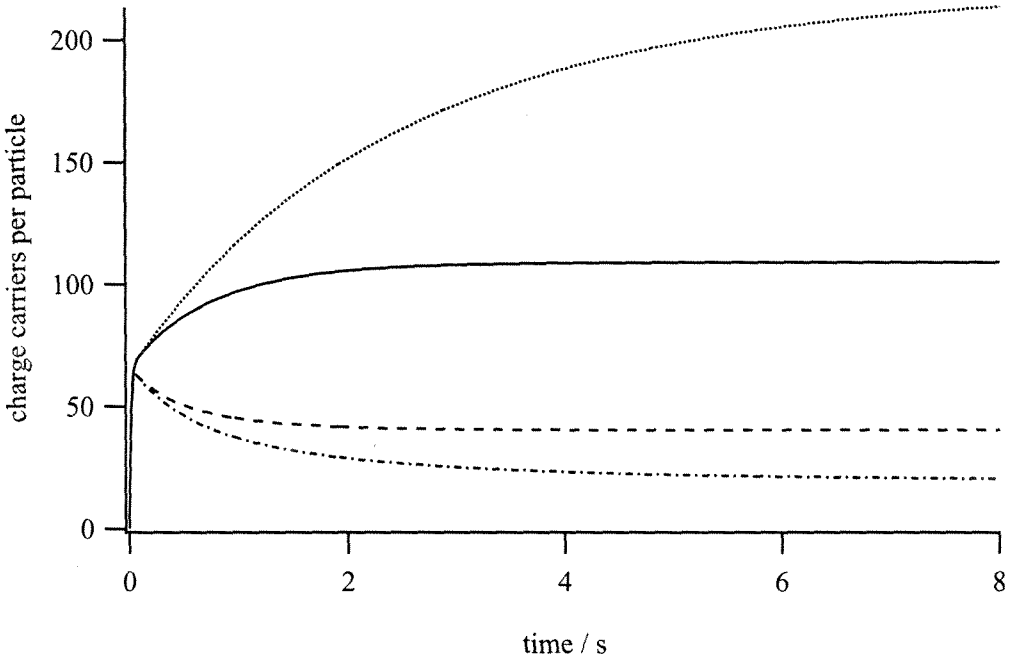

Figure 6.10. Simulated concentrations of intermediates, including the Butler-Volmer equation (reducing (solid line) and oxidizing (dashed line) intermediates) and omitting the Butler-Volmer equation (reducing (dotted line) and oxidizing (dot-dashed line) intermediates, under continuous illumination (at pH 6.25).

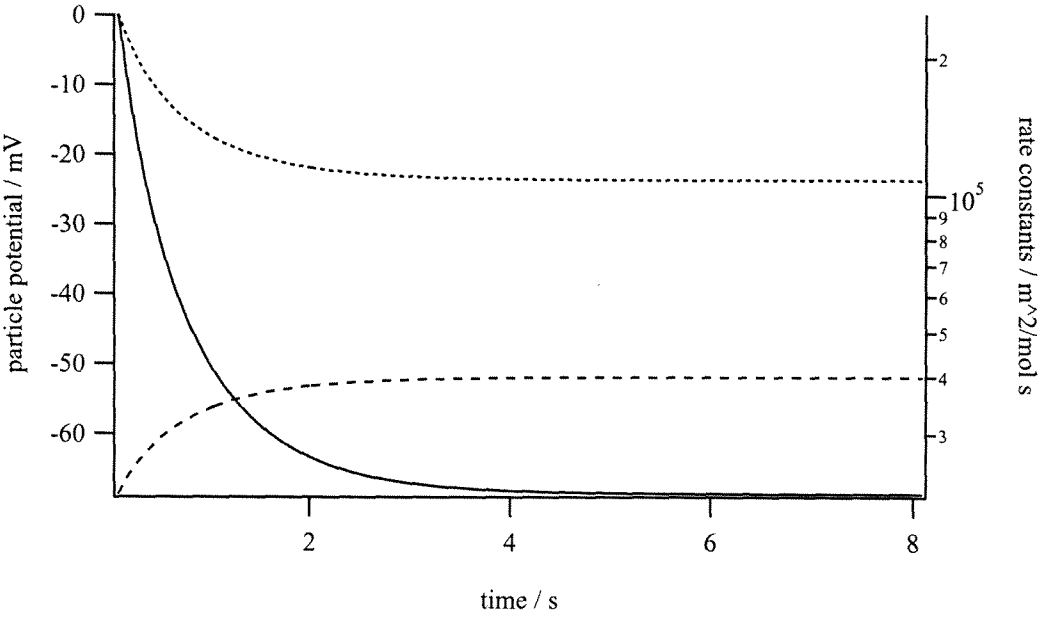

Figure 6.11. Simulated evolution of the particle potential (solid line) and the rate constants for reduction (dashed line) and oxidation (dotted line) to steady state under continuous illumination (at pH 6).

6.5 Conclusions

We verified that a simplified set of reactions – including only generation of a reducing and an oxidizing intermediate, interfacial transfer to an electron acceptor and donor respectively, and recombination – combined with the Butler-Volmer formulation for the interfacial transfer rates, is sufficient to reproduce qualitatively the main features observed in our previously presented experimental results, such as the occurrence of two transitions in the degradation rate (or quantum yields) vs. τ_L, the limits on the degradation rate under periodic illumination set by the continuous illumination case, and the shifts of the transitions as a function of the pH.

It is likely that there are different combinations of initial conditions and kinetic constants that result in transitions at the given light times. Some of those combinations may correspond better to our experimental conditions, and may also reproduce the experimentally observed shifts of the transitions with duty cycle and photon absorption rate. It is equally possible that some of the discrepancies are related to limitations of the model, and that a more complete reaction mechanism – e.g., incorporating a variable number of surface sites with pH, back reactions and further reactions with A^- and D^+ – must be used to achieve better agreement with the experimental results.

6.6 References

(1) Minero, C. *Catal. Today* **1999**, *54*, 205.

(2) Nosaka, Y.; Fox, M. A. *J. Phys. Chem.* **1988**, *92*, 1893.

(3) Upadhya, S; Ollis, D. F. *J. Phys. Chem. B* **1997**, *101*, 2625.

(4) Sczechowski, J. G.; Koval, C. A.; Noble, R. D. In *Photocatalytic Purification and Treatment of Water and Air*; by Ollis, D. F., Al-Ekabi, H., Eds.; Elsevier: Amsterdam, 1993, 121.

(5) Sczechowski, J. G.; Koval, C. A.; Noble, R. D. *J. Photochem. Photobiol. A: Chem.* **1993**, *74*, 273.

(6) Grela, M. A., Colussi, A. J. *J. Phys Chem.* 1996, *100*, 18214.

(7) Brett, C. M. A.; Oliveira-Brett, A. M. *Electrochemistry: Principles, Methods, and Applications*, Oxford University Press, 1993.

(8) Calvert, J. G.; Pitts, J. N., Jr. *Photochemistry*, Wiley & Sons, Inc., 1966, Chapter 6.

(9) Gerischer, H. *Electrochim. Acta* **1993**, *38*, 3.

(10) Augugliaro, V.; Palmisano, L.; Sclafani, A.; Minero, C.; Pelizzetti, E. *Toxicol. Environ. Chem.* **1988**, *16*, 89.

(11) Manuera, G.; Rives-Arnau, V.; Saucedo, A. *J. Chem. Soc., Faraday Trans.* **1979**, *75*, 736.

6.7 Appendices

Printout of the Igor program used to carry out the simulations

```
#pragma rtGlobals=1          // Use modern global access method.

Function degradation(pw, xx, yw, dydx)
// Used with SolveODE to model pulsed photocatalysis with the following reaction mechanism
// carrier generation: h nu –> e- + h+ (Ia)
// reduction:          e- + A –> A- (k1)
// oxidation:          h+ + D –> D+ (k2)
// recombination:      e- + h+ –> heat (k3)

    Wave pw    // parameter wave (input)
            // pw[0] = Ia
            // pw[1] = k1
            // pw[2] = k2
            // pw[3] = k3
            // pw[4] = s/Cdl
    Variable xx // x value at which to calculate derivatives
            // time
    Wave yw    // wave containing y[i] (input)
            // yw[0] = [e-]
            // yw[1] = [h+]
            // yw[2] = [A]
            // yw[3] = [D+]
            // yw[4] = [D]
    Wave dydx  // wave to receive dy[i]/dx (output)
            // dydx[0] = d[e-]/dt = Ia - k1 [e-][A] -k3[e-][h+]
            // dydx[1] = d[h+]/dt = Ia - k2 [h+][D] -k3[e-][h+]
            // dydx[2] = d[A]/dt = 0 bubbling oxygen
            // dydx[3] = d[D+]/dt = k2 [h+][D]
            // dydx[4] = d[D]/dt = 0

    NVAR pH = pH
    Variable Pot = ((yw[1]-yw[0])*pw[4]) + (6.25-pH)*0.059      // charged particle potential =
([h+]-[e-])*s/Cdl
        // correct for pH with pH_zpc=6.25

    NVAR t_light = t_light, duty_cycle = duty_cycle
    Variable Ia = pw[0]      // charge carrier generation rate
    If(mod(xx,t_light/duty_cycle)>t_light)      // pulsed illumination
        Ia /= 2000
    EndIf
    Variable Red = pw[1]*exp(-8.55*Pot)*yw[0]*yw[2]          // Butler Volmer reduction rate
    Variable Ox = pw[2]*exp(12.2*Pot)*yw[1]*yw[4]            // Butler Volmer oxidation rate
```

```
    Variable Rec = pw[3]*yw[0]*yw[1]  // recombination rate

    // mass balance equations
    dydx[0] = Ia -Red - Rec
    dydx[1] = Ia - Ox - Rec
    dydx[2] = 0
    dydx[3] = Ox
    dydx[4] = 0
End

Macro RunDegradation(S_mechanism, S_rate_constants, S_concentrations, V_timestep, species)
    String S_mechanism="degradation"
    String S_rate_constants="rate_constants"
    String S_concentrations="concentrations"
    Variable V_timestep = .01
    Variable species = 3 // use third species to calculate degradation rate

    PrintRateConstants(S_rate_constants)
    RunOneDegradation(S_mechanism, S_rate_constants, S_concentrations, V_timestep)
    PrintDegradationRate(S_Concentrations,species) *.642e-9 // convert to nM/s
End

Macro RunIntensitySeries(S_mechanism, S_rate_constants, S_concentrations, S_intensity,
S_timesteps, species, S_result)
    String S_mechanism="degradation"
    String S_rate_constants="rate_constants"
    String S_concentrations="concentrations"
    String S_intensity="intensity"
    String S_timesteps="timesteps_vs_I"
    Variable species = 3 // use third species to calculate degradation rate
    String S_result="rate_vs_I"

    PrintRateConstants(S_rate_constants)
    Variable i = 0
    Variable V_timestep
    do
        $S_rate_constants[0] = $S_intensity[i]
        V_timestep = $S_timesteps[i]
        RunOneDegradation(S_mechanism, S_rate_constants, S_concentrations, V_timestep)
        $S_result[i] = PrintDegradationRate(S_concentrations,species) *.642e-9 // convert to
nM/s
        i += 1
    while (i < numpnts($S_intensity))
End

Macro RunPulsedSeries(S_mechanism, S_rate_constants, S_concentrations, S_lighttimes,
S_timesteps, species, S_result)
    String S_mechanism="degradation"
    String S_rate_constants="rate_constants"
    String S_concentrations="concentrations"
    String S_lighttimes="lighttimes"
```

```
    String S_timesteps="timesteps_vs_t"
    Variable species = 3 // use third species to calculate degradation rate
    String S_result="rate_vs_t"

    PrintRateConstants(S_rate_constants)
    Variable i = 0
    Variable V_timestep
    do
        t_light = $S_lighttimes[i]
        V_timestep = $S_timesteps[i]
        RunOneDegradation(S_mechanism, S_rate_constants, S_concentrations, V_timestep)
        $S_result[i] = PrintDegradationRate(S_concentrations,species) *.642e-9 // convert to
nM/s
        i += 1
    while (i < numpnts($S_lighttimes))
End

Function RunOneDegradation(S_mechanism, S_rate_constants, S_concentrations, V_timestep)
    String S_mechanism, S_rate_constants, S_concentrations
    Variable V_timestep

    WAVE rate_constants = $S_rate_constants
    NVAR t_light = t_light, duty_cycle = duty_cycle
    Variable intensity = rate_constants[0]
    Variable period = t_light/duty_cycle
    printf "intensity=%4.2W1Peinstein/l/s\t", intensity
    printf "light time=%4.2W1Ps\t", t_light
    printf "duty cycle=%g\t", duty_cycle
    printf "timestep=%4.2W1Ps\r", V_timestep
    if (duty_cycle<1)
        // mod(n*div,div) returns div when the numerical error is negative
        if (abs((period/V_timestep)-round(period/V_timestep)) > 1e-3)
            printf "WARNING: wave scaling does not divide evenly into illumination period."
            printf "\r\t(%6.4W1Ps / %6.4W1Ps) = ", period, V_timestep
            printf "%g%+g\r", round(period/V_timestep), (period/V_timestep)-
round(period/V_timestep)
        endif
        if (abs((t_light/V_timestep)-round(t_light/V_timestep)) > 1e-3)
            printf "WARNING: wave scaling does not divide evenly into illumination light
time."
            printf "\r\t(%6.4W1Ps / %6.4W1Ps) = ", t_light, V_timestep
            printf "%g%+g\r", round(t_light/V_timestep), (t_light/V_timestep)-
round(t_light/V_timestep)
        endif
    endif
    SetScale/P x t_light/2,V_timestep,"s", $S_concentrations
    Make/O/N=(DimSize($S_concentrations, 1)) W_tol= 1e-15
    IntegrateODE/U=40/F=3/S=W_tol $S_mechanism, $S_rate_constants, $S_concentrations
End

Function PrintRateConstants(S_rate_constants)
```

```
    String S_rate_constants

    printf "rate constants:"
    WAVE rate_constants = $S_rate_constants
    Variable index=1
    do
        printf "\t%s=%#g", GetDimLabel($S_rate_constants, 0, index), rate_constants[index]
        index += 1
    while (index<DimSize($S_rate_constants, 0))
    printf "\r"
End

Function PrintDegradationRate(S_concentrations, i)
    String S_concentrations
    Variable i

    WAVE W_C = $S_concentrations
    NVAR duty_cycle = duty_cycle
    NVAR t_light = t_light
    Variable period = t_light/duty_cycle
    Variable timestep = DimDelta($S_concentrations, 0)
    Variable stop = DimSize($S_concentrations, 0)-1
    Variable start = stop-period/timestep
    if (start<0)
        period = stop * timestep
        start = 0
    endif
    Variable degradation_rate = -(W_C[start][i] - W_C[stop][i])/period
    printf "degradation rate: %#4.2g/s", degradation_rate
    printf " (%#4.2g from %#5.3g", W_C[start][i] - W_C[stop][i], W_C[start][i]
    printf " to %#5.3g in %4.2W1Ps)\r", W_C[stop][i], period
    Return degradation_rate
End

Function FitDegradationRate(w,t_exp,duty_cycle_exp,Ia_exp,pH_exp) : FitFunc
    Wave w
    Variable t_exp
    Variable duty_cycle_exp
    Variable Ia_exp
    Variable pH_exp

    //CurveFitDialog/ These comments were created by the Curve Fitting dialog. Altering them
will
    //CurveFitDialog/ make the function less convenient to work with in the Curve Fitting dialog.
    //CurveFitDialog/ Equation:
    //CurveFitDialog/ Use integrateODE to calculate degradation rate
    //CurveFitDialog/ DegradationRate
Ia+k1+k2+k3+Cdl*t_exp*pH_exp*duty_cycle_exp*Ia_exp
    //CurveFitDialog/ End of Equation
    //CurveFitDialog/ Independent Variables 4
    //CurveFitDialog/ t_exp
```

```
    //CurveFitDialog/ duty_cycle_exp
    //CurveFitDialog/ Ia_exp
    //CurveFitDialog/ pH_exp
    //CurveFitDialog/ Coefficients 6
    //CurveFitDialog/ w[0] = Ia
    //CurveFitDialog/ w[1] = k1
    //CurveFitDialog/ w[2] = k2
    //CurveFitDialog/ w[3] = k3
    //CurveFitDialog/ w[4] = Cdl
    //CurveFitDialog/ w[5] = phi

    WAVE concentrations = concentrations
    WAVE rate_constants = rate_constants
    NVAR duty_cycle = duty_cycle
    NVAR t_light = t_light
    NVAR pH = pH

    rate_constants[0] = Ia_exp
    PrintRateConstants("rate_constants")
    // set initial electron and hole concentrations to steady-state at average intensity
    concentrations[0][0,1] = 0
    rate_constants[0] = Ia_exp * duty_cycle_exp; duty_cycle = 1
    Variable rise_time = 1/sqrt(rate_constants[0]*rate_constants[3])
    SetScale x 0,50*rise_time,"s", concentrations
    Make/O/N=(DimSize(concentrations, 1)) W_tol= 1e-15
    IntegrateODE/U=2000/F=3/S=W_tol degradation, rate_constants, concentrations
    concentrations[0][0,1] = concentrations[Inf][q]

    // run degradation simulation
    t_light = t_exp
    duty_cycle = duty_cycle_exp
    rate_constants[0] = Ia_exp
    pH = pH_exp
    RunOneDegradation("degradation", "rate_constants", "concentrations", t_exp/10)
    return PrintDegradationRate("concentrations", 3) *.642e-9 // convert to nM/s
End
```

Chapter 7

General conclusions

In this work, we rationalized earlier reports of improved quantum yields for photocatalysis under periodic illumination, by comparison with those obtained under continuous illumination. In agreement with the literature, we found that the quantum yields under periodic illumination are equal to or larger than those under continuous illumination with the same *maximum* photon absorption rate. In addition, we demonstrated conclusively that these improvements do not require mass transfer limitations. However, we also found that the quantum yields under periodic illumination are constrained above by those under continuous illumination with the same *average* photon absorption rate.

This finding implies that in the application of photocatalysis, it is not possible to achieve a higher quantum yield, using a given photon flux, than in the ideal case where all photons are absorbed uniformly, both in space and in time, over the volume of the reactor. If the photon flux is not absorbed uniformly, it is still possible to obtain the same quantum yield as in the ideal case, provided that the photon flux on each photocatalyst particle averages out to the average photon flux on a sufficiently short timescale. Periodic illumination experiments, like the ones carried out in this work, can be used to determine what that timescale is.

The quantum yield under periodic illumination was shown to rise from its lower limit to its upper limit, not via one – as observed in homogeneous photochemistry – but via two transitions. These transition times are related to the lifetimes of (two) intermediates involved in the photocatalytic reactions at the TiO_2/solution interface.

One intermediate's lifetime was found to increase exponentially with pH, while that of the other decreases exponentially. Combined with the known dependence of the charge carrier's reducing or oxidizing powers on the pH – because of the shift of the band edge positions to more negative values by 59 mV for every one pH unit increase – and the concurrent dependence of the reaction rates on the pH (Butler-Volmer equation), this relationship between the lifetimes and the pH led us to conclude that the intermediate with a decreasing lifetime with pH is a reducing species, while the other one is an oxidizing species. The lifetimes of both intermediates are equal at pH 8.2, where only one transition is observed. If this were a general finding, it would imply that below pH 8.2, where most photocatalytic systems are operated, interfacial electron transfer to oxygen is the slowest step.

From the comparison of the quantum yields for photocatalytic formate oxidation on Degussa P25 and on Tiona PC105 TiO_2, it seems that the lifetimes are insensitive to the anatase/rutile ratio of the TiO_2 photocatalyst particles. This would be inconsistent with the reasoning presented above, since the conduction band edge of rutile is 0.2 V lower than that of anatase. This should result in a decreased reducing power, and a longer lifetime of the reducing (long-lived) intermediate on P25 (70% anatase, 30% rutile) vs. PC105 (100% anatase), which is not observed experimentally. A tentative explanation to bring these two conflicting observations in agreement involves the inactivity of the rutile phase, under our experimental conditions, for formate photocatalysis. Rutile might be much less efficient in absorbing photons with a wavelength around 360 nm than anatase, or may for some other reason not catalyze formate photooxidation, which would account for the apparent absence of any influence of the rutile phase on the lifetime of the

reducing intermediate. This hypothesis could be tested by performing some (formate) degradation experiments on rutile particles under the same conditions as the previous series of experiments (especially the range of wavelengths used).

A disadvantage of the technique of periodic illumination is that the identity of the observed intermediates must be deduced by other means. From spectroscopic measurements, it is known that the lifetimes of free electrons or holes are much shorter than those measured with the technique of periodic illumination. The latter are, however, not inconsistent with the lifetimes of superoxide radicals (a reducing species), and hydroxyl radicals, surface trapped holes and surface-bound hydroxyl radicals (oxidizing species). To gain more certainty on the identity of the observed intermediates, experiments could be performed in which for example the electron acceptor is varied, or the solvent, or the TiO_2 surface.

Although not all issues concerning the interpretation of the results have been resolved, this work clearly demonstrates the versatility of the technique of periodic illumination in the determination of characteristic timescales in photocatalysis. The technique can be used with any electron donor and acceptor of interest, in the presence of any other reagent of interest, without the necessity to add probe molecules that might interfere with the redox reactions. It can be used in the actual environment of interest, in a slurry or a fixed bed reactor, in aqueous phase or in the gas phase. In fact the comparison of the lifetimes of the rate-determining intermediates in aqueous phase vs. those in the gas phase might provide some insights into the causes of the lower quantum yields typically observed in aqueous phase photocatalysis.

The utility of the technique could be further enhanced by combining it with various other techniques that have been used to study photocatalysis, e.g., using UV laser illumination to precisely control photon energy, pulse timing and intensity, or using a rotating disk electrode to study mass transfer effects and/or electrochemically measure transient reaction rates. Techniques enabling time-resolved measurement of reaction rates and/or concentrations of intermediates would be of particular interest for answering questions about the relative rates of different steps in the reaction mechanism.

Photocatalyst configurations where the oxidation and reduction occur on different surfaces in different environments, with the photocatalyst physically separating the two environments, also offer intriguing prospects both for study and applications of photocatalysis, if the concomitant engineering challenges can be solved.